Schriftenreihe IWAR

270

TECHNISCHE UNIVERSITÄT DARMSTADT

IWAR

Vanessa Acevedo Alonso

Modelling Biofilm Systems for Wastewater Treatment: Impact of Microscale Features on Global Modelling Results

Herausgeber:
Verein zur Förderung des Instituts IWAR der TU Darmstadt e. V.

Modelling Biofilm Systems for Wastewater Treatment: Impact of Microscale Features on Global Modelling Results

Vom Fachbereich Bau- und Umweltingenieurwissenschaften
der Technischen Universität Darmstadt
zur Erlangung des akademischen Grades einer
Doktor-Ingenieurin (Dr.-Ing.) genehmigte Dissertation

von

M.Sc. Vanessa Acevedo Alonso
aus Bogotá

Erstgutachterin: Prof. Dr. Susanne Lackner
Zweitgutachter: Prof. Dr. Eberhard Morgenroth

Darmstadt 2022
D 17

Vanessa Acevedo Alonso

Modelling Biofilm Systems for Wastewater Treatment: Impact of Microscale Features on Global Modelling Results.

Darmstadt, Technische Universität Darmstadt

Hrsg.: Verein zur Förderung des Instituts IWAR der TU Darmstadt e. V.
Darmstadt: Eigenverlag, 2022
(Schriftenreihe IWAR 270)

ISSN 0721-5282
ISBN 978-3-940897-71-8

URI: https://tuprints.ulb.tu-darmstadt.de/id/eprint/21670

URN: urn:nbn:de:tuda-tuprints-216704

Referentin: Prof. Dr. Susanne Lackner
Korreferent: Prof. Dr. Eberhard Morgenroth

Tag der schriftlichen Einreichung: 19.04.2022
Tag der mündlichen Prüfung: 24.06.2022

Herstellung: Lasertype GmbH
Holzhofallee 19
64295 Darmstadt

Vertrieb: Institut IWAR
TU Darmstadt
Franziska-Braun-Straße 7
64287 Darmstadt
Telefon: 06151 / 16 20301
Telefax: 06151 / 16 20305

Abstract

Biofilm models are effective tools that allow the mathematical description of biofilm systems, the prediction of their removal performance as well as their conceptual exploration. Models have the advantage of being less resource and time consuming than laboratory experiments and being more flexible regarding the scenarios that can be analyzed. Due to the high complexity of biofilms, it is virtually impossible to develop a model that comprises all the phenomena occurring within the biofilm. Simplifications are considered a substantial part of the modelling process, and even the most comprehensive models developed until now make use of assumptions and simplifications. Nevertheless, the vast majority of models fulfill their purpose and are useful to both researches and practitioners (Wanner et al. 2006).

The decision on which model is better for which modelling task relies on the data available, the level of understanding of the phenomena occurring in the system and the objective of the modelling task. In the specific case of biofilms, a trade-off between microscale features and global modelling results is often present. A more detailed description of the microscale features does not necessarily lead to more compelling modelling results, and occasionally it can compromise the identifiability and the determination of relevant parameters. However, neglecting microscale features can result in inaccurate representations of the system and thus the explanatory power of the model may be diminished. Depending on the system and its specific conditions, the modeler is presented with a dilemma: Which microscale features are worth including, which simplifications can be afforded and which simplifications are compulsory due to the lack of information.

Two microscale features are of special interest in this work: microbial community composition and dimensionality. Three biofilm systems were used to explore the impact that these two microscale features have on the global modelling results and on the model's explanatory power: A biologically active Granular Activated Carbon (bGAC) filter, a Moving Bed Bioreactor (MBBR) and a Membrane Aerated Biofilm Reactor (MABR). An individual publication is dedicated to each one of these systems. These systems were used to showcase alternative modelling approaches and to illustrate the effect of choosing simple or more complex descriptions of the microscale features of interest.

The first and second publication, P1 and P2 respectively, focus on the microbial community composition. Publication P1 deals with DOC removal from WWTP effluents in a bGAC-filter. Within the filter, DOC is removed by simultaneous adsorption and biodegradation, therefore a suitable model should include both mechanisms. It proposes a model that integrates a traditional one-dimensional biofilm model with the ideal adsorbed solution theory that can be applied within the activated sludge model framework. A simplified microbial community composed solely composed of aerobic heterotrophic bacteria is selected. The developed model is able to describe the DOC breakthrough curves at different empty bed contact times and it also shows the relative contribution of biodegradation and adsorption to the total DOC removal.

Publication P2 analyzes the behavior of heterotrophic bacteria in an MBBR reactor operating as a Partial Nitritation/ Anammox (PN/A) system. It discusses the growth strategies that heterotrophic bacteria pursue when facing substrate scarcity. The effect of the yield-strategy is

analyzed in two scenarios. In the first scenario a group of heterotrophic bacteria growing on endogenous COD is investigated, whereas in the second scenario, external COD is allowed into the system and a second group of heterotrophs (rate strategist) growing on the more available external COD is added. The competition between both groups over space, and electron acceptor is assessed. In both scenarios the pursuing of the yield strategy seems to be crucial for the diversity of the heterotrophic community. Effluent concentrations as well as heterotrophic produced dinitrogen gas is strongly affected by the growth-strategy that the heterotrophs selected, higher denitrification activities are observed when the yield strategy is selected.

Finally dimensionality is the microscale feature of interest in the third publication P3. An MABR reactor used for PN/A is modelled. Publication P3 compares a traditional one-dimensional model and different pseudo two-dimension models that allow the implementation of concentration gradients in the bulk liquid and the gas phase, individually and simultaneously as well as in counter or parallel flow. The results show that the one-dimensional model underestimates the effluent's total dissolved nitrogen concentration in comparison to the prediction delivered by the pseudo two-dimensional models. Differences in the axial gradients in the biofilm are also observed between the two evaluated modelling approaches. P3 also demonstrates that the concentration gradients in the gas phase have a more significant impact on the modelling results than the concentration gradients in the bulk liquid.

The importance of the microscale features: microbial composition and dimensionality is explored. Alongside, the implications on the global modelling results, product of the simplifications of microscale features are investigated. In the case of microbial composition, although more information has been made available due to the new experimental techniques (molecular biology, imagining etc.) there are still disparities between what can be determined experimentally and how this can be implemented into the existent modelling frameworks. In the case of dimensionality, longitudinal gradients seem to be more influential than it was previously assumed and need to be taken into account to better describe MABRs. The adequate level of complexity required for a microscale feature and in general for a model should be decided based on the modelling goals, the current understanding of the system and the available data.

Kurzfassung

Biofilmmodelle sind wirksame Instrumente, die die mathematische Beschreibung von Biofilmsystemen, die Vorhersage ihrer Abbauleistung sowie die konzeptionelle Erforschung dieser Systeme ermöglichen. Modelle haben den Vorteil, dass sie weniger ressourcen- und zeitaufwändig sind als Laborexperimente und dass sie hinsichtlich der zu analysierenden Szenarien flexibler sind. Aufgrund der hohen Komplexität von Biofilmen ist es praktisch unmöglich, ein Modell zu entwickeln, das alle im Biofilm vorkommenden Phänomene umfasst. Vereinfachungen sind ein wesentlicher Bestandteil des Modellierungsprozesses. Selbst die umfassendsten Modelle, die bisher entwickelt wurden, treffen zahlreiche Annahmen. Dennoch erfüllt die überwiegende Mehrheit der Modelle ihren Zweck und so bleiben sie sowohl für die Forschung als auch für die Praxis nützlich (Wanner et al. 2006).

Die Entscheidung, welches Modell für welche Modellierungsaufgabe besser geeignet ist, hängt von den verfügbaren Daten, dem Grad des Verständnisses der im System auftretenden Phänomene und dem Ziel der Modellierungsaufgabe ab. Im speziellen Fall von Biofilmen besteht häufig ein Kompromiss zwischen *microscale features* und globalen Modellierungsergebnissen. Eine detailliertere Beschreibung der *microscale features* führt nicht notwendigerweise zu verbesserten Modellierungsergebnissen und kann gelegentlich die Identifizierbarkeit des Biofilms und die Bestimmung der relevanten Parameter beeinträchtigen. Die Vernachlässigung von *microscale features* kann jedoch zu ungenauen Darstellungen des Systems führen und damit die Aussagekraft des Modells verringern. Je nach System und seinen spezifischen Bedingungen steht der Modellierer vor einem Dilemma: Welche *microscale features* sind es wert, einbezogen zu werden, welche Vereinfachungen kann man sich leisten und welche sind aufgrund des Mangels an Informationen zwingend erforderlich.

Zwei *microscale features* sind in dieser Arbeit von besonderem Interesse: die Zusammensetzung der mikrobiellen Gemeinschaft und die Dimensionalität. Drei Biofilmsysteme wurden verwendet, um die Auswirkungen dieser beiden *microscale features* auf die globalen Modellierungsergebnisse und die Aussagekraft des Modells zu untersuchen: Eine biologisch aktiver granulierter Aktivkohle (bGAK) Filter, ein *Moving Bed Bioreactor* (MBBR) und ein *Membrane Aerated Biofilm Reactor* (MABR). Jedem dieser Systeme ist eine eigene Veröffentlichung gewidmet. Diese Systeme wurden verwendet, um unterschiedliche Modellierungsansätze vorzustellen und die Auswirkungen der Wahl einfacher oder komplexerer Beschreibungen der interessierenden *micro features* zu veranschaulichen.

Die erste und zweite Veröffentlichung, P1 bzw. P2, konzentrierten sich auf die Zusammensetzung der mikrobiellen Gemeinschaft. Die Veröffentlichung P1 befasst sich mit der Entfernung von DOC aus Kläranlagenablauf in einem bGAK-Filter. Innerhalb des Filters wird DOC durch gleichzeitige Adsorption und biologischen Abbau entfernt, weshalb ein geeignetes Modell beide Mechanismen berücksichtigen sollte. Ein Modell wurde entwickelt, das ein traditionelles eindimensionales Biofilmmodell mit der *ideal adsorbed solution* Theorie verbindet, die im Rahmen der *activated sludge models* angewendet werden kann. Es wurde eine vereinfachte mikrobielle Gemeinschaft ausgewählt, die ausschließlich aus aeroben heterotrophen Bakterien

besteht. Das entwickelte Modell ist in der Lage, die DOC-Durchbruchskurven bei unterschiedlichen Leerbett-Kontaktzeiten zu beschreiben und zeigt auch den relativen Beitrag von biologischem Abbau und Adsorption zur gesamten DOC-Entfernung.

Publikation P2 analysiert das Verhalten heterotropher Bakterien in einem MBBR-Reaktor, der als partielle Nitritation/Anammox (PN/A) betrieben wird. Sie erforscht die Wachstumsstrategien, die heterotrophe Bakterien bei Substratknappheit verfolgen. Die Auswirkung der *yield strategy* wird in zwei Szenarien analysiert. Im ersten Szenario wurde eine Gruppe heterotropher Bakterien untersucht, die auf endogenem CSB wächst, während im zweiten Szenario den System externer CSB zugeführt wurde und eine zweite Gruppe heterotropher Bakterien (*rate strategists*) hinzugefügt wurde, die auf dem besser verfügbaren externen CSB wächst. Der Wettbewerb zwischen beiden Gruppen um Platz und Elektronenakzeptoren wurde untersucht. In beiden Szenarien schien die Verfolgung der *yield strategy* ausschlaggebend für die Diversität der heterotrophen Gemeinschaft zu sein. Die Abwasserkonzentrationen sowie der von den Heterotrophen produzierte gasförmige Stickstoff wurden stark von der von den Heterotrophen gewählten Wachstumsstrategie beeinflusst, wobei höhere Denitrifikationsaktivitäten beobachtet wurden, wenn die *yield strategy* gewählt wurde.

In der dritten Veröffentlichung P3 war die Dimensionalität das *microcale feature* von Interesse. Es wurde ein MABR-Reaktor modelliert, der für PN/A verwendet wird. In der Veröffentlichung P3 werden ein traditionelles eindimensionales Modell und verschiedene pseudo-zweidimensionale Modelle verglichen, die die Implementierung von Konzentrationsgradienten in der Flüssigkeits- und der Gasphase ermöglichen, und zwar sowohl einzeln und gleichzeitig als auch im Gegen- oder Parallelstrom. Die Ergebnisse zeigen, dass das eindimensionale Modell die Gesamtkonzentration des gelösten Stickstoffs im Abwasser im Vergleich zu den Vorhersagen der pseudo-zweidimensionalen Modelle unterschätzt. Auch bei den axialen Gradienten im Biofilm wurden Unterschiede zwischen den beiden evaluierten Modellierungsansätzen festgestellt. P3 zeigte auch, dass die Konzentrationsgradienten in der Gasphase einen stärkeren Einfluss auf die Modellierungsergebnisse hatten als die Konzentrationsgradienten in der Flüssigkeitsphase.

Die Bedeutung der *microscale features:* mikrobielle Zusammensetzung und Dimensionalität wird untersucht. Außerdem werden die Auswirkungen auf die globalen Modellierungsergebnisse untersucht, die sich aus den Vereinfachungen der *microscale feature*s ergeben. Im Fall der mikrobiellen Zusammensetzung stehen mehr Informationen zu Verfügung, dank der neuen experimentellen Techniken (Molekularbiologie, *Imaging* usw.), dennoch kann nicht alles, was experimentell bestimmt werden kann, direkt in herkömmliche Modelle implementiert werden. Was die Dimensionalität betrifft, haben Konzentration Gradienten in der Fließrichtung einen größeren Einfluss als bisher angenommen und müssen berücksichtigt werden, um MABRs besser zu beschreiben. Das angemessene Maß an Komplexität, das für ein *microscale feature* und allgemein für ein Modell erforderlich ist, sollte auf der Grundlage der Modellierungsziele, des aktuellen Verständnisses des Systems und der verfügbaren Daten entschieden werden.

Contents

List of Figures

List of Tables

Part I: Synopsis

1. Introduction

Biofilms are the most widespread form of microbial organization, which can be found in several environments ranging from geothermal fields to medical devices. Although biofilm formation is often perceived as disadvantageous, biofilms have found extensive application in drinking water and wastewater treatment. Various treatment processes rely on biodegradation within a biofilm and take advantage of the unique conditions that biofilms have to offer e.g. localized concentration gradients, cooperation between the microorganisms and more resistance and tolerance to changes (Flemming et al. 2016).

Modelling is widely recognized as a powerful tool to investigate biological systems without the constrained resources inherent to experimental set-ups. Modelling a biofilm system not only allows the prediction of the overall system behavior but also provides a conceptual framework for the understanding of the phenomena occurring within the system (Vannecke 2015). In the last years the understanding of biofilms has increased, due to new experimental techniques that allow the exploration and measurement of a wider range of biofilm characteristics. Valuable insight into the structural heterogeneity of the biofilm has been gained thanks to new imaging techniques such as: fluorescent in situ hybridization, fluorescent staining combined with confocal scanning laser microscopy etc. Imaging techniques deliver interesting information about the initial biofilm formation phases (attachment), spatial distribution of bacteria and the extracellular polymer matrix, and the environment's influence on the biofilm structure (Lewandowski and Beyenal 2009). Alongside the imaging techniques new molecular technologies have also played a central role in the investigation of biofilm features. The application of omics techniques has shed some light on biofilm community structures, metabolic profiling and the biofilm genetic coding potential of biofilms (Franklin et al. 2015). The rise of such experimental techniques has shifted the perspective, as more information about several biofilm features has become available and as consequence, more complex models could be developed.

With increasing information, models can be enriched, however the development of unnecessarily complex models is risked. A more detailed descriptions of some biofilm microscale features may be irrelevant to the macroscale results. Therefore, a careful consideration of whether or not to translate all the new gained information into the model is needed. It is generally accepted that both the modelling objectives (mainly directed to the macro scale result e.g. effluent concentrations), and the available data may serve as guideline for the definition of the adequate complexity. Nevertheless a standardized process to find the right complexity level is lacking and is hard to define (Hill 2006).

This work focuses on two microscale features that are crucial when modelling a biofilm system: microbial community composition and dimensionality. It analyses the effect that these microscale features have on the macroscale predictions as well as on the model's explanatory power. This thesis aimed to qualitatively describe the necessity of taking into account such microscale features and the level of complexity that is required to obtain sound modelling results. Three currently relevant biofilm systems were selected for this purpose.

In the first, publication P1, a biologically active Granular Activated Carbon (bGAC) filter used for the removal of DOC from a Wastewater Treatment Plant (WWTP) effluent is modelled. P1

investigates the combination of biodegradation and multi-component adsorption. Given that the biofilm is formed by a highly complex community that influences the mass transfer from the bulk liquid into the GAC surface, P1 deals with the microbial community composition as a relevant microscale feature. Taking this into consideration, the following **research hypotheses for P1** were proposed**:**

- There is an adequate way to include biological degradation into a multi-component adsorption model for DOC removal.
- The implementation of a simplified microbial community is sufficient to predict the experimentally observed removal of DOC via adsorption and biodegradation.
- Such a model is able to provide interesting insights about the contribution of adsorption and biodegradation to the total DOC removal and the possible interactions between the two removal mechanisms.

Publication P2 studies a second biofilm system: a Moving Bed Biofilm Reactor (MBBR) for the treatment of municipal wastewater through a Partial Nitritation Anammox (PN/A) process. In P2 the microbial community composition was also the targeted microscale feature. The functional diversity of the heterotrophic community, the ecological adaptations they undergo under substrate-limited conditions and how a common kinetic model can reflect it, led to the **research hypotheses for P2**:

- Growth strategies that microbial communities undergo when faced with substrate-limited conditions modify the microbial community structure as well as the macro modelling results.
- The yield strategy plays an important role in the behavior of heterotrophic bacteria growing in fully autotrophic systems.
- The current modelling framework is able to reflect such ecological adaptations.

Finally, in publication P3 a Membrane Aerated Biofilm Reactor (MABR) used for the treatment of municipal wastewater through PN/A was analyzed. Dimensionality was in P3 the microscale feature of interest. The mismatch between the longitudinal heterogeneity observed experimentally in MABRs and the traditional modelling approaches that represent all phases, i.e. bulk liquid, biofilm and gas phase as homogeneous, brought me to the formulation of the **research hypotheses for P3:**

- In fully autotrophic MABRs, concentration gradients in the bulk liquid but especially in the gas phase have a significant impact on the biofilm micro features, especially on the community composition and thus on the global modelling results.
- A one-dimensional model is sufficient to conceptually evaluate the magnitude of these effects.

These three modelling exercises aim to highlight the effect that microscale features: microbial composition and dimensionality can have on macroscale or global modelling results. They also show how rather simple modelling approaches can be implemented to include relatively complex microscale features without sacrificing mechanistically meaning but rather strengthening it.

The present thesis is divided into two parts: Part I: Synopsis and Part II: Publications. The Synopsis presents the theoretical background and gives an overview of the fundamental concepts and terminology required for the understanding of this work. Likewise, it presents a general discussion that explores the relationship between the three publications and places them a more general modelling context. Finally, it draws some general conclusions from the results delivered by the three publications and proposes prospective future work. The second part contains the scientific publications that form the cumulative part of this dissertation as listed below:

Publication P1: Acevedo, V., Kaiser, T., Babist, R., Fundneider, T. and Lackner, S. (2021) A multi-component model for granular activated carbon filters combining biofilm and adsorption kinetics. Water Research 197, 117079.

Publication P2: Acevedo, V. and Lackner, S. (2022) Are K-strategists yield-strategists in disguise? An example from autotrophic nitrogen removal. Biotechnology and Bioengineering, 1–11

Publication P3: Acevedo, V. and Lackner, S. (2019) Membrane Aerated Biofilm Reactors – How longitudinal gradients influence nitrogen removal – A conceptual study. Water Research 166, 115060.

2. Background

2.1. What is a Biofilm?

Biofilms have been known since the 17th century when the Dutch scientist Antoni van Leeuwenhoek observed for the first time a microbial film growing on the surface of teeth, however only until lately this form of bacterial organization started being deeply investigated, due to the apparition of new optic and molecular techniques, which enabled a closer look. Biofilms are often defined as a group of microorganisms growing on a surface in a permanent manner and held together by a polysaccharide matrix (Flemming et al. 2016, Hall-Stoodley et al. 2004), the polysaccharides that form this matrix are known as Extracellular Polymer Substances (EPS) and are produced by the bacteria living within the biofilm. Although biofilms sustain the existence of millions of cells, bacteria take up only around 1 to 2% of the total biofilm volume, with water being the main constituent (Quan et al. 2021). Despite the dominant role that the water fraction has, the behavior of sessile bacteria i.e. bacteria growing in biofilms differs greatly from the behavior of those living in planktonic states. Studies have shown that bacteria living in biofilms have a specific phenotype in regard to velocity of growth and gene transcription. In addition they possess specialized mechanisms to attach/detach themselves onto/from surfaces and are able to form structured environments (Donlan 2002). Flemming et al. (2016) pointed out several biofilm properties specific to biofilm structures that are unlikely to occur under planktonic conditions. The presence of the EPS matrix fosters the formation of substrate gradients along the biofilm depth and thus the diversity of the community thanks to the formation of several metabolic niches. Alongside localized gradients, the EPS matrix confers the microorganisms' resistance/tolerance to antibiotics, acts as a sorbent for external nutrients and retains enzymes allowing external digestion. Social interactions as well as synergic relationships are also stimulated within biofilms. Figure 1 as taken from Flemming et al. (2016) is a graphical review of the properties mentioned above.

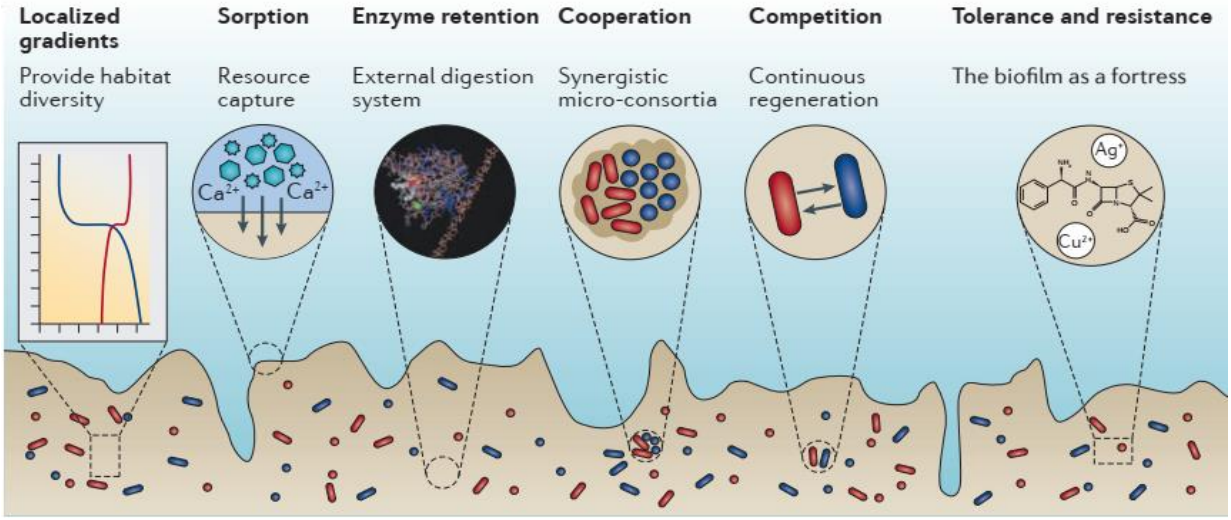

Figure 1. Schematic representation of the biofilm characteristics (Flemming et al. 2016).

2.2. Fundamentals of Biofilm Modelling

Biofilm models can be classified into different categories depending on the method used to solve the differential equation system that represents the processes occurring within the biofilm: pseudo analytical, analytical and numerical. Due to the high complexity of biofilms analytical solutions are only possible for very simplified versions of the systems, as consequence numerical methods are state of the art. Numerical models can be further classified into one-dimensional (1D) two-dimensional (2D) numerical and three-dimensional (3D) (Boltz et al. 2010). This chapter introduces the fundamental aspects common to all biofilm models and focuses on the 1D dynamic model as it is the most relevant to this study. A more comprehensive overview of other important biofilm models in the wastewater context can be found in the work of Wanner et al. (2006).

2.2.1. Model Phases

A biofilm model can be divided into three different phases: substratum, biofilm and bulk liquid, occasionally in specific applications a gas phase can also be included. Each of the phases is an independent compartment that interacts with others through an interface. The individual mass balances of each substance in each phase and the boundary conditions defined by the nature of the interfaces conform the differential equation system, which mathematically describes a biofilm process. Figure 2 shows a scheme of the basic phases that have to be taken into account in a basic biofilm model.

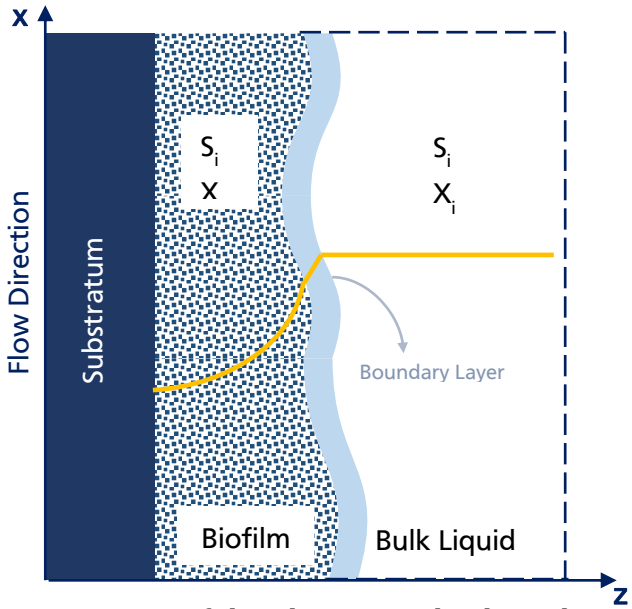

Figure 2. Schematic respresentation of the phases involved in a basic biofilm model. S_i represents the concentration of a dissolved substance i and X_i the concentration of a particulate substance i. The yellow line is the concentration gradient of s_i troughout the layers.

The substratum is the surface onto which biofilm attaches and grows. Depending on the specific application it can be seen as an impermeable or as a permeable boundary, likewise the substratum can be considered inert or reactive i.e. transformation processes take place in it. If

the substratum is impermeable and inert, there is no mass transport between it and the biofilm and the corresponding boundary condition is written as follows:

$$\frac{\partial S_i}{\partial z} = 0 \; ; \; \frac{\partial X_i}{\partial z} = 0 \qquad (1)$$

where S_i is the concentration of the dissolved substance i and X_i is the concentration of the particulate substance i; z represents the direction of biofilm growth

In the majority of the biofilm systems used for wastewater treatment the substratum belongs to this category. A prominent example of this are MBBRs. In such systems the carriers act solely as support for the biofilm and do not allow substance exchange beyond its limits. If the substratum is permeable or semi-permeable, the net flux of a given substance that crosses the substratum in any direction (from or to the biofilm) is different to 0 and should be modelled accordingly. MABRs are an example of a biofilm system with a semi-permeable substratum. In these systems the membrane serves as support of the biofilm and simultaneously allows the transport of air into the biofilm.

The biofilm is a porous matrix composed of a solid and a liquid phase. Bacteria and all other particulate substances are part of the solid phase whereas the liquid phase is a mixture of water and dissolved substances. The control volume for the mass balances is defined by the biofilm thickness, which, depending on the specific conditions, may be constant or variable. The easiest way to approach the modelling of a biofilm is to consider it homogenous and flat; however, the morphology of biofilms varies greatly and the decision of introducing more complexity in the model in terms of geometry and heterogeneity depends on the final aim of the study. 1D models account for heterogeneity along the biofilm thickness through the numerical discretization of the biofilm into different layers. In each layer, the concentration of particulate and dissolved substances is the same at any point in the space i.e. each layer is represented as a completely mixed reactor, the number of layers becomes then a key parameter in the modelling of the biofilm. An insufficient number of layers may result in modelling results that greatly deviate from experimental measurements, especially in multi-species biofilms (Boltz et al. 2011). Multi-dimensional models often offer a better representation of the biofilm morphology but are in turn more time and data intensive.

The liquid phase above the biofilm is known as the bulk liquid. The bulk liquid acts as supplier of nutrients and as receptor of the substances produced within the biofilm. The bulk liquid is mostly considered as a completely mixed reactor and is modelled accordingly. The bulk liquid can also exchange biomass with the biofilm through either attachment (fixation of planktonic biomass onto the biofilm) or detachment (separation of biomass from the biofilm). For reactors in which biomass has to be removed to control biofilm thickness or to avoid blockage, modelling approaches to detachment are of great importance and have to be adapted to each specific configuration. Depending on the quantity of biomass that is suspended in the bulk liquid, this phase can also be biologically active and in consequence the reactor can be regarded as a hybrid process.

In between biofilm surface and the bulk liquid is located the diffusion boundary layer (DBL). This layer is an either stationary or laminar flow region, where the mass transport from the

bulk liquid into the biofilm can only occur due the diffusional forces created by the concentration gradient across it. The DBL is contained in the hydrodynamic boundary layer (HBL), which is the region where a gradient in the flow velocity is observed due to the non-slip condition (flow velocity at a solid boundary is zero) (Bishop et al. 1997). Both boundary layers are closely related and the effective transport occurring within the DBL is highly correlated to the flow regime and thus to the HBL. Turbulent regimes foster the mass transfer and lead to a reduction in the concentration gradient, on the contrary low velocity flow increases the difference in the concentration between biofilm and bulk liquid (Boltz et al. 2011). The diffusive transport that takes place within the DBL can be represented trough the flux expression in equation (2)(Stewart 2012):

$$J = k_L(S_{BL} - S_{BF})\ ;\ k_L = \frac{D}{L_{DBL}} \qquad (2)$$

Where J is the flux of a substance trough the DBL, k_L is the mass transfer coefficient composed of D: diffusion coefficient and L_{DBL}: the DBL thickness. S_{BL} is the concentration at the bulk liquid and S_{BF} the concentration at the biofilm surface.

The thickness of the boundary layer is one of the most influential parameters in biofilm systems and a proper description of the gradients within the boundary layer is of vital importance to obtain good modelling results. At low flow velocities, the DBL can be assumed to be parallel to the substratum. In contrast, at high flow velocities the DBL adopts the biofilm geometry. Although, the simplification that the mass transport resistances are concentrated exclusively in the DBL delivers satisfactory modelling results, in cases of intermediate flow regimes and complex biofilm structures, it does not suffice. In such instances the convection might play an important role in the mass transfer and therefore the calculation of the velocity flow filed in the bulk face is essential (Picioreanu et al. 1999).

2.2.2. Model Scales

Although the global modelling results of a system are the product of the interactions of all phases, generally a differentiation between macro and microscale results is made. On the one hand the results related to the bulk liquid and to the system as a whole are known as macroscale results. On the other hand, the modelling outcomes associated to the biofilm, its morphology and its spatial organization are known as microscale results. Macroscale results typically comprise biomass accumulation, biomass loss and removal/ production rates referred to the complete system. These results come from a global mass balance between influent and effluent and can be easily compared to experimental measurements, additionally production/removal rates are a key parameter for reactor design. In many applications only macroscale results are relevant or even measurable and therefore microscale results are subordinate to them. Frequently certain levels of inaccuracy of the microscale results are accepted as trade-off for obtaining good macroscale results. Lewandowski and Boltz (2011) and Eberl and Wade (2020) recognize the antagonism between macro and microscale results and the challenges that the current modelling practice faces to reconcile them. The appearance of new techniques and methods that allow the closer exploration of the microscale features often expose disparities between the experimental microscale measurements and the microscale results delivered by the models. It

is generally accepted that in a sufficiently big system divergences in the microscale do not greatly affect the macroscale results and thus such divergences can be allowed. Nevertheless, the question whether such deviations constrain the explanatory power of the models and the possibilities to investigate complex theoretical scenarios still remains. The decision about the level of complexity and the desired accuracy of the microscale results is intertwined with the dimensionality of the model, its objectives, the experimental set-up and the available computational power.

Time plays also an important role in the modelling of biofilm systems. The traditional differentiation between steady-state and dynamic model is also applied in this context, however due to the various processes that occur within a biofilm reactor and the disparity between their dynamics can lead to virtually mixed states. Processes related to the biofilm (growth, decay, attachment, detachment) have characteristic times that range between 10^5 and 10^7 seconds. In contrast, mass transport processes such as convection and diffusion range between 10^{-3} and 10 seconds (Picioreanu et al. 2000). In practice, this means that during the same period of time the bulk liquid concentrations may undergo changes and recover while the biofilm structure, e.g. biofilm thickness, remains the same. In this case, it could be assumed a steady-state condition for the biofilm phase and dynamic conditions for the bulk liquid. Systems of differential equations that have such an imbalance in the dynamics of the components are known as stiff systems. In order to avoid instability in the calculation of results, special numerical methods are required. All current software uses numerical solvers capable of dealing with this kind of differential systems, nevertheless the simulation of very complex systems may still be subject of instability, inconsistencies and special care needs to be taken to assure that the results adequately represent the reality.

2.2.3. The One-Dimensional Dynamic Model

The 1D dynamic model can be regarded as the most sophisticated amongst the low dimensionality models. As its name indicates it represents the system in one dimension, this one dimension being the biofilm thickness, under the assumption the steepest concentration gradients occur in this direction and that the biomass in the biofilm can be assumed as a continuum. Such a model allows the user to include as many substances (dissolved or particulate) and as many bacterial species as the modelling task requires. The model does not define the nature of the transformation processes, which makes it very flexible and easy to adapt to numerous microbial kinetics. It most conventional formulation is implemented in the software AQUASIM (Reichert 1994). The present chapter explains the fundamentals of this model based on the 1D multi-species model first published by Wanner and Gujer (1986).

Modelling a biofilm requires the inclusion of three parameters related to the volume occupied by the biofilm: biomass density (ρ_i), volume fraction (f_i) (each specific to a given microbial species) and the biomass displacement velocity with respect to the substratum (u). The biomass flux (g_i) can be written using these three parameters as shown in equation (3)

$$g_i(t,z) = u(t,z)\rho_i f_i(t,z) \qquad (3)$$

where t is the time and z the biofilm thickness.

The mass balance for each of the microbial species also needs to be expressed in terms of these parameters as seen in equation (4)

$$\frac{\partial f_i}{\partial t} = \mu_{net,i} f_i - \frac{1}{\rho_i}\frac{\partial g_i}{\partial z} \qquad (4)$$

where $\mu_{net,i}$ is the net/observed specific growth rate of a microbial species i.

In order to determine *u*, the definition of flux g_i from equation (3) has to be integrated into the mass balance presented in equation (4). Considering that *u* is a parameter that describes the behavior of the entire biomass, the summation of the mass balance of each microbial species *i* has to be made. Conducting these operations and rearranging terms equation (5) arises:

$$\sum_{i=0}^{n}\frac{\partial f_i}{\partial t} = \sum_{i=0}^{n}\mu_{net,i} f_i - \frac{\partial u}{\partial z}\sum_{i=0}^{n} f_i - \sum_{i=0}^{n}\frac{\partial f_i}{\partial z} \qquad (5)$$

where n is the total number of microbial species in the system.

Two further definitions need to be implemented for the model to be complete. Equation (6) shows that the sum of all the volumetric fractions should be equal to 1, as expected. Equation (7) defines the net growth rate of the total biomass $\overline{\mu_{net}}$ as the weighted average of the specific net growth rates in relation to the volumetric fraction; the value of $\overline{\mu_{net}}$ depends on the time and on the location (z) along the biofilm thickness.

$$\sum_{i=0}^{n} f_i \overset{\text{def}}{=} \sum_{i=0}^{n}\frac{V_i}{V} = 1 \qquad (6)$$

$$\overline{\mu_{net}}(t,z) \overset{\text{def}}{=} \sum_{i=0}^{n}\mu_{net,i}(t,z)\, f_i(t,z) \qquad (7)$$

If we assume that the volumetric fraction (f_i) remains constant with time and along the biofilm thickness and thus $\partial f_i/\partial t$ and $\partial f_i/\partial z$ are zero the substitution of equations (6) and (7) in equation (5) gives the change of the velocity of biomass displacement along the biofilm thickness. Equation (8) presents its differential form as well as the result of the integration over the biofilm thickness i.e. from z=0 to z=L_f.

$$\frac{\partial u(t,z)}{\partial z} = \overline{\mu_{net}} \quad \text{integrating it becomes} \quad u(t,z) = \int_0^{L_f}\overline{\mu_{net}}\,(t,z)dz \qquad (8)$$

When the integral for *u* described in equation (8) is evaluated at the substratum-biofilm interface (z=0) and considering an impermeable substratum, equation (1) holds, and the velocity *u* must be equal to zero. In the case of the biofilm-bulk liquid interface (z=L_f) a term that accounts for the biomass exchange velocity (σ) between bulk liquid and biofilm is required. In this way equation (8) becomes equation (9) at the bulk liquid biofilm interface.

$$u(t,L_f) = \int_0^{L_f}\overline{\mu_{net}}\,(t,z)dz + \sigma(t) \qquad (9)$$

Analogously to the case of microbial species, a mass balance has to be written for all the substances in the system. The mass balance includes a term representing the production/consumption rate of any substance i (r_i) and a term that describes the flux of substance from or into the system (j_i). Equation (10) summarizes the mass balances of a dissolved substance S_i.

$$\frac{\partial S_i(t,z)}{\partial t} = r_i(t,z) - \frac{\partial j_i(t,z)}{\partial z} \qquad (10)$$

The first Fick's law states that the flux of a substance is proportional to a concentration gradient and that both are related through a proportionality constant, in this case the specific diffusivity of the substance in a given fluid (D_i). This law can be used to express the substance flux between biofilm and bulk liquid. Equation (11) shows its mathematical expression.

$$j_i(t,z) = -D_i \frac{\partial S_i(t,z)}{\partial z} \qquad (11)$$

As already mentioned in section 2.2.1, 1D models have to account for a mass transfer boundary layer to be able to properly represent the concentration gradient that occurs between the fully mixed bulk liquid and the biofilm surface ($z=L_f$). The mass transfer boundary layer constitutes the first spatial boundary condition of the mass balance presented in equation (10). Equation (12) mathematically describes this external mass transfer resistance.

$$\frac{\partial S_i(t,L_f)}{\partial z} = \frac{D_{BL,i}}{L_{BL} D_i}\left(S_i(t,BL) - S_i(t,L)\right) \qquad (12)$$

where L_{BL} is the thickness of the mass transfer boundary layer, BL indicates the location of the boundary layer and $D_{BL,L}$ the diffusivity of a substance i at the boundary layer.

The second boundary condition is evaluated at the substratum-biofilm interface (z=0) and here equation (1) holds and the flux j_i equals zero at that location.

The consumption/production rate (r_i) is left open so the model remains flexible and can be adapted according to the requirements of each specific system. Typically, this rate is coupled to the microbial growth rate of a species that uses the substance as substrate or produces it as part of its metabolism. Stoichiometric coefficients such as the yield relate the growth kinesics with the production/consumption rate of each substance S_i.

2.2.4. Biokinetic Model: Activated Sludge Model

In addition to the description of the physical processes in a system, a model for the representation of the biochemical processes that occur within the biofilm, e.g. biomass growth, substrate consumption etc., is also required. In the wastewater modelling practice, the Activated Sludge Models (ASM) are widely accepted and applied, as it was the case of the publications that conform this work.

ASMs were developed in the late 80s by a special task group of the international water association. The main objective was to find the simplest model able to predict in a satisfactory manner the performance of activated sludge systems where organic matter oxidation, nitrification and denitrification take place. For this purpose, COD was selected as the adequate parameter to quantify organic matter in the models. A fractionation of the COD was proposed depending

on its solubility and biodegradability, likewise a fractionation of the nitrogenous matter was also introduced. The bacterial community present in the activated sludge was initially divided into autotrophic nitrifying and heterotrophic biomass, aiming to match the biological processes of interest. Additionally, a series of transformation processes where considered: biomass growth and decay, hydrolysis of organic matter and ammonification of organic nitrogen. Each process represents a biochemical reaction and relates trough stoichiometric coefficients the concentration of reactants and products that take part in the reaction. As well, a kinetic expression is assigned to every process. One characteristic of the ASMs is the matrix notation used for summarizing the information contained in the model. This representation form is composed by two main elements: a stoichiometric matrix and accompanying rate vector. The components/substances are listed in the matrix columns whereas the transformation processes in the rows, and the matrix cells are then filled with the corresponding stoichiometric parameters. The rate vector has the same number of rows as the matrix and lists the kinetic expressions of the transformation processes. The ASM1 is the first and simplest model of the ASM family, it was characterized by a one-step nitrification and denitrification reactions and a first order kinetics decay. After the publication of the ASM1, several modifications / new models have appeared with the aim of extending the biological processes or improving the representation of the existing ones. The ASM2 model introduced biological phosphor removal while in the ASM3 model the decay concept was replaced with the endogenous respiration one, to take advantage of the newest knowledge about storage substances and its role in the microbial metabolism (Henze et al. 2006).

The ASM framework achieved not only the completion of comprehensive models, but it also created a common platform for all the users to extend or to adapt the existing models depending on the specific system needs. Despite ASMs successful implementation and the application of the basic concepts in new models, some drawbacks have been also recognized. The fundamental mechanisms of the transformation processes are not completely understood and the processes descriptions included in the models correspond rather to the assumptions and simplifications made in order to obtain a good fit between the predictions and the observed data. This leads to a lost in the explanatory power of the models and might be detrimental for the extrapolation of the model to less conventional applications (Hauduc et al. 2013). Other authors also argue that with a growing number of biochemical processes to be considered, the complexity of extending and calibrating the models increases and additional supporting tools and/or fundamental changes in the model structure may be needed (Sin and Al 2021).

2.3. Biological Processes

This section shortly presents the biological processes relevant to this work. The focus lays on two processes: Nitrogen removal trough Partial Nitrogen/Anammox (PN/A) including denitrification sustained by organic substances produced by decay processes within the biofilm, and DOC removal in bGAC-filters for the treatment of WWTP effluents.

2.3.1. Partial Nitritation/ Anammox

PN/A exploits two metabolic pathways of the nitrogen cycle. The partial oxidation of NH_4^+ until NO_2^- and the further reduction of NO_2^- to dinitrogen gas using NH_4^+ as electron donor.

For the first part Ammonium Oxidizer Bacteria (AOB) are responsible while Anaerobic Oxidizing Bacteria (AnAOB) also known as Anammox are in charge of the second part.

The implementation of PN/A processes in a biofilm-based configuration requires the simultaneous existence of aerobic and anoxic zones within the biofilm. In an aerobic zone oxygen is available as free molecule, whereas an anoxic zone oxygen is present bound in a compound such as NO_2^- and/or NO_3^- . To achieve the coexistence of both aerobic and anoxic zones, the oxygen penetration depth must be carefully controlled trough a regulated air supply.

A major challenge of single stage PN/A systems is the suppression of Nitrate Oxidizing Bacteria (NOB). NOB utilize oxygen as electron donor to oxidize NO_2^- to NO_3^-, competing with AOB over oxygen and with AnAOB over NO_2^- . An imbalance in the amount of NOB with respect to the other microbial groups may result in the failure of the system, therefore it is vital to repress their growth. Two main strategies are accepted to control NOB growth: adjustment of SRT and restriction of the dissolved oxygen concentration. In biofilm systems, it is unfeasible to use the STR as NOB control strategy due to near to complete biomass retention onto the carrier. Nevertheless, substrate gradients within biofilmd make the DO control strategy a suitable approach for NOB suppression. Adequate DO concentrations can be obtained either by assuring low DO concentration in the bulk phase i.e. real time DO controlling or through intermittent aeration coupled with NH_4^+ availability (Regmi et al. 2014, Wang et al. 2019). Low DO levels are the only way to create anoxic zones in which AnAOB can survive avoiding reversible inhibition by the DO. Free ammonia (FA) and free nitrous acid (FNA) inhibition is also recognized as a successful strategy for NOB suppression. It is known that once the FA and FNA concentrations surpass a given threshold 0.08–0.82 mg /l for FA and 0.06–0.83 mg /l in the case of FNA, the growth of NOB slows down whereas the growth of AOB remains practically unaffected (Cao et al. 2017). Such FA and FNA concentrations can be easily attained under side stream conditions due to the high ammonia concentrations that the wastewater from the dewatering process has, however under mainstream conditions the use of FA/FNA NOB control strategy is less viable due to the low ammonia concentrations present in the municipal wastewater.

Alongside NOB suppression, maintenance of suitable conditions for AnAOB is another critical factor for a PN/A system to work properly. The main obstacles are inhibition caused by dissolved oxygen and NO_2^- and the potential biomass washout caused by the characteristic long doubling time of AnAOB (7-14 d) (Strous et al. 1998). These restrictions are dealt with by taking advantage of two special features of biofilm systems: the substrate gradients that are formed along the biofilm thickness and the virtually infinite SRT. These features allow biofilms to support microorganism within a wide range of growth rates, both slow growing (AnAOB) and fast growing microorganism (NOB, AOB) have a chance to survive (Lackner et al. 2014).

Although PN/A are considered fully autotrophic processes, the presence of heterotrophic bacteria subsisting on solely the decay products and the organic compounds produced by the autotrophic community has been reported (Agrawal et al. 2017, Persson et al. 2017). Therefore denitrification processes play an important role in the total dissolved nitrogen removal observed in PN/A systems. In biofilm systems, depending on their configuration (co and counter-

diffusion) the heterotrophic community can affect the system's performance differently (Lackner et al. 2008b). Denitrification is a sequential process in which NO_3^- is stepwise reduced until N_2, as showed in equation (13). Each of these steps is mediated by a specific enzyme and requires the presence of an electron donor, typically organic matter but not exclusively.

$$NO_3^- \rightarrow NO_2^- \rightarrow NO \rightarrow N_2O \rightarrow N_2 \qquad (13)$$

Denitrifying bacteria are classified in different groups according to their functional capabilities. Bacteria that have the complete set of enzymes and thus are able to fully reduce NO_3^- to N_2 are known as canonical denitrifiers whereas microorganisms that can only carried out the reduction from NO_2^- to N_2 are known as partial denitrifiers. Some bacteria have truncated reduction paths and reduce NO_3^-/ NO_2^- only until nitrogen oxides NO/N_2O, such organisms are referred as incomplete denitrifiers. Finally bacteria capable of reducing the NO and N_2O to N_2 are grouped as nitrogen oxide reducers(Lu et al. 2014). Understanding the functional diversity of the denitrifier community is of vital importance in PN/A processes, due to the role it plays as either sink or source of N_2O emissions, the competition for electron acceptors (O_2, NO_2^-) with other bacterial groups (AOB and AnAOB) and the competition for space in the case of biofilm.

2.3.2. Removal of Residual DOC

WWTP effluents contain residual DOC that cannot be biologically removed during the conventional treatment, but that can be potentially biodegraded in advanced treatment systems such as bGAC-filters (Fundneider et al. 2021, Simpson 2008) or even in the receiving water bodies. The degree at which such residual DOC can be used by microorganisms varies depending on its quality i.e. its bioavailability and its energy content (Eiler et al. 2003). DOC in WWTP effluents is a highly heterogeneous mixture of different organic compounds and thus its characterization can be challenging. As consequence the determination of DOC biodegradability and the involved metabolic pathways is not trivial. Wang et al. (2014) quantified the biodegradability of the several WWTP effluents (using a dark 5 days bioassay) and concluded that only 20-30% of the DOC was biodegradable. Additionally, they found a strong correlation between the molecular weight of the DOC fraction and its biodegradability.

Although direct heterotrophic activity, i.e. consumption of organic matter as electron donor and conversion of DOC into biomass, is the most common metabolic pathway for biological DOC removal, several experiments have shown that the co-metabolic transformation of DOC, especially of organic micropollutants (OMP), can be relevant in the wastewater context. During co-metabolic processes DOC is transformed alongside the main metabolism of the microorganism, and can thereby be modified or completely biodegraded (Fetzner 2011). In contrast to the case where DOC is used in the main metabolism, in co-metabolism DOC does not serve either as energy or carbon source. Both heterotrophic and autotrophic co-metabolism processes have been observed. Helbling et al. (2012), Rattier et al. (2014) and Margot et al. (2015) found that some OMPs, such as acetaminophen and naproxen seem to be removed by AOB via co-metabolism, whereas other OMPs like paracetamol, gabapentin, diclofenac are rather related to the denitrification co-metabolism activity.

2.4. Biofilm Processes in Wastewater Treatment

The fundamental principle of biological water treatment is the accumulation of active biomass within the system and its retention during a sufficiently long period. In order to avoid biomass washout, it has to be assured that the amount of produced biomass is at equilibrium with the amount wasted from the system. To achieve the required Sludge Retention Time (SRT), processes that use suspended biomass rely mainly upon the recirculation of a portion of the produced sludge, while the remaining part of the biomass is taken out and further treated. In contrast to suspended sludge systems, biofilm systems have the advantage of achieving biomass retention due to the irreversible attachment of the biomass to a surface, this permanent attachment makes biofilm systems independent from separation processes downstream, in contrast to most the suspended sludge counterparts. Biomass concentrations of approximately 10–60 gVSS/L can be achieved in biofilm systems whereas in suspended sludge systems concentrations of 3-8 gVSS/L are to be expected (Lewandowski and Boltz 2011). High biomass concentrations result in smaller reactor volumes but also can lead to mass transfer limitations for the transport of substrate and nutrients from the bulk phase into the different biofilm layers. This dichotomy is central to biofilm applications and might be decisive for some operational aspects depending on each specific system. Traditionally, biofilm systems are preferred for the treatment of effluents with high volumetric flows but low concentrations of the substance of interest. Under such conditions the ability to retain biomass within the system becomes valuable in comparison to suspended sludge processes (Van Loosdrecht and Heijnen 1993).

Depending on the way the biofilm is brought into the reactor different system configurations can been used. Decisive is, whether the biofilm grows in a fixed or mobile carrier. On the one hand, in fixed bed reactors the biofilm grows onto an immobile carrier within the reactor and the influent flows through the bed. This flow configuration may cause the appearance of longitudinal concentration profiles along the bed as the reactor acts as a plug-flow. On the other hand, in fluidized bed reactors the mobile carrier material (and the biofilm) are fully mixed in the reactor (Rittmann 1982). Fluidized bed reactors often achieve fully mixed conditions and can be regarded as continued stirred tank reactors (CSTR). Due to this high degree of mixing fluidized bed reactors are believed to have higher mass and heat transfer rates between the bulk liquid and the biofilm (Wang and Zhong 2007).

Ticking filters are one of the first known applications of biofilm-based processes, they dominated the German wastewater practice from the late 19th century onwards before activated sludge systems came and replaced them around 1950 (Seeger 1999). Over the years, new technologies arose and improved various features such as biofilm surface area, mixing conditions etc. In the late 1980s there was as breakthrough with the emergence of the Moving Bed Biofilm Reactor (MBBR) concept, a process that takes the best of both biofilm-based and suspended sludge system. Section 2.4.1 is dedicated entirely to this process. Lately hybrid systems, referred as integrated fixed-film activated sludge (IFAS), that combine suspended sludge and a biofilm have been gaining importance. Normally, IFAS systems use a fixed or mobile biofilm carrier to augment the treatment capacity of an activated sludge system and have the advantage of leveraging existing resources. The simultaneous presence of biofilm and suspended sludge

separates the reactor into two different environments, which may be advantageous for the subsistence of all the microbial groups required to efficiently perform nutrient (Boltz et al. 2009).

Granular sludge can be also considered as a biofilm system due to the heterogeneous biomass distribution observed in the granules and the diffusion limited mass transport (Hubaux et al. 2015). Traditionally granular sludge is encountered in anaerobic processes such as digesters and up flow anaerobic sludge bed reactors, however full scale applications of aerobic granular systems have been also successfully developed (Campos et al. 2017). Aerobic granular systems have been applied for nutrient removal of municipal wastewater and PN/A for the treatment of effluents generated during the sludge dewatering (Boltz et al. 2017).

This chapter addresses only the three biofilm systems of interest for this work: MBBR, Membrane Aerated Biofilm Reactors (MABR) and biologically active filters. Each section focuses on a specific system and its application, likewise the most significant modelling aspects are also explored.

2.4.1. The Moving Bed Biofilm Reactor (MBBR)

A Moving Bed Biofilm Reactor is a reactor configuration in which biomass grows attached to mobile carriers that move freely within the reactor and are kept within the system by built-in retention structures. The mobile carriers are designed to enhance biomass retention, provide larger specific surface areas for growth, prevent clogging and backwashing (Ødegaard 2006). Various mobile carrier types have been developed since the apparition of MBBRs, the carries differ in specific area, geometry, dimensions (height, diameter) and maximal achievable biofilm thickness. The presence of carriers leads to a high biomass density (biomass per unit reactor volume) within the system. In addition the use of carriers makes the system very compact with high conversion rates allowing so the system to have low hydraulic retention times and to be space-saving (Revilla et al. 2016).

Aerobic and anoxic/anaerobic processes can be implemented in MBBRs. In the case of aerobic processes, the delivered air aids the mixing and simultaneously supplies the biofilm with oxygen. In the case of anoxic/ anaerobic processes mechanical mixing is required.

MBBRs are normally modelled as CSTR i.e. the concentration of any compound can be considered the same in any location of the reactor as well as in the reactor's outlet. This assumption also implies that all carriers behave the same and that an equivalent biofilm that grows onto all of them. Regularly, zero-dimensional (diffusion-free) and 1D models are preferred and used more often for engineering purposes. As explained in chapter 2.2.3, 1D models assume that the biofilm has a homogenous structure parallel to the substratum, but in contrast it shows gradients transversal to the substratum. As a consequence, concentration gradients are neglected in the parallel direction but considered as dominating in the perpendicular one. If the substratum is inert, as is the case of MBBR's carriers, this corresponds to a so called co-diffusional biofilm and the concentration profiles along the biofilm thickness look like the ones depicted in Figure 2.

To account for the biofilm heterogeneity perpendicular to the substratum, the biofilm is divided into various layers and each of those are treated as a CSTR. The biofilm that grows on the

carriers is represented through a singular surface that has an area equivalent to the total area of all the carriers with the reactor, and that holds the same amount of biomass that all the carriers (Barry et al. 2012). The simplest modelling approach of an MBBR corresponds then more or less to the trivial application of the 1D biofilm model. To investigate operational features of MBBRs such aeration configuration, filling ratio (carrier volume in relation to total volume) and mixing more elaborated models are required as for instance computational fluid dynamic simulations coupled with biokinetic models (Wang et al. 2021).

2.4.2. The Membrane Aerated Biofilm Reactor (MABR)

MABRs differentiate themselves from other biofilm reactors in their substratum. MABRs do not use a conventional substratum but instead they have a semi-permeable membrane that acts as biofilm support and simultaneously supplies oxygen/air through it. As consequence, at the membrane-biofilm interface, diffusive mass transfer takes place. While the electron acceptor (oxygen) diffuses in the direction of the biofilm surface, the electron donor (e.g. NH_4^+, COD etc.) is in turn supplied via the bulk liquid and diffuses in the opposite direction i.e. from the biofilm surface to its base. This particular configuration of the concentration gradients is known as counter-diffusion and is responsible for the MABR's main features: singular microbial community organization, mass transport limitations at high biofilm thickness and profiting of the boundary layer, due to the resistance to the mass transport imposed by the boundary layer to the substrate supplied by the membrane (Nerenberg 2016). Figure 3 is a scheme of the phases and concentration profiles in a counter-diffusional biofilm e.g. an MABR. It is noticeable that in contrast to a co-diffusional biofilm a fourth phase: the gas phase is added to the biofilm system and that the substratum acts as a semi-permeable membrane. These features are key when modelling an MABR and must be added to the traditional 1D model to properly describe a counter-diffusional biofilm. Due to counter-diffusion the zones of the biofilm with the highest activity expand from the surface (in the case of co-diffusional biofilms) to the whole biofilm thickness, thereby creating a particular microbial community structure. Several activity niches are formed along the biofilm thickness enabling the growth of different bacterial groups at different locations of the biofilm. One of the most interesting applications that profit from such a microbial structure is the simultaneous nitrogen and COD removal. In such an MABR, at the biofilm base, oxygen concentration is the highest whereas COD concentration is the lowest, which gives nitrifying bacteria an advantage to develop. At the biofilm base both oxygen and ammonia are available for nitrifying bacteria but the competition over oxygen with heterotrophic bacteria is less due to the COD scarcity. The distribution of the substrates along the biofilm thickness brings the heterotrophic bacteria to grow in the layers near to the biofilm surface, protecting the bacteria that grow in the inner layers (nitirifiers) from shear and chemical stress (Martin and Nerenberg 2012). Likewise, the stratification of the biofilm can be beneficial for the implementation of PN/A processes. Nitrifying bacteria can grow in the inner (aerobic) zone of the biofilm and produce NO_2^- for AnAOB to reduce it in presence of NH_4^+. At the same time, AnAOB can grow in the outer part of the biofilm where oxygen concentration does not reach inhibitory levels and NH_4^+ concentration is the highest. Various studies have experimentally verified the capacity of MABR system to support PN/A processes (Bunse et al. 2020, Gilmore et al. 2012), however two shortcomings still need to be addressed: the

accumulation of NOB in the inner biofilm layers that may prove difficult to reverse and the over exposition to shear and chemical stress that AnAOB may face on the biofilm surface.

In counter-diffusional biofilms, the biofilm thickness has a different effect on the substrate-fluxes than the one it has on conventional co-diffusional biofilms. At the beginning an increase in the biofilm thickness stimulates the mass transport from the membrane lumen and the bulk liquid into the biofilm due to higher microbial activity. However, after a certain thickness is reached, the activity in both outer and inner biofilm layers decreases due to limitation of the substrate that is supplied from the other side of the biofilm. In order to maintain the activity at an appropriate level the biofilm thickness should be carefully dealt with. Another difference from conventional biofilms is the role that the mass transfer-boundary layer plays in the system. Normally, as the biofilm thickness increases the boundary layer excerpts a greater resistance against the substrate transfer from the bulk liquid. In an MABR, however, the boundary layer may help to retain substrate supplied by the membrane within the biofilm. Under substrate non-limiting conditions in the bulk liquid the boundary layer might benefit the biofilm activity (Nerenberg 2016).

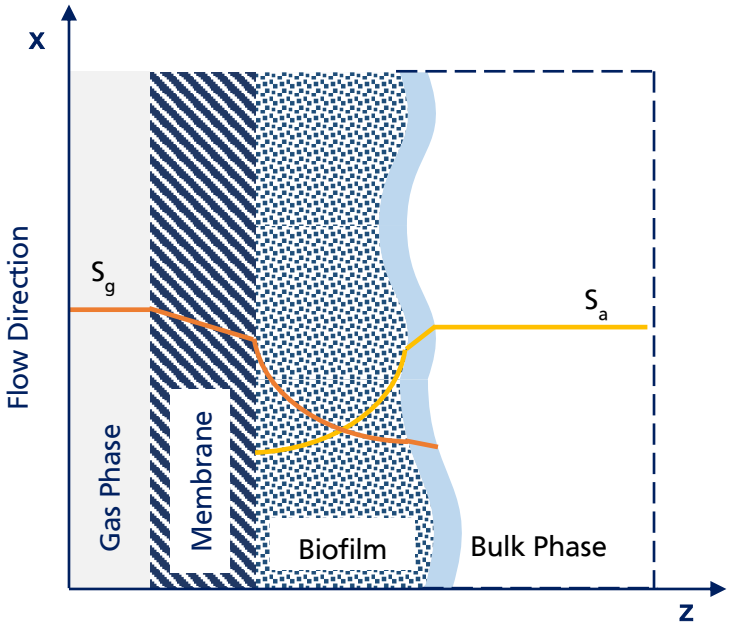

Figure 3. Schematic representation of the model phases and the concentration profiles in the z-direction (biofilm thickness) for a counter-diffusional biofilm.

The existence of an additional phase in the system, in this case a gas phase, requires also a further modelling formulation. At the interface between the gas and the membrane lumen a thin film is formed analogous to the mass transfer boundary layer at the biofilm-bulk liquid interface. However, the mass transfer resistance exerted by this gas-film can be neglected. The transfer of the oxygen/air through the membrane is driven by a concentration gradient across the membrane, the flux generated by this gradient can be mathematically described as in equation (14).

$$J_{O2} = HS_{MG}K_M\left(\frac{p}{H} - S_{O2,M}\right) \; ; \; S_{MG}K_M = \frac{P}{t_M} \qquad (14)$$

where J_{O2} is the oxygen flux through the membrane, H is the Henry coefficient, SMG is the gas/membrane partition coefficient, p is the partial pressure of the gas, $S_{O2,M}$ is oxygen concentration at the membrane-biofilm interface, P is the membrane permeability and t_M the membrane thickness

As equation (14) shows, the resistance is defined mostly by the physical properties specific to the membrane. On the other hand, the concentration gradient is greatly influenced by the presence of the biofilm on top of the membrane (Pellicer-Nàcher et al. 2013). Due to oxygen consumption by anaerobic microbial processes within the biofilm, oxygen concentration at the membrane-biofilm interface ($S_{O2,M}$) is lower than in the case of a clean membrane (without biofilm); this low concentration enlarges the gradient and ultimately the oxygen transfer profits from it (Martin and Nerenberg 2012).

2.4.3. Biologically Active Filters

Biologically active filters (BAF) are central to the drinking water treatment (Basu et al. 2016) and have become more relevant for the wastewater treatment, especially for the removal of micropollutants(Zhang et al. 2017). The term biologically active filter is typically understood as fixed bed of a carrier material on which a biofilm is able to grow. Sand, plastic media, granular active carbon (GAC), anthracite amongst other are normally used as filter media. BAFs are used in several applications ranging from removal of natural organic matter (NOM), sulfates, NO_3^-, iron ions and recently OMP (Zhu et al. 2010). In most of the applications the media can be regarded as inert and does not play any role in the treatment other than supporting the biofilm. GAC however, is a noticeable exception of this. This section focuses exclusively on the biologically active filters using GAC as supporting media also known as bGAC-filters.

In contrast to other filter media, GAC has the ability of binding numerous substances onto its surface and thereby contributing to their removal. The exceptional adsorption capacity of GAC is of greater interest in many applications than its ability to support biological growth. Normally the adsorption performance of the GAC is prioritized over the biofilm establishment. A long operation time leads to GAC saturation, however biofilm profits from it by adapting itself to the environmental conditions and in doing so, getting more specialized. Despite this apparent contradiction, synergies between the biological and adsorptive removal have been observed. Many authors have found that the presence of a biofilm within GAC-filters may help to extend the life span of the GAC. Biodegradation of NOM is one of the mechanisms responsible for the positive effect that the biofilm has on the adsorptive removal. NOM tends to block the pores of the GAC and in consequence hinders the removal of other compounds such as OMP. When a biofilm is present on the GAC surface, it degrades a part of the NOM decreasing the blockage of the pores and prolonging the duration of the GAC. Alongside the enhanced performance, the simultaneous occurrence of biological and adsorptive removal increases the system robustness and improves its response to fluctuations in the influent (Ross et al. 2019). Biofilm growth on the GAC surfaces presents some disadvantages such as the accumulation of biomass that may eventually clog the filter bed generating a high pressure drop along it. In addition, the release of pathogens into the effluent, negative competition with adsorption for

specific compounds and enhanced transfer of antibiotic resistance genes cannot be excluded (Olmstead and Weber 1991, Zhu et al. 2020).

Biofilm and GAC interact on the microscale in various manners that are still only partially understood. It has been theorized that the synergetic effect between biodegradation and adsorption relies substantially on bioregeneration. Two possible mechanisms to explain bioregenation have been suggested, the first one proposes that the substances adsorbed on the GAC surface are degraded by the action of exoenzymes originating in the biofilm. The products of this degradation are believed to become available for the microorganism for biodegradation. A part of the biodegradation products can again be readsorbed onto the GAC. The second theory states that once a critical biodegradation rate is reached the concentration gradients may get reversed and the mass transport would occur in the opposite direction i.e. from the GAC into the biofilm and desorption may take place. In this way some of the desorbed substance may become available for the biofilm (Sirotkin et al. 2001).

Removal in bGAC-filters is a dynamic process that is believed to be divided into three stages. In the first stage adsorption on the GAC surface is fully responsible for the DOC removal in the system, whereas biodegradation does not play a substantial role in the removal. In this early stage the biofilm establishes itself on the GAC and thus the DOC removed via biodegradation is still negligible. Once the biofilm is fully established the second phase begins, where biodegradation and adsorption occur in parallel. In this stage the GAC saturation starts happening. Finally, in the third stage the effect of adsorption is very little due to the high saturation degree of the GAC and so the biological removal dominates. Figure 4 presents a theoretical DOC removal curve over time, and indicates the three removal stages and the contribution of adsorption and biodegradation in each stage. The yellow line indicates the adsorptive DOC removal whereas the black line represents the biological DOC removal. Figure 4 also shows that in water treatment applications, there is a fraction of the DOC that cannot be removed, neither by adsorption nor by biodegradation (orange arrow) and it sets a limit to the maximum achievable removal. This description of removal development in a bGAC filter over the time is a very simplified one and intends only to explain the macroscale observations.

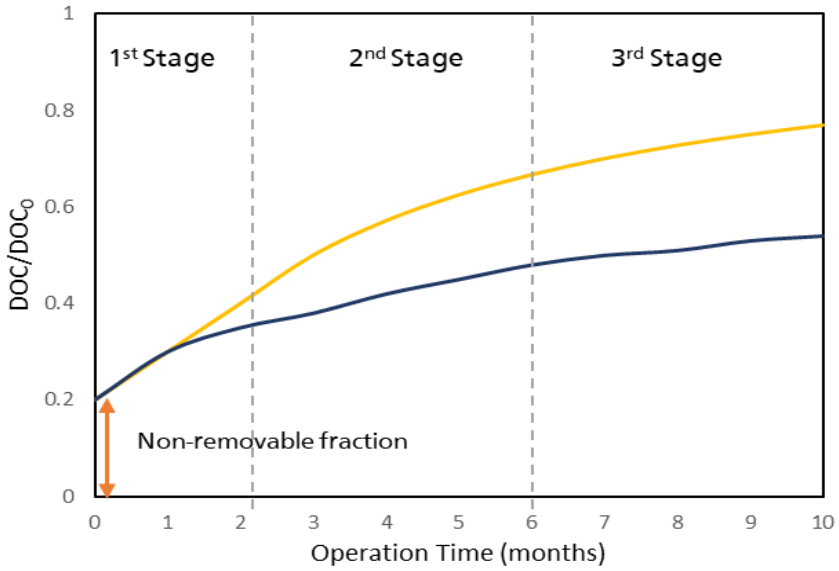

Figure 4. Schematic representation of the DOC removal in a bGAC-filter. Adapted from (Simpson 2008).

Modelling a bGAC-filter implies the combination of a biofilm and an adsorption model. Adsorption is an equilibrium process where individual states depend on the pair adsorbent (GAC)/ adsorbate (DOC) and the environmental conditions of the systems such as temperature, pH etc. Typically, these equilibrium states are studied at a constant temperature and describe through mathematical expressions known as adsorption isotherms. Isotherms illustrate the equilibrium relationship between the concentration of the adsorbate in the fluid phase (c_{eq}) and the amount of it on the adsorbent surface, also known as load (q_{eq}). A general expression of an adsorption isotherm looks as presented in Equation (15).

$$q_{eq} = f(c_{eq}, T)\ ;\ T = constant \qquad (15)$$

The mathematical function *f* can differ for each specific system. There are several recognized expressions for adsorption isotherms and the decision which one suits the system better can only be taken by fitting experimental results. The Freundlich isotherm (Equation (16)) has been proved to be suitable for systems using active carbon for the treatment of wastewater and drinking water. On the one hand, it has the advantage of satisfactorily describing the medium concentration range but on the other hand it fails to represent the saturation effect as well as the linear behavior observed at very low concentrations (Worch 2021).

$$q_{eq} = KC_{eq}^{n} \qquad (16)$$

where K is is the Freundlich constant and n is the Freundlcih coefficient.

The Freundlich isotherm is a single-component expression that describes the adsorption of an individual dissolved component. However, wastewater is considered a multi-component solution and should be modelled as such. For this purpose, the Ideal Adsorption Solution Theory (IAST) is often applied. This theory accounts for the competition for adsorption sites between the various components of the solution. In multi-component solutions the equilibrium loading of each component ($q_{eq,i}$) is a function not only of the respective liquid phase concentration ($c_{eq,i}$) but it also depends on the equilibrium concentrations of all the other components. The

IAST allows the calculation of a multi-component isotherm in terms of the parameters of individual isotherms, it assumes that the liquid phase as well as the solid phase (GAC) can be considered as ideal solutions. Additionally, the GAC surface is believed to be available for all components equally. On the basis of the IAST an adsorption analysis can be conducted. This analysis divides the DOC into different fictive fractions according to their adsorbability and in doing so, overcomes the problem of the unknown composition of the DOC and allows the application of the IAST.

IAST determines the solutes distribution between the liquid phase and the GAC surface using the spreading pressure term (φ_i) resulting from the Gibbs isotherm. φ_i can be defined as a function of the mass specific surface of the adsorbent (A_m), the gas constant (R), and the temperature. It can also be written in terms of the single-component concentrations in both the liquid phase and GAC as shown in Equation (17). For Equation (17) to hold, it has to be assumed that all the components in the system are assumed to have φ_i.

$$\frac{\pi_i A_m}{RT} = \int_0^{c_i^0} \frac{q_i^0}{c_i^0} dc_i^0 = \varphi_i \qquad (17)$$

where πi is the spread pressure and is given by the difference between the surfaces tension of the water-GAC and component-solution interfaces.

The IAST introduces the molar fraction on the GAC surface (z_i) to associate the concertation in the liquid phase of each component (c_i) with its correspondent equilibrium concentration in a single-solute system (c_i^0). Likewise, it uses z_i and the adsorbed concentration of the solute in a single-solute system (q_i^0) for the determination of the system the total adsorbed concentration (q_T). The mathematical expression of these relationships is given by Equation (18). These expressions constitute the fundament of modelling adsorption of multi-component systems and are widely applied within the drinking water practice and in a lesser extend in the wastewater practice.

$$c_i = c_i^0 z_i \; and \; q_T = \left[\sum_{i=1}^{N} \frac{z_i}{q_i^0}\right]^{-1} \qquad (18)$$

3. Discussion

The Occam's razor principle translates into a fundamental modelling premise " A model should be as simple as possible, and only as complex as needed" (Wanner et al. 2006). The ASM models were developed on this basis and are, after almost 20 years, still state of the art. ASM models prioritized the accuracy of the macroscale results over the exact and comprehensive representation of the microscale features of the system. As result of this compromise, ASMs predict the most important macroscale features of a wastewater system fairly well: effluent concentrations, sludge production and oxygen consumption, although other characteristics of the system like microbial diversity, concentration gradients around/within flocs are not fully portrayed. Despite the several simplifications that the ASM models contain, they still have a substantial explanatory power. Many experimental observations can be explained by the use of ASM models, moreover operational strategies and knowledge of the system can be gained from them. Biofilm models were developed under the same modelling premise as ASM models and the compromise between simplicity and explanatory power is equally valid for the biofilm models, if not of greater importance. Due to the temporal disparity of the modelling development and the technical possibilities to accurately measure different biofilm properties such as biomass composition, thickness, morphology etc., assumptions regarding the microscale characteristics needed to be done to obtain satisfactory macroscale results. With the advances in experimental and computational techniques, more information about biofilm systems can be gathered, and the question of whether or not to include all the available information into the model arises. How simple is too simple and vice versa how complex is too complex? The decision of which level of complexity is adequate for the model depends on the objective of the modelling task as well as on the available information. The objective serves as main guideline for the decision-making process while the available information acts more as constrain of the model (Wanner et al. 2006). I explored two decisive microscale features of a biofilm system: microbial community and dimensionality and examined the level of complexity of the model in the relation to the understanding of the system and the obtained insights.

3.1. Microbial Community Composition

One of the most important modelling decisions is the definition of the microbial community that on the one hand, can be successfully represented (information constraints e.g. kinetic parameters) and on the other hand that needs to be included so the system is appropriately described. This is a tipping-point during the modelling. It dictates the biochemical processes that are going to take place within the system and in consequence it limits the model to a certain extend. Appropriately choosing the microbial community that has to be implemented into a model not only depends on the *a priori* knowledge of the composition but it also depends strongly on the available kinetic and stoichiometric information. In addition, measurements of the substances that play a role in the microbial metabolism are vital when deciding how to describe the microbial community. My first research hypotheses deal with the adequate representation of the microbial community that grows on the GAC surface of a bGAC-filter, and some of the central factors that have to be taken into consideration when implementing a biofilm into a GAC adsorption model.

The first publication P1 focuses on the need of having a simplified microbial community as a reasonable compromise for attaining the objective of assembling two complex preexisting models. P1 aimed to construct a multi-component model able to describe the simultaneous biological and adsorptive removal of DOC in bGAC-filters. The resulting model from P1 is a combination of two well established models: a one-dimensional biofilm model and a multi-component adsorption model. When combining these two models several challenges appeared. The composition of the microbial community was one of the most prominent issues aside from the role that the biofilm played in the mass transfer between the bulk liquid and the GAC.

The composition of the biomass that grew on the bGAC-filters that I used for the modelling exercise in P1 was known, so the question of whether or not to use a multi-species biofilm model had to be asked. Figure 5 shows the relative abundance of the bacteria phyla found in the backwashing sludge from three bGAC-filters treating a WWTP effluent (bGAC-filter 1, bGAC-filter 2, bGAC-filter 3) and the relative abundance found in the activated sludge from the correspondent WWPT (WWTP). In Figure 5 can be observed that all the sampes contained bacterial phyla typical to WWTP, like *Nitrospira*, *Proteobacteria*, *Planctomycetes*, *Armatimonadetes* and *Actinobacteria.*

Figure 5. Microbial community composition of the sludge in the backwash water of three bGAC-filters at different points in time (Provided by Dr. Laura Orschler).

Altough the results in Figure 5 provided information about the microbiological composition of the system, it is still very difficult to directly incorporate molecular biology information into the traditional models, as was the case of P1. Altough the taxonomic composition of the microbial community in P1 is to a certain extend known, I decided to not include all the species

present in the biomass and rather to include a simplified version of it that serves to the goblal objective of succsesfully representing the cocurrent biological and adsoprtive DOC removal and of properly describing the influence of the EBCT on the bGAC-filter performance. For this pourpose and to keep the model as identifiable as possible, I selected a biofilm featuring only one heterotrophic species that uses DOC as electron donor and oxygen as electron acceptor and follows a Monod kinetic law. It allowed me to focus on the model structure and the role of the biofilm in the mass transport. Although the information shown in Figure 5 gives insight to the composition of the microbial community present in the bGAC-filters, it does not provide enough information about the functionality of the different members of the community, which is the key input needed to develop a traditional biochemical model. In addition, the biodegradation of the DOC remaining in WWTP's effluents involves complex processes, which mechanism are not yet fully understood. For the specific case of micropollutants is been observed that their biodegradation is linked not only to the main metabolism of heterotrophic bacteria but also to co-metabolic processes of both heterotrophic and autotrophic bacteria, which makes the accurate representation of the biochemical processes within the biofilm even more intricate. Taking advantage of the molecular biology data would require more targeted measurements directed to the functional bacterial groups rather than the specific species present in the biofilm.

As suggested before, the impracticability of including such information derives in part from a mismatch between what it is meant by microbial composition in a model versus what it means in the microbiological context. In the traditional ASM modelling framework the focus is on the functionalities of the microbial community rather than on the actual species that can be identified. In other words, in a model, bacteria are classified by the specific biochemical processes they take part in, whereas the composition (relative abundance) obtained by the molecular biology techniques is a pure taxonomic classification as in the case of Figure 5.Further molecular techniques such as transcriptomics, metabolomics etc. answer to the questions of what the bacteria are capable of, and how they behave at a given time and, therefore they may give a better insight of the microbial community from the modelling point of view. Although these omics techniques provide essential qualitative information about microbial communities, there is still a significant knowledge gap regarding how to transform such kind of data into physiological parameters relevant for the traditional mechanistic models e.g. affinity constants, maximum growth rates etc. (Prosser 2015). The work of Vieira-Silva and Rocha (2010) is a compelling approach to calculating physiological parameters from genomic data. The contribution explores the possibility of calculating the maximal growth rate of bacteria and archaea using information derived from their genomes. Nevertheless, the presented approach seems to be subjected to the bias of culture methods that tend to select fast growing strains. More research is needed to expand the model to bacteria growing in suboptimal conditions e.g. natural biofilms, substrate-limited conditions.

In addition to the estimation of physiological parameters, it is still challenging to incorporate the dynamics and the spatial dimension of the communities into the omics data. Most of the studies analyze the microbial community at a specific point in time and location, which only reflect a transitory state of the community and are difficult to link with the actual state of the

system. Overcoming this so called " temporal and spatial heterogeneity" requires time and cost intensive measuring campaigns that continue to be somewhat impractical (Prosser 2015).

Despite the various open questions, some studies recognize the importance of including molecular biology data into the modelling, however they also acknowledge that the current ASM framework is not yet ready for it (Sin and Al 2021, Vannecke 2015). Sin and Al (2021) argue that traditional ASM models seem unable to keep up with the new information and data inflow and even consider that they have reached their limits. They also propose a methodology for the explicit integration of molecular biology results into a relatively traditional ASM model scheme. The authors propose the introduction of dynamic metabolic pathways into the model that otherwise is based in the assumption of fixed metabolic pathways. The information provided by the metagenomics and metatranscriptomics data can be used to predict the metabolic state of the system and to adjust the model accordingly. The application of machine learning techniques is suggested for linking the traditional model structure and the molecular biology data. Although this seems to be a promising approach, I expect the amount of data needed to appropriately train a data-driven algorithm to be the bottleneck to the practical implementation of this concept, as the collection of omics information from microbial communities continues to be laborious.

In the same way, McDaniel et al. (2021) explore different potential applications of the omics data in the water engineering field. The authors summarize some studies aiming to integrate molecular biology data within traditional modelling frameworks. Especially interesting is the contribution of Weinrich et al. (2019). In this work the conventional model for anaerobic digestion ADM1 was extended by combining it with a Flux-Balance-Analysis, which allows the prediction of intracellular fluxes and it opens the possibility to calibrate the extended ADM1 model using omics data. Likewise in their work Reed et al. (2014) developed an interesting method to quantify the production of genes relevant to the nitrogen cycle in marine environments (nitrate reductase (narG), nitrite reductase (nirK) amongst others) by modifying the traditional Monod growth expression. The authors introduced a thermodynamic factor that accounts for the chemical energy and a second factor that incorporates the gene abundance. The model is divided into functional groups associated to a metabolic pathway and to its related genes reconciling in doing so, molecular biology information and a traditional modelling framework (comparable to the ASM one).

The developed model uses a very simplified version of the microbial community, however, it serves as a proxy for the DOC removal that cannot be attributed to adsorption and for the mass transport phenomena caused by the existence of a biofilm on the GAC surface. I expected that the DOC removal attained by the modelled biofilm corresponds to the biological DOC removal measured in the filters. Likewise, the modifications to the concentration gradient of all the DOC fractions should be comparable to the ones that took place in the bGAC-filters. Figure P1.2 compares the results delivered by the model with the experimental measurements from the pilot bGAC-filters. A good agreement between the experimental and simulated effluent DOC concentrations can be observed, as well as the capability of the model to describe the effect that the EBCT has on the bGAC-filter performance. In Figure P1.3 the breakthrough

curves of the different DOC fractions are presented. Figure P1.3 was used to validate the rationality of the model structure and to evaluate the behavior of the DOC fractions depending on its absorbability and/or biodegradability. The effect of the temperature on the biodegradable fractions is very clear. Likewise, desorption of the better adsorbable fractions can be observed when the WWTP effluent was diluted i.e. the DOC concentration in the bulk phase was lower than the one on the GAC surface. The model also enabled the tracking of the distribution of the DOC removal as shown in Figure P1.7. The distribution observed in the figure corresponds to the description proposed by Simpson (2008) and is explained in chapter 2.4.3. At the beginning of the operation adsorptive removal dominates until the biofilm is sufficiently developed and starts contributing to the removal, until virtual saturation of the GAC is reached. During this phase both biodegradation and adsorption take place simultaneously. Once the GAC is nearly saturated, the biofilm is responsible for the majority of the observed removal. Depending on the EBTC, biodegradation sets in earlier. At short EBCTs the effect of biodegradation on the global DOC removal becomes noticeable earlier than in the case of long EBCTs. This may suggest that short EBCTs are beneficial for the biofilm development, which contradicts previous findings reported in the literature. Longer EBCTs are believe to foster the biofilm growth due to the longer exposure of the biofilm to the substrates and the possible interactions between the adsorbed DOC and the biofilm (Fundneider et al. 2021, Terry and Summers 2018). The observed behavior in the model can be explained by the fact that at lower EBCTs the filters receive a higher flow and thus a higher DOC mass is available for the bacteria to grow. In consequence the biofilm develops faster and its contribution to the removal can be seen earlier. This deviation is a drawback resulting from the simplification of the microbial community and points towards the necessity to better model the potential interactions between the adsorbed DOC and the biofilm. Despite of the various simplifications that the model developed in P1 encompasses, it is a satisfactory first approach to the modelling of simultaneous biodegradation and adsorption of DOC from a WWTP effluent. It establishes a methodology to connect a biofilm and a multi-component adsorption model. It also lays a strong foundation for the inclusion of individual micropollutants and for the potential extension of the microbial community for it to include more species and better represent the actual diversity of it. The fact that the model is built within the ASM framework is also advantageous for the perspective inclusion of the model and bGAC-filters into plant wide models.

The issue of the microbial composition in P1 constitutes a typical case where simplification is needed despite the fact that a deeper understanding of the system is available. Some authors have discussed the relationship between complexity and understanding in a modelling context. They theorized that the complexity of a model increases along with the understanding of the system and that the modeller can make the decision of either keeping a simplified model while continuing to expand the understanding of the system and thereby attainig “elegant simplicity” or to try and develop a model as complex as possible, risking in doing so a state of “hypercomplexity” where models do not add to the knowledge of the system (Schwartz et al. 2017). Considering the results of P1, I argue the complexity level that a model is able to achive is defined not only by the understanding of the system, but it is determined to a great extend by the useful information that is accesible to the modeler. The amount of scientific knowlegde that exists about a system and the posibility of capturating it in a model is limited by an

information gap. Figure 6 is a schematic representation of the concept presented by Schwartz et al. (2017) and the explained information gap. New discoveries about a system and its underlying mechanims do not directly translate into usable information for the models since the gathering of information (especially in the microscale) continues to be restrictive, time and resource consuming. Additionally, it is difficult to know beforehand which parameters are going to be needed for the perspective models and the measurements may be disconnected from the parameters required by the model. Closing this information gap requires a stronger feedback between the modelling and the experimental research and a better use of the model explanatory power, considering that models do not have the sole purpose of reproducing experimental data but also of contributing to the general understanding of a process.

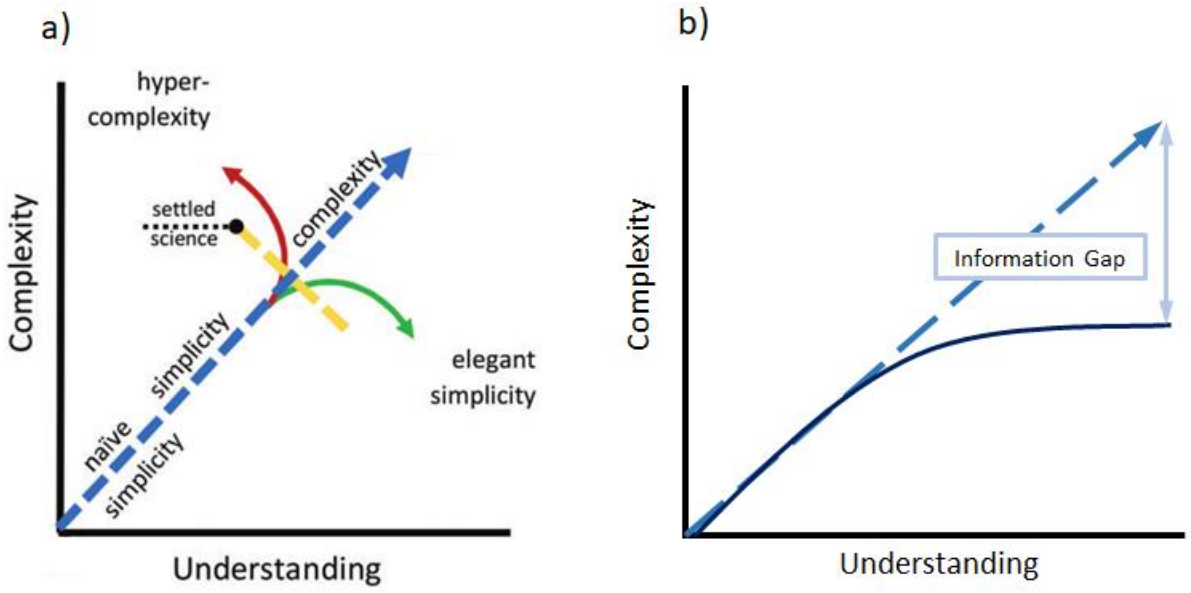

Figure 6. Comparison of the concept presented by (Schwartz et al. 2017) and the proposed relationship between information, understanding and complexity.

If the information gap cannot be bridged by means of experimental measurements specific to the system, sometimes it my be convenient to transfer some of the parameters from well-studied comparable systems or to use established/ accpeted values. As it was the case in P1, accurate kinetic information related to biofilm consortia is still lacking and therefore in many cases the best available information is still the one stemming from the activated sludge systems. On the one hand, this lack of information occurs due to the difficulties to measure some of the required biofilm parmeters. On the other hand, the so called pure culture paradigm plays also a conceptual role.

Most of the microbiological knowledge built until now, is based mainly on the pure culture paradigm. A species is cultivated in a chemostat under perfect mixing conditions and its behavior is determined on the basis of the experimental results. Kinetic parameters, metabolic pathways amongst other specific characteristics of bacteria are studied through pure cultures. The information gathered using such an experimental set-up is valuable and has been vital in the development of microbial applications, however the extent to which these findings can be

compared and extrapolated to the behavior of natural communities and in special of biofilms remains under discussion. Several works from the medical field recognize the limitations of planktonic cultures and the bias that they might have caused in the understanding of microbiological phenomena (Wolcott and Ehrlich 2008). The essential critique to this paradigm is that culture conditions usually differ greatly from those bacteria would experiment in nature. Sufficient supply of substrates and nutrients, controlled pH, sufficient water activity, absence of interactions are the rule in planktonic cultures and the exception in natural environments. Relevant information about secondary metabolites, communication, cooperation and competition may get lost due to the optimal growth conditions used in pure/planktonic cultures (Nai and Meyer 2018). The research hypotheses of the second publication P2 originate from this fact, the way microorganisms interact and behave in rich environments and in suspended cultures greatly deviates from the behavior in biofilms under limited-substrate conditions. Yet, the question remains of whether these differences in behavior have an important effect on the macroscale modelling results. Moreover can these differences be explored using the current modelling framework? One interesting feature of microorganism growing in structured environments under substrate limiting conditions is their ability to cooperate and select the common good over their individual fitness. Bacteria under such conditions are believed to undergo the so called yield strategy. Bacteria would rather increase their growth yield and trade it for a decrease in growth rate, which may be considered as indirect passive cooperative behavior. In contrast, bacteria growing at a high growth rate at the expense of their growth yield are believed to be rate-strategists and are associated with rich substrate environments and planktonic conditions (Kreft and Bonhoeffer 2005b).

In P2, I theoretically investigated the effect that the growth yield has on different features like microbial composition, diversity and on the bulk liquid concentrations. I use a MBBR dedicated to fully autotrophic nitrogen removal i.e. PN/A and analyzed the behavior of the heterotrophic community under various pairings of yield (Y) and growth rate (μ). To simulate different levels of substrate availability, three scenarios with different values of the affinity constant (K) were also studied. In doing so I was able to simulate instances where the heterotrophs acted as yield strategists and as rate strategists, and I compare the implications of each strategy on the macroscale results especially on the nitrogen gas production by the heterotrophic community and on the microscale features more specifically the microbial composition/ diversity.

The first scenario was dedicated to a reactor operated in absence of external COD (COD_{Ex}) and focused on the competition of three different heterotrophic bacteria surviving on the same scarce electron donor: the organic matter produced by the biomass decay (COD_{Bf}) .Figure P2.1 shows the production of nitrogen gas by the HB2 (using NO_2^- as electron acceptor), by the HB3 (using NO_3^- as electron acceptor) and the sum of both contributions. It is clear, that the nitrogen gas production depends highly on the yield and is almost insensitive to μ and K. Interestingly enough HB2 do not produce N_2 i.e. do not grow unless a high yield is assigned to the heterotrophic bacteria.

In scenario 1, the growth yield was determinant for the composition of the heterotrophic community. The diversity of the heterotrophic community may be closely related to the yield growth as only at the highest yields a diverse biofilm was observed in the results. Figure P2.2

shows the biomass concentration profiles along the biofilm thickness at different μ-Y pairings for a K equal to 10 $gCOD_{BF}/m^3$. Variations in the concentration profiles can be observed, higher values of yield result, as expected, in higher biomass concentrations and in a diverse community, moreover the diversity of the community seems to depend exclusively on the yield. The results shown in P2.2 suggest as well that the growth yield affects not only the composition of the heterotrophic community but also its spatial structure.

I also analyzed the effect of the yield strategy, when the heterotrophic community growing on COD_{Bf} faces the competition of a second heterotrophic community growing on a more abundant substrate (COD_{EX}). I found that the growth yield positively affects the production of N_2 by HB2, however it does not do so for the production of N_2 by HB3. After a yield of approx. 0.35 $gCOD_x/gCOD_{Bf}$ the N_2 production by HB3 slightly decreases and then stabilizes, which in turn means that the best strategy for the community in terms of diversity would not be necessarily the yield-strategy. Nevertheless, the total N_2 production reaches its maximum when the yield takes the highest possible value. The well-known k-strategy and the yield-strategy were also shortly compared in P2 on the light of the postulates of the microbial transition state theory. This theory proposes a direct relationship between the affinity constant and the growth yield, which implies that both k and yield-strategy are outcomes of the same adaptation strategy to substrate limited conditions and should be probably investigated jointly rather than individually.

P2 used a traditional modelling set up to conceptually explore the implications of behavioral changes in the heterotrophic microbial community on the macroscale results of a fully autotrophic process. I showed that the heterotrophic community pursuing a yield-strategy has implications not only on the microscale (microbial composition and diversity) but also on the macroscale features like N_2 production and total dissolved nitrogen. The use of models to explore different hypothesis in relation to the growth strategies being pursued by the bacteria can lead to interesting results and could strengthen the link between the modelling and the experimental practice. In their work Costa et al. (2006) used the findings of the kinetic theory and of their previous models to predict the existence of comammox (complete ammonium oxidation) bacteria and their preference for the yield strategy. Moreover, they were able to propose different experimental set-ups with the aim to facilitate the isolation and further investigation of such bacteria. Recently Kits et al. (2017) corroborated the hypothesis proposed by Costa et al. (2006) by isolating *Nitrospira inopinata*. They found that *Nitrospira inopinata* have a high growth yield, a low maximum rate of NH_4^+ oxidation and a high affinity NH_4^+, which confirms that they undergo the yield strategy.

3.2. Dimensionality

The second studied microscale feature of this work is dimensionality. Dimensionality plays a central role in biofilm modelling. An essential modelling decision is the selection of the number of dimensions that the model requires, 1D models find application in both research and engineering contexts, whereas models with higher dimensionality are used especially for research and educational purposes. High dimensionality models are very often used in the microbial ecology to explain biofilm structure an interactions between the microorganisms, however they are rarely applied in engineering contexts. (Wanner et al. 2006)

1D models assume that the concentration gradients along the biofilm thickness are steep enough so that they dominate over the gradients in all other directions. However, longitudinal concentration gradients in the bulk liquid and or in the gas phase can be found, likewise differences in the biofilm along the length of the reactor are observed. This is valid especially in the case of MABRs, where depending on the reactor specific configuration, pronounced concentration gradients might arise. Determinant for the apparition of such gradients are the membrane configuration: flow through or dead-end as well as the presence or not of a recirculation in the bulk liquid (Hibiya et al. 2003, Martin and Nerenberg 2012, Pankhania et al. 1999, Shanahan and Semmens 2006). The second hypothesis of this work originates from these kind of observations. In fully autotrophic MABRs, the longitudinal concentration gradients in the membrane lumen and in the bulk liquid influence the biofilm microscale features (biomass distribution), in such a way that macroscale results reflect it. I hypothesize that a low-dimensionality model can be used to assess the magnitude of these effects. Publication P3 addresses this problem by comparing a traditional 1D biofilm model with a pseudo 2D biofilm model. This pseudo 2D model is composed of various fully mixed compartments connected in series, which simulates the mixing conditions of a plug flow reactor in both gas and bulk phase. Figure P3.1 alongside with Table P3.1 explains all the configurations explored. The model had the flexibility to include the gradients individually or simultaneously in each of the phases (gas phase and bulk liquid). In addition, the number of fully mixed compartments (n), was also varied in the model.

The conceptual comparison of the model configurations demonstrated that the oxygen gradient is the most influential gradient in terms of biomass distribution and in terms of the global reactor performance. Figure P3.5 shows the distribution of the total biomass for all the studied configurations alongside with their respective Total Dissolved Nitrogen (TDN) in the effluent. Despite the differences in TDN between each configuration and the 1D model, the total biomass distribution is very similar in all the cases, except for the apparition of NOB in the configurations featuring only the oxygen gradient. The occurrence of NOB seems to logically provoke an increase in the final TDN. When looking at the biomass distribution along the reactor length (Figure P3.6), very different biomass distribution profiles can be seen. In the configurations with an oxygen gradient the biomass composition varies greatly along the length, whereas in the configuration with only a substrate concentration gradient (bulk liquid as PFR, but gas phase as fully mixed reactor) the biomass distribution is nearly the same along the reactor length and very similar to the biomass distribution predicted by the 1D model, being the main difference the accumulation of particulate inert components. Table 1 summarizes the most important results from the P3. It compares the modelling results of all configuration using

the 1D model as a baseline. In Table 1 it can be seen that a substrate gradient alone (configuration 5) has almost none effect on the TDN, however in combination with the oxygen gradient, it seems to slightly counterbalance the effect of the oxygen gradient.

Table 1. Summary of the main results of Publication1. Comparison of the effect of longitudinal gradients on the total dissolved nitrogen and the biomass distribution

Configuration	n	Difference (*)	TDN (mgN/L)	Oxygen Gradient	Substrate Gradient	Biomass Distribution (along the reactor length)
2	3	76%	25.1	✓	x	Heterogenous
2	5	113%	30.3	✓	x	Heterogenous
3	3	30%	18.5	✓	✓	Heterogenous
3	5	-30%	9.9	✓	✓	Heterogenous
5	3	-1%	14.1	x	✓	Homogeneous
5	5	-6%	13.4	x	✓	Homogeneous
1D model	—	—	14.2	x	x	Homogeneous

(*)with respect to the TDN from the 1D model

In an MABR, the key to sustain the microbial communities that performed PN/A is the oxygen penetration depth as demonstrated in several experimental studies (Casey et al. 1999a, Schramm et al. 2008). Oxygen should not penetrate the entire biofilm so an anoxic zone is established and adequate growth conditions for AnAOB are present. An excessive oxygen concentration would hinder AnAOB growth and the system would act rather as a nitrification system. As discussed in P3, the airflow is crucial to obtain a good reactor performance and can be set in relation to the incoming NH_4^+ load, making in doing so oxygen the limiting substrate. As consequence, it is to be expected that the influence of the oxygen longitudinal gradient dominates over the influence of the correspondent substrate gradient, as I illustrated in P3.

The structure of the model also allowed the analysis of two flow arrangements: counter and parallel flow. Flow arrangements did affect the performance of the modelled reactor, the parallel flow being the only arrangement that showed sufficient nitrogen removal. In other applications such as chemical reactors and heat exchangers counter flow arrangements has proved to be advantageous, due to the re-localization of the concertation or temperature gradients in such a way that the driving force of the transport (mass or heat) is bigger than the one occurring in parallel flow. However, according to my observations this is not the case in MABR applications used for PN/A processes. When a counter flow arrangement is in place, the maximal oxygen concentration occurs in one extreme of the reactor whereas the maximal NH_4^+ occurs in the other one, resulting in a lack of a growth niche for AOB. If AOB are not able to grow, the whole nitrogen removal chain truncates and thus the MABR shows a poor performance. At first glance, this finding may seem trivial. However, such a comparison between two flow arrangements is not possible when using a traditional 1D model. Only by assuming the existence of longitudinal concentration gradients and by developing a model that is able to represent them, the possibility of physically having two flow arrangements and of investigating them opens. P3 also contributed to elucidate the effects of these flow configurations on the performance of an MABR applied to PN/A.

A similar approach to attain higher dimensionality was used also in P1. The tricking filter process unit on which the model is based, employs three different completely mixed reactors

connected in series to simulate the longitudinal profiles along the bGAC-filter. Due to the fixed bed characteristic of the bGAC-filters it is clear from the start that longitudinal profiles are going to be present in the bulk phase, the GAC and the biofilm. DOC concentration and composition in the bulk liquid change considerably along the GAC-bed due to the preferential adsorption of some of the DOC fractions and the asynchronous saturation of the different filter bed areas. As a result of this, the time in which the microbial community fully develops its composition, biofilm thickness etc. vary according to the location within the GAC-bed.

The use of a pseudo 2D model configuration proved in this case yet again to be sufficient to reflect these longitudinal variations without introducing unnecessary complexity to the model. As shown in Animation 1 and Animation 2 from P1, the data delivered by the model is sufficient to reproduce the DOC advection fronts in the bGAC filters. These fronts show the profiles of the DOC concentration along the filter length and across the biofilm thickness, moreover desorption events can be observed in the two directions (filter length and biofilm thickness).

With regard to the microbial community composition the model was also capable of describing the differentiated growth along the filter bed, however only in terms of the time at which the biofilm was fully developed. Figure P1.6 in the supplementary material of P1 shows how the biofilm in the top compartment of the filter bed reaches the maximal concentration ($X_{HB,\ SP}$) biofilm concentration first, followed by the middle and bottom compartment. Due to the simplification of the microbial community composition (inclusion of only one species) it is not possible for the model to reflect the potential longitudinal profiles of the microbial community composition. However, there is experimental evidence that microbial composition varies strongly depending on the filter bed location. A closer look into Figure 5 reveals such differences in the microbial community composition. The relative abundance of the microbial species in bGAC-filter 1, the one that is closest to the influent inlet, differs greatly from the one in the bGAC-filters 2 and 3, which are further downstream with respect to the influent inlet.

The problem of dimensionality showcases that fundamental understanding of a system that may be considered as settled science, does not always have a straightforward translation into a model or even more it should not be necessarily included into it. As mentioned in the section before (3.3), higher complexity cannot be achieved without sufficient information. Not all the parameters that a model needs can be determined experimentally and not all of them can be fitted using a model and parameter estimation procedures. It is clear that biochemical processes take place in all the three dimensions of a biofilm, nonetheless as showed in P1 a pseudo 2D model is capable of satisfactorily describe the most relevant macroscale results and to facilitate other models to encompass more complexity in the microbial community as well in the influent composition. In contrast, the result of P3 showed that in the case of MABR the simplest approach (1D model) neglects crucial system microscale features such as the longitudinal gradients, which may have a significant effect on the macroscale results and thus on the reactor performance. In this case a pseudo 2D model seems to be more appropriate for describing the phenomena occurring within the reactor.

4. Conclusions

The focus of this work was the relationship between the microscale and macroscale features when modelling a biofilm system, especially when a substrate is limited. On the one hand, it is difficult to assess beforehand whether the inclusion of a microscale feature would significantly impact the global modeling results, which are very often the priority. On the other hand the inclusion of microscale features may be beneficial for the explanatory power of the model and its mechanistic meaning.

For the bGAC-filter I demonstrated in P1 that a very simple representation of the microbial community seems to be sufficient especially at early modelling stages. It allows the construction of a model capable of describing the removal of DOC as a simultaneous multi-component adsorption and biodegradation. Moreover, it favors the development of a methodology on how to combine these two processes (multi-component adsorption and biodegradation) and on how to further extend the model for it to have more components and more microbial species.

In terms of dimensionality, the pseudo 2D- model in P1 proved to be sufficient for the investigation purposes. Using this kind of model, DOC advective fronts were generated and a visual representation of the DOC (and its fractions) concentration gradients along the filter bed and along the biofilm depth, was generated. Through these results the modelled interaction of the biofilm and the GAC can be easily explore and inconsistencies/ potential improvement points can be recognized. On the one hand, a lower dimensionality approach i.e. 1D model would have neglected the longitudinal gradients, yielding an oversimplified and incorrect model. On the other hand a higher complexity model, i.e. a 3D model, would have required information about the GAC and biofilm that was not available and would have taken the focus from the simultaneous implementation of the multi-component adsorption and the biodegradation.

In P2 I illustrated the impact that the growth yield has on the composition and activity of a heterotrophic community growing under fully autotrophic conditions (PN/A system). The results suggest that the diversity of the community highly depends on the growth yield, thus, high yields being favorable for the coexistence of all the heterotrophic species sharing the scarce substrate. The relationship between the k-strategy and the yield-strategy was shortly discussed, and the need to investigate them as a whole rather than separate were also briefly addressed. Due to the imbalance between understanding and information, the deliberate decision of keeping a model simple despite of having deep knowledge of the system can turn the model into a more profitable tool. A simpler model or a model featuring elegant simplicity can bring forward the understanding of the system. The use of simple conceptual models can serve as guideline to the experimental practice of what to search for or where to focus more when measuring. P2 is an example of such a situation. Despite of not including the latest biofilm modelling theories like the Extracellular Polymeric Substances (EPS) theory, a simpler model was able to shed light upon an ecological trait of the microbial community that may be worth a deeper investigation and could probably help to find an explanation of some macroscale observations.

In the case of the MABR, the results of P3 conceptually showcase the impact that longitudinal concentration gradients have on the macroscale results. My results suggest that depending on

the specific reactor configuration a 1D model may not be sufficient to describe an MABR and that a relatively simple pseudo 2D model can deliver better results. The 1D model predicted lower total dissolved nitrogen concentrations than the ones predicted by the pseudo 2D model in all the evaluated scenarios. In the worst case, the difference between the predictions was threefold. Furthermore, the implementation of longitudinal gradients also showed an impact on the gradients along the biofilm depth. The case study of P3 constitutes an example when oversimplification may be risky in terms of explanatory power and quality of the predictions.

Throughout this work I also examined the relationship between the information available of the system and the general understanding of the phenomena taking place in a system, and the complexity level that a model (representing the system) may achieve. I argue that the achievable complexity of a model is certainly related to the existing understanding but it is limited by the usable information accessible to the modeler. As simplifications could be actively pursued, they can be also forced upon the model if it is no capable to integrate the new information or the produced information does not fit the model structure. I show for the case of the microbial community in P1 that although a big amount of knowledge is available about the composition of the microbial community, it does not correspond entirely with the information required by the model and thus the translation of the knowledge into the model is not straight forward.

5. Outlook

This section is dedicated to give an overview of the potential future work that originates from the contributions that composed this work. It also shortly discusses some research questions that opened up while conducting this investigation.

For P1, the implementation of OMP removal into the developed model should be prioritized. OMPs may be included into the model using the fractionation methodology applied for DOC, however parameters of the individual adsorption isotherms of each OPM in the respective wastewater matrix are a prerequisite. In addition, the difference between the orders of magnitude of DOC and OPM concentrations may be a challenge to overcome. In regard to the microbiological composition in P1, modifications are still required. The expansion of the microbial composition to include microorganisms able to biodegrade OMPs should come along with the introduction of OMPs into the model. Nitrifiers are believed to have the ability to co-metabolize some OMPs parallel to their main metabolism, therefore the exploration of the influence of the nitrifier community on the biological removal of the OPMs may be worthwhile. Including the nitrogen species into the model may as well increase its explanatory power in terms of the final effluent quality. Regarding the dimensionality, the model presented in P1 represents in a very simplified way the GAC structure. A more complex representation of the GAC may further enhance the model quality. The incorporation of a differentiated pore volume (micro, meso, and macro) can be crucial when OMP concentrations are targeted with the model.

For P2, several questions are still open with respect to the behavior of heterotrophic bacteria in fully autotrophic systems. The relationship between the yield strategy and the EPS theory is worth exploring experimentally. Is the yield strategy the preferred one when SMP are the only carbon source? Has the yield the same influence on the composition and on the diversity of the community if the postulates of the EPS are considered? Does the scarce carbon source and the need of undergoing yield strategy influence the nitrogen conversion processes as well, for instance is incomplete denitrification more likely to occur? Finally, yield and k strategy should be studied together rather than individually in order to have a better understanding of the fundamental mechanism of the behavior of the heterotrophic community under substrate limited conditions.

In the case of P3 experimental calibration and validation of the conceptual model is still required. Verification of the steepness of the longitudinal gradients is required to determine the number of compartments that deliver the most realistic description of the longitudinal gradients and of the system. The potential occurrence of biological processes in the bulk phase and its implications on the macroscale results could be also looked into. Through the compartments approach a heterogeneous biofilm (along the reactor's length) in terms of biofilm thickness and density can be also implemented. Finally, a multi-compartment model, like the one developed in P3, can become a tool for testing different operational strategies featuring targeted longitudinal gradients in both bulk and gas phase.

References

Agrawal, S., Karst, S.M., Gilbert, E.M., Horn, H., Nielsen, P.H. and Lackner, S. (2017) The role of inoculum and reactor configuration for microbial community composition and dynamics in mainstream partial nitritation anammox reactors. MicrobiologyOpen 6(4), e00456.
Barry, U., Choubert, J.-M., Canler, J.-P., Héduit, A., Robin, L. and Lessard, P. (2012) A calibration protocol of a one-dimensional moving bed bioreactor (MBBR) dynamic model for nitrogen removal. Water Science and Technology 65(7), 1172-1178.
Basu, O.D., Dhawan, S. and Black, K. (2016) Applications of biofiltration in drinking water treatment – a review. Journal of Chemical Technology & Biotechnology 91(3), 585-595.
Bishop, P.L., Gibbs, J.T. and Cunningham, B.E. (1997) Relationship Between Concentration and Hydrodynamic Boundary Layers over Biofilms. Environmental Technology 18(4), 375-385.
Boltz, J., Morgenroth, E., Brockmann, D., Bott, C., Gellner, W. and Vanrolleghem, P. (2011) Systematic evaluation of biofilm models for engineering practice: components and critical assumptions. Water Science and Technology 64(4), 930-944.
Boltz, J.P., Johnson, B.R., Daigger, G.T. and Sandino, J. (2009) Modeling integrated fixed-film activated sludge and moving-bed biofilm reactor systems I: Mathematical treatment and model development. Water Environment Research 81(6), 555-575.
Boltz, J.P., Morgenroth, E. and Sen, D. (2010) Mathematical modelling of biofilms and biofilm reactors for engineering design. Water Science and Technology 62(8), 1821-1836.
Boltz, J.P., Smets, B.F., Rittmann, B.E., van Loosdrecht, M.C.M., Morgenroth, E. and Daigger, G.T. (2017) From biofilm ecology to reactors: a focused review. Water Science and Technology 75(8), 1753-1760.
Bunse, P., Orschler, L., Agrawal, S. and Lackner, S. (2020) Membrane Aerated Biofilm Reactors for Mainstream Partial Nitritation / Anammox: Experiences using real Municipal Wastewater. Water Research X 9.
Campos, J.L., Val del Río, A., Pedrouso, A., Raux, P., Giustinianovichc, E.A. and Mosquera-Corral, A. (2017) Granular biomass floatation: A simple kinetic/stoichiometric explanation. Chemical Engineering Journal 311, 63-71.
Cao, Y., van Loosdrecht, M.C.M. and Daigger, G.T. (2017) Mainstream partial nitritation–anammox in municipal wastewater treatment: status, bottlenecks, and further studies. Appl Microbiol Biotechnol 101(4), 1365-1383.
Casey, E., Glennon, B. and Hamer, G. (1999a) Oxygen mass transfer characteristics in a membrane-aerated biofilm reactor. Biotechnol Bioeng 62(2), 183-192.
Costa, E., Pérez, J. and Kreft, J.U. (2006) Why is metabolic labour divided in nitrification? Trends Microbiol 14(5), 213-219.
Donlan, R.M. (2002) Biofilms: microbial life on surfaces. Emerging infectious diseases 8(9), 881-890.
Eberl, H.J. and Wade, M.J. (2020) Recent Trends in Biofilm Science and Technology. Simoes, M., Borges, A. and Chaves Simoes, L. (eds), pp. 359-383, Academic Press.
Eiler, A., Langenheder, S., Bertilsson, S. and Tranvik, L.J. (2003) Heterotrophic bacterial growth efficiency and community structure at different natural organic carbon concentrations. Applied and Environmental Microbiology 69(7), 3701-3709.
Fetzner, S. (2011) BIODEGRADATION OF XENOBIOTICS.
Flemming, H.-C., Wingender, J., Szewzyk, U., Steinberg, P., Rice, S.A. and Kjelleberg, S. (2016) Biofilms: an emergent form of bacterial life. Nature Reviews Microbiology 14(9), 563-575.
Franklin, M.J., Chang, C., Akiyama, T., Bothner, B., Ghannoum, M., Parsek, M., Whiteley, M. and Mukherjee, P. (2015) New Technologies for Studying Biofilms. Microbiol Spectr 3(4), 3.4.27.

Fundneider, T., Acevedo, V., Wick, A., Albrecht, D. and Lackner, S. (2021) Implications of biological activated carbon filters for micropollutant removal in wastewater treatment. Water Research 189, 116588.
Gilmore, K.R., Terada, A., Smets, B.F., Love, N.G. and Garland, J.L. (2012) Autotrophic Nitrogen Removal in a Membrane-Aerated Biofilm Reactor Under Continuous Aeration: A Demonstration. Environmental Engineering Science 30(1), 38-45.
Hall-Stoodley, L., Costerton, J.W. and Stoodley, P. (2004) Bacterial biofilms: from the Natural environment to infectious diseases. Nature Reviews Microbiology 2(2), 95-108.
Hauduc, H., Rieger, L., Oehmen, A., Van Loosdrecht, M., Comeau, Y., Héduit, A., Vanrolleghem, P. and Gillot, S. (2013) Critical review of activated sludge modeling: state of process knowledge, modeling concepts, and limitations. Biotechnol Bioeng 110(1), 24-46.
Helbling, D.E., Johnson, D.R., Honti, M. and Fenner, K. (2012) Micropollutant Biotransformation Kinetics Associate with WWTP Process Parameters and Microbial Community Characteristics. Environmental Science & Technology 46(19), 10579-10588.
Henze, M., Gujer, W., Mino, T. and van Loosedrecht, M. (2006) Activated Sludge Models ASM1, ASM2, ASM2d and ASM3, IWA Publishing.
Hibiya, K., Terada, A., Tsuneda, S. and Hirata, A. (2003) Simultaneous nitrification and denitrification by controlling vertical and horizontal microenvironment in a membrane-aerated biofilm reactor. Journal of Biotechnology 100(1), 23-32.
Hill, M.C. (2006) The Practical Use of Simplicity in Developing Ground Water Models. Groundwater 44(6), 775-781.
Hubaux, N., Wells, G. and Morgenroth, E. (2015) Impact of coexistence of flocs and biofilm on performance of combined nitritation-anammox granular sludge reactors. Water Research 68, 127-139.
Kits, K.D., Sedlacek, C.J., Lebedeva, E.V., Han, P., Bulaev, A., Pjevac, P., Daebeler, A., Romano, S., Albertsen, M., Stein, L.Y., Daims, H. and Wagner, M. (2017) Kinetic analysis of a complete nitrifier reveals an oligotrophic lifestyle. Nature 549(7671), 269-272.
Kreft, J.U. and Bonhoeffer, S. (2005b) The evolution of groups of cooperating bacteria and the growth rate versus yield trade-off. Microbiology (Reading) 151(Pt 3), 637-641.
Lackner, S., Gilbert, E.M., Vlaeminck, S.E., Joss, A., Horn, H. and van Loosdrecht, M.C.M. (2014) Full-scale partial nitritation/anammox experiences – An application survey. Water Research 55, 292-303.
Lackner, S., Terada, A. and Smets, B.F. (2008b) Heterotrophic activity compromises autotrophic nitrogen removal in membrane-aerated biofilms: Results of a modeling study. Water Research 42(4), 1102-1112.
Lewandowski, Z. and Beyenal, H. (2009) Biofilms in the Food and Beverage Industries. Fratamico, P.M., Annous, B.A. and Gunther, N.W. (eds), pp. 99-130, Woodhead Publishing.
Lewandowski, Z. and Boltz, J.P. (2011) Treatise on Water Science. Wilderer, P. (ed), pp. 529-570, Elsevier, Oxford.
Lu, H., Chandran, K. and Stensel, D. (2014) Microbial ecology of denitrification in biological wastewater treatment. Water Research 64, 237-254.
Margot, J., Lochmatter, S., Barry, D.A. and Holliger, C. (2015) Role of ammonia-oxidizing bacteria in micropollutant removal from wastewater with aerobic granular sludge. Water Science and Technology 73(3), 564-575.
Martin, K.J. and Nerenberg, R. (2012) The membrane biofilm reactor (MBfR) for water and wastewater treatment: Principles, applications, and recent developments. Bioresource Technology 122, 83-94.
McDaniel, E.A., Wahl, S.A., Ishii, S.i., Pinto, A., Ziels, R., Nielsen, P.H., McMahon, K.D. and Williams, R.B.H. (2021) Prospects for multi-omics in the microbial ecology of water engineering. Water research 205, 117608.

Nai, C. and Meyer, V. (2018) From Axenic to Mixed Cultures: Technological Advances Accelerating a Paradigm Shift in Microbiology. Trends Microbiol 26(6), 538-554.
Nerenberg, R. (2016) The membrane-biofilm reactor (MBfR) as a counter-diffusional biofilm process. Current Opinion in Biotechnology 38, 131-136.
Ødegaard, H. (2006) Innovations in wastewater treatment: –the moving bed biofilm process. Water Science and Technology 53(9), 17-33.
Olmstead, K.P. and Weber, W.J. (1991) INTERACTIONS BETWEEN MICROORGANISMS AND ACTIVATED CARBON IN WATER AND WASTE TREATMENT OPERATIONS. Chemical Engineering Communications 108(1), 113-125.
Pankhania, M., Brindle, K. and Stephenson, T. (1999) Membrane aeration bioreactors for wastewater treatment: completely mixed and plug-flow operation. Chemical Engineering Journal 73(2), 131-136.
Pellicer-Nàcher, C., Domingo-Félez, C., Lackner, S. and Smets, B.F. (2013) Microbial activity catalyzes oxygen transfer in membrane-aerated nitritating biofilm reactors. Journal of Membrane Science 446, 465-471.
Persson, F., Suarez, C., Hermansson, M., Plaza, E., Sultana, R. and Wilén, B.-M. (2017) Community structure of partial nitritation-anammox biofilms at decreasing substrate concentrations and low temperature. Microbial Biotechnology 10(4), 761-772.
Picioreanu, C., van Loosdrecht, M. and Heijnen, S. (1999) Modelling and Predicting Biofilm Structure.
Picioreanu, C., Van Loosdrecht, M.C. and Heijnen, J.J. (2000) Effect of diffusive and convective substrate transport on biofilm structure formation: A two-dimensional modeling study. Biotechnol Bioeng 69(5), 504-515.
Prosser, J.I. (2015) Dispersing misconceptions and identifying opportunities for the use of 'omics' in soil microbial ecology. Nature Reviews Microbiology 13(7), 439-446.
Quan, K., Hou, J., Zhang, Z., Ren, Y., Peterson, B.W., Flemming, H.-C., Mayer, C., Busscher, H.J. and van der Mei, H.C. (2021) Water in bacterial biofilms: pores and channels, storage and transport functions. Critical Reviews in Microbiology, 1-20.
Rattier, M., Reungoat, J., Keller, J. and Gernjak, W. (2014) Removal of micropollutants during tertiary wastewater treatment by biofiltration: Role of nitrifiers and removal mechanisms. Water Research 54, 89-99.
Reed, D.C., Algar, C.K., Huber, J.A. and Dick, G.J. (2014) Gene-centric approach to integrating environmental genomics and biogeochemical models. Proceedings of the National Academy of Sciences 111(5), 1879-1884.
Reichert, P. (1994) AQUASIM – A TOOL FOR SIMULATION AND DATA ANALYSIS OF AQUATIC SYSTEMS. Water Science and Technology 30(2), 21-30.
Revilla, M., Galán, B. and Viguri, J.R. (2016) An integrated mathematical model for chemical oxygen demand (COD) removal in moving bed biofilm reactors (MBBR) including predation and hydrolysis. Water Research 98, 84-97.
Rittmann, B.E. (1982) Comparative performance of biofilm reactor types. Biotechnol Bioeng 24(6), 1341-1370.
Ross, P.S., van der Aa, L.T.J., van Dijk, T. and Rietveld, L.C. (2019) Effects of water quality changes on performance of biological activated carbon (BAC) filtration. Separation and Purification Technology 212, 676-683.
Schramm, A., de Beer, D., Gieseke, A. and Amann, R. (2008) Microenvironments and distribution of nitrifying bacteria in a membrane-bound biofilm. Environmental Microbiology 2, 680-686.
Schwartz, F.W., Liu, G., Aggarwal, P. and Schwartz, C.M. (2017) Naïve Simplicity: The Overlooked Piece of the Complexity-Simplicity Paradigm. Groundwater 55(5), 703-711.
Seeger, H. (1999) The history of German waste water treatment. European Water Management 2, 51-56.

Shanahan, J. and Semmens, M. (2006) Influence of a nitrifying biofilm on local oxygen fluxes across a micro-porous flat sheet membrane. Journal of Membrane Science 277(1-2), 65-74.
Simpson, D.R. (2008) Biofilm processes in biologically active carbon water purification. Water Research 42(12), 2839-2848.
Sin, G. and Al, R. (2021) Activated sludge models at the crossroad of artificial intelligence—A perspective on advancing process modeling. npj Clean Water 4(1), 16.
Sirotkin, A.S., Koshkina, L.Y. and Ippolitov, K.G. (2001) The BAC-process for treatment of waste water Containing non-ionogenic synthetic surfactants. Water Research 35(13), 3265-3271.
Stewart, P.S. (2012) Mini-review: Convection around biofilms. Biofouling 28(2), 187-198.
Strous, M., Heijnen, J.J., Kuenen, J.G. and Jetten, M.S.M. (1998) The sequencing batch reactor as a powerful tool for the study of slowly growing anaerobic ammonium-oxidizing microorganisms. Appl Microbiol Biotechnol 50(5), 589-596.
Terry, L.G. and Summers, R.S. (2018) Biodegradable organic matter and rapid-rate biofilter performance: A review. Water Research 128, 234-245.
Van Loosdrecht, M.C.M. and Heijnen, S.J. (1993) Biofilm bioreactors for waste-water treatment. Trends in Biotechnology 11(4), 117-121.
Vannecke, T. (2015) Modelling of microbial populations in biofilm reactors for nitrogen removal from wastewater, Ghent University.
Vieira-Silva, S. and Rocha, E.P.C. (2010) The Systemic Imprint of Growth and Its Uses in Ecological (Meta)Genomics. PLOS Genetics 6(1), e1000808.
Wang, J., Ying, X., Huang, Y., Chen, Y., Shen, D., Zhang, X. and Feng, H.J. (2021) Numerical study of hydrodynamic characteristics in a moving bed biofilm reactor. Environmental Research 194, 110614.
Wang, S.-J. and Zhong, J.-J. (2007) Bioprocessing for Value-Added Products from Renewable Resources. Yang, S.-T. (ed), pp. 131-161, Elsevier, Amsterdam.
Wang, S., Zhang, X., Wang, Z.-W., Li, X. and Ma, J. (2014) In-depth characterization of secondary effluent from a municipal wastewater treatment plant located in Northern China for advanced treatment. Water Science and Technology 69(7), 1482-1488.
Wanner, O., Eberl, H., Morgenroth, E., Noguera, D., Picioreanu, C., Rittmann, B. and van Loosdrecht, M. (2006) Mathematical Modeling of Biofilms.
Wanner, O. and Gujer, W. (1986) A multispecies biofilm model. Biotechnol Bioeng 28(3), 314-328.
Weinrich, S., Koch, S., Bonk, F., Popp, D., Benndorf, D., Klamt, S. and Centler, F. (2019) Augmenting Biogas Process Modeling by Resolving Intracellular Metabolic Activity. Frontiers in Microbiology 10.
Wolcott, R.D. and Ehrlich, G.D. (2008) Biofilms and Chronic Infections. JAMA 299(22), 2682-2684.
Worch, E. (2021) Adsorption technology in water treatment, de Gruyter.
Zhang, S., Gitungo, S.W., Axe, L., Raczko, R.F. and Dyksen, J.E. (2017) Biologically active filters – An advanced water treatment process for contaminants of emerging concern. Water Research 114, 31-41.
Zhu, I.X., Getting, T. and Bruce, D. (2010) Review of biologically active filters in drinking water applications. Journal AWWA 102(12), 67-77.
Zhu, L., Chen, T., Xu, L., Zhou, Z., Feng, W., Liu, Y. and Chen, H. (2020) Effect and mechanism of quorum sensing on horizontal transfer of multidrug plasmid RP4 in BAC biofilm. Science of The Total Environment 698, 134236.

Part II: Publications

P1. A multi-component model for granular activated carbon filters combining biofilm and adsorption kinetics

Vanessa Acevedo Alonso, Tobias Kaiser, Roman Babist, Thomas Fundneider, Susanne Lackner. In: Water Research, Volume 197, 1 June 2021, 117079.

https://doi.org/10.1016/j.watres.2021.117079

Abstract

Along with the rise of biological active granular activated carbon (bGAC) filtration as advanced treatment technology for wastewater treatment plant (WWTP) effluents, the mathematical representation of such systems is gaining increasing importance. This work introduces a model that describes the performance of bGAC-filters for Dissolved Organic Carbon (DOC) removal from a WWTP effluent. The DOC removal within bGAC-filters is accomplished by two mechanisms: adsorptive removal and biological transformation. An appropriate representation of the adsorptive removal requires the DOC to be divided into fictive fractions according to its adsorbability. Likewise, a further DOC classification according to its biodegradability is necessary. Modeling a bGAC-filter then becomes a multi-component adsorption problem, with the simultaneous occurrence of DOC degradation within a biofilm. For dealing with this modeling task, this work integrated the Ideal Adsorbed Solution theory into a traditional biofilm model compatible with the Activated Sludge Model Framework. For the description of the adsorption dynamics, a Freundlich isotherm for the equilibrium and a pseudo first order model for the kinetics were selected. The biofilm consisted of heterotrophic bacteria able to oxidize DOC using oxygen as electron acceptor. The correctness of the model was evaluated using experimental data from a pilot plant. The predicted DOC breakthrough curve satisfactorily fitted the experimental measurements for empty bed contact times (EBCT) of 6, 12, 24 and 33 min. Moreover, the model predicted the relationship between EBCT, DOC removal and bGAC-filter lifespan. The developed model is the first that combines multi-component adsorption and biofilm kinetics in a wastewater treatment context.

1. Introduction

Granular activated carbon (GAC) filtration is an established treatment technology in the drinking water sector. With the emergence of more stringent discharge regulations for wastewater, the implementation of GAC-filters as advanced treatment for micropollutants and DOC removal from municipal wastewater has become more important. An interesting feature of GAC-filters is the development of a biofilm on the GAC surface and their transition to biological activate GAC filters (bGAC-filters). Several studies have demonstrated that the presence of such a biofilm may enhance the overall DOC removal as well as the removal of individual micropollutants (Simpson 2008, Yapsakli and Çeçen 2010).

Mass transfer processes in GAC-filters, adsorption equilibria and kinetics have been extensively researched. Several models intending to predict the behavior of GAC-filters for removing organic substances have been published. Chang and Rittmann (1987) presented a model able to describe the removal of a single component in a bGAC-filter, later on Kim and Min

(1993) developed and compared two different modeling approaches for the removal of dissolved organic matter in a biofiltration system. More recently, Shim et al. (2004) provided a review of the models that existed at the time and proposed a new modeling approach, that successfully implemented backwashing of biomass from the GAC-filter bed in a single-component system.

The interactions between wastewater, biofilm, GAC and the processes occurring within are intricate and component specific, which makes mathematical modeling of such a multi-component systems challenging. From the adsorption point of view, there are several models capable to describe the adsorption behavior of complex mixtures. The Ideal Adsorbed Solution (IAS) theory first introduced by Radke and Prausnitz (1972) continues to be one of the most frequently used approaches for describing adsorption in a multi-solute system, as the theory can be applied in combination with any single-solute adsorption isotherm. The IAS theory or extensions of it have been implemented along with conventional breakthrough models. Nowotny et al. (2007) modeled the competitive adsorption between a set of micropollutants and the background organic matter presented in a Wastewater Treatment Plant (WWTP) effluent. Similarly, Worch (2010) compared two model approaches capable of predicting breakthrough curves of multi-component systems, specifically the competition for adsorption between micropollutants and Natural Organic Matter (NOM) in drinking water treatment; Pürschel et al. (2014) in turn, applied the same concept for modeling the NOM removal in anion exchange resins. Schideman et al. (2006) proposed a model with three fictive components for natural waters; this model is capable to describe several competition phenomena between NOM and micropollutants. Nevertheless, the models proposed in all these studies do not account for biofilm growth onto the media surface, thereby neglecting the influence of the biological processes on the filter performance, especially after long-term operation.

Although the mechanisms and the basic mathematical principles are well known for biological and adsorption processes, a comprehensive modeling approach that incorporates both of these concepts is still lacking. The modeling practice in the wastewater field is widely dominated by the Activated Sludge Model (ASM) framework and there is agreement about the need of extending the current framework to include physicochemical models as for instance adsorption (Batstone et al. 2012). However, until now, a standardized methodology for introducing adsorption processes into the ASM-framework is not available.

This paper presents a mathematical model capable of describing the biological GAC- filtration as advanced treatment stage for DOC removal in a municipal WWTP. To the best of our knowledge, our model is the first attempt to combine a multi-component adsorption approach with a biofilm model. The model was developed to be compatible to the ASM framework and is therefore easy to implement and replicate.

2. Model Development

Figure P1.1a shows a schematic representation of a bGAC-filter and its main features. The model describes the flow of wastewater through a fixed bed filter filled with GAC. The GAC-particles are considered to be a rectangular prism instead of a sphere and their surface is able to support the growth of a biofilm. In the same way, adsorbed components (q_i) are considered unavailable for the biological reactions and can be desorbed only if the concentration gradient reverses in the X-axis. Mechanical dispersion in the X-axis was not taken into consideration.

Figure P1.1 b shows the model's X-axis divided into three different compartments: bulk phase, biofilm, and GAC that are linked through diffusive mass transport.
The mass transfer resistances are connected in series and include the diffusion from the bulk phase to the biofilm through a liquid boundary layer, within the biofilm and within the GAC-particle. The vertical dashed lines in the figure mark points on the X-axis. These points indicate the location of the interfaces between compartments and their corresponding abbreviations.
In the specific case of biodegradable substances, the consumption within the biofilm is also considered. As a simplification of the mass transfer phenomena, the concentration of qi is assumed to be homogeneous in the GAC-particle and to be located exclusively at the end of the GAC compartment (at X = R). This means that the surface diffusion is not considered and equation P1.1 holds:

$$\frac{\partial q_i}{\partial x} = 0 \qquad \text{(P1.1)}$$

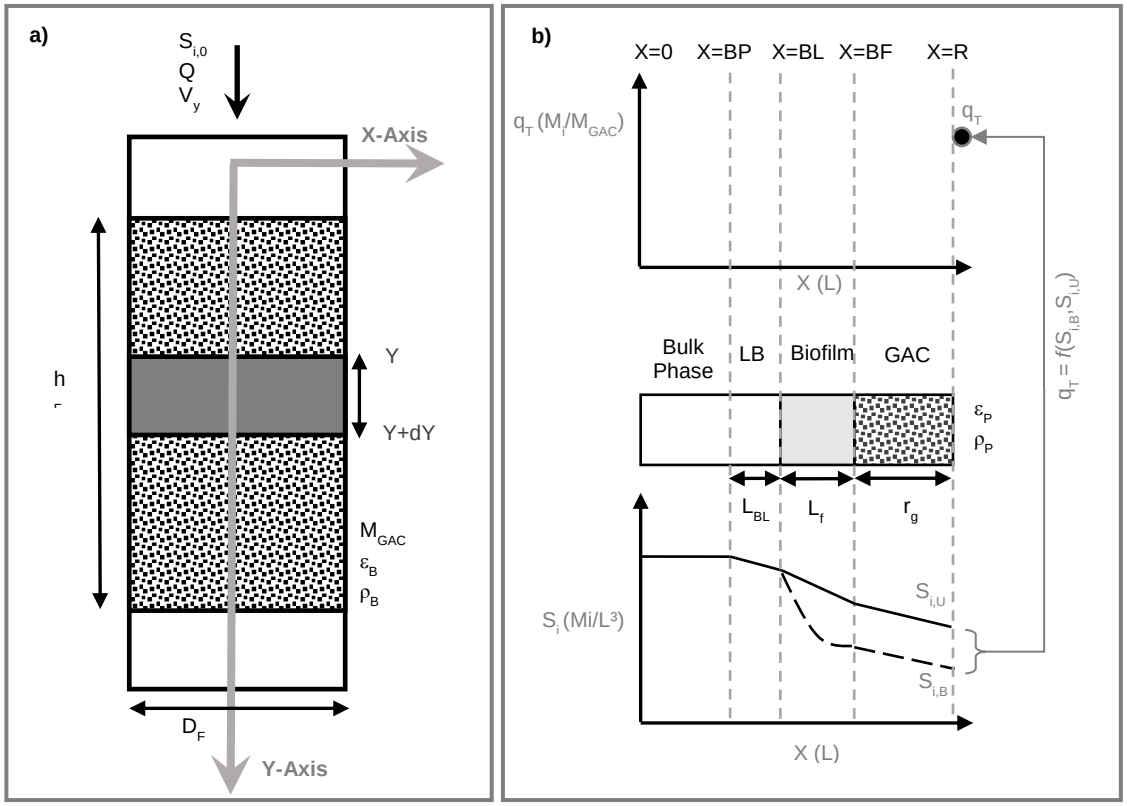

Figure P1. 1. a) Schematic representation of the modeled system, including the relevant dimensions of the bGAC-Filter. b) Description of the compartments along the X-axis, and the mass transfer and adsorption equilibrium assumptions made in the model. The upper part shows the X coordinates of the interfaces between compartments, the middle schema shows the three compartments in the X-axis: bulk phase, biofilm and GAC, it also includes the Liquid Boundary Layer (BL) between the bulk phase and the biofilm. The bottom diagram shows the theoretical concentration profiles of a non-biodegradable substance ($S_{i,U}$) and a biodegradable one ($S_{i,B}$) along the X-axis. The concentration profiles are based on the assumption that $S_{i,U}$ and $S_{i,B}$ are equally adsorbable and have the same diffusion coefficient

Finally, Figure P1.1b also shows that the model uses several dissolved components differentiated according to their adsorbability and biodegradability ($S_{i,U}$ and $S_{i,B}$) whereas for the adsorbed phase a lumped variable for the total adsorbed DOC concentration (q_T) is introduced. The dissolved and adsorbed variables are related through a multi-component equilibrium isotherm. The system is a non-steady state system, due to the accumulation of adsorbed DOC in the GAC and the continuous growth of biofilm.

2.1. Fractionation of the Influent

The model is meant for predicting the behavior of the DOC concentrations during bGAC treatment. Similar to the chemical oxygen demand (COD) fractionation in ASM type models (Henze et al. 2006), the first step in developing this model was a fractionation of the DOC. DOC was divided into several fictive fractions according to its biodegradability and adsorbability. This step is the one that allows the model to describe a multicomponent adsorption.
Initially, the DOC was divided into two fractions depending on its biodegradability: biodegradable and non-biodegradable. Subscript B refers to the biodegradable fractions, whereas subscript U refers to the non-biodegradable ones. According to this classification, the model has two types of dissolved state variables $S_{i,B}$ and $S_{i,U}$. Likewise, the DOC can also be divided into fictive fractions according to its absorbability as described in the work of Johannsen and Worch (1994). Using this adsorption analysis the AdsANA software (version 1.5) was developed (Worch 2016). AdsANA fits experimental data to a multicomponent Freundlich-Isotherm based on the IAS theory. For the fractionation of DOC in municipal WWTP effluents, the use of five fictive fractions is suggested (Fundneider 2020). As result of the fractionations, the influent DOC in our model is represented by 10 different state variables, since both, the biodegradable and non-biodegradable DOC were also classified according to their adsorbability.

2.2. Mass Balances

To completely describe the GAC-system, an individual mass balance for the dissolved and adsorbed components is required. In the same way, a single mass balance for each model compartment (BP, BF, and GAC) in the X-axis is needed. Equation P1.2 shows the mass balance for the dissolved components in the bulk phase:

$$\frac{\partial S_{i,BP}}{\partial t} = V_y \frac{\partial S_{i,BP}}{\partial y} - D_{BP,i} \frac{\partial^2 S_{i,BP}}{\partial x^2} \qquad \text{(P1.2)}$$

The right hand side of the equation P1.2 shows the advection term along the Y-Axis (filter depth) and the diffusion through the liquid boundary layer. To be solved the equation P1.1 needs an initial condition, one boundary condition for the Y-axis and two for the X-axis. The initial condition, the boundary condition for the Y-axis and one for the X-axis are given by $S_{i,BP}$ (t=0, X,Y)= $S_{i,BP}$ (t, X,Y=0) = $S_{i,BP}$ (t, X=0,Y) =Si,0, respectively.

The second boundary condition in the X-axis corresponds to the mass transfer at the interface between bulk phase and biofilm surface i.e. the liquid boundary layer (X=BL). It can be described as follows:

$$D_{BP,i}\frac{\partial S_{i,BP}}{\partial x} = \frac{D_{BP,i}}{L_{BL}}\left(S_{i,BP} - S_{i,BL}\right) \qquad \text{(P1.3)}$$

The area relevant to this boundary condition is the one from the biofilm (ABF).

Equation P1.4 describes the mass balance in the biofilm for the dissolved components:

$$\frac{\partial S_{i,BF}}{\partial t} = D_{BF}\frac{\partial^2 S_{i,BF}}{\partial x^2} - v_{i,bio}\gamma_{i,bio} \qquad \text{(P1.4)}$$

Where $\gamma_{i,bio,}$ is the biodegradation rate and the $v_{i,bio}$ is the respective stoichiometric parameter. Alongside with biodegradation, equation P1.4 includes the mass entering the biofilm from the liquid boundary layer as well as the mass leaving to the GAC.

Equation P1.4 requires an initial condition and two boundary conditions for the X-axis. We assume that at the beginning of the operation the biofilm is free from any substance Si and hence the initial condition reads $S_{i,BF}$ (t=0, X,Y) = 0.

The first boundary condition at X=BL describes the flux of Si entering the biofilm:

$$D_{BP,i}\frac{\partial S_{i,BF}}{\partial x} = \eta_{BF}\frac{D_{BP,i}}{L_F}\left(S_{i,BL} - S_{i,BF}\right) \qquad \text{(P1.5)}$$

As equation P1.5 states, the diffusion coefficient for the biofilm is lesser than in the bulk phase and is decreased by an empirical factor (η_{BF}). The area relevant to this boundary condition is the one from the biofilm (A_{BF}).

The second boundary condition is found at the interface between the biofilm and the GAC (X=BF) and is written in equation P1.6:

$$D_{BP,i}\frac{\partial S_{i,BF}}{\partial x} = \frac{\varepsilon_P}{\tau}\frac{D_{P,i}}{r_g}\left(S_{i,BF} - S_{i,R}\right) \qquad \text{(P1.6)}$$

Here the diffusion has to be related to the porosity of the GAC particle and decreased by a tortuosity factor, which reflects the heterogeneity of the GAC pores.The corresponding area to this boundary condition is the thus internal GAC surface (A_{GAC}).

Finally, equation P1.7 shows the mass balance of the dissolved components in the GAC.

$$\frac{\partial S_{i,GAC}}{\partial t} = D_{GAC}\frac{\partial^2 S_{i,GAC}}{\partial x^2} - v_{i,ad}\gamma_{i,ad} - v_{i,des}\gamma_{,i,des} \qquad \text{(P1.7)}$$

$\gamma_{i,ad}, \gamma_{i,des}$ are the adsorption, and desorption rates. The terms $v_{i,ad}, v_{i,des}$ correspond adsorption and desorption stoichiometric parameters. Equation P1.7 is associated with one initial condition and two boundary conditions in the X-Axis. Similarly to the mass balance in the biofilm it is assumed that the GAC does not content any substance Si at the beginning of the operation and hence Si,GAC (t=0, X,Y) = 0. Given that the GAC and biofilm have a common interface, the boundary condition described in equation P1.6 must be also valid for equation P1.7. The end of the GAC compartment (X=R) corresponds to an impermeable limit and the second boundary condition should satisfy equation P1.8:

$$\frac{\partial S_{i,GAC}}{dx} = 0 \qquad \text{(P1.8)}$$

Given that adsorbed components appear only in the GAC compartment, the mass balance has to be conducted only in this compartment as shown in equation P1.9:

$$\frac{\partial q_{i,t}}{\partial t} = v_{i,des,q}.\gamma_{i,des} + v_{i,ad,q}\gamma_{ad} \qquad \text{(P1.9)}$$

Here the rates ($\gamma_{i,ad}, \gamma_{i,des}$) are the same as in the equation P1.7, however the stoichiometric parameters are specific for the adsorbed components and hereby different from the ones of the dissolved components.

2.3. Adsorption Equilibrium and Kinetics

The mass balances in the GAC compartment (equations P1.7 and P1.9) require a kinetic expression that gives γ_{ad} i.e. the rate at which adsorption occurs. The Pseudo First Order (PFO) model as described in Guo and Wang (2019) was used to describe the adsorption kinetics. Equation P1.10 shows the PFO expression.

$$\gamma_{i,ad} = k_{PFO}\left(q_{i,e} - q_{i,t}\right) \qquad \text{(P1.10)}$$

Where $q_{i,e}$ is the adsorbed concentration of a component i at equilibrium and $q_{i,t}$ at a given time t. PFO model requires as well an expression capable of predicting the adsorption equilibrium. In accordance to the fractionation methodology, the Freundlich-Isotherm was selected to describe the adsorption equilibrium of the DOC-fractions onto the activated carbon. Equation P1.11 is the mathematical expression of the isotherm:

$$q_{i,e} = K_{f,i} * S_{i,e}^{n_f} \qquad \text{(P1.11)}$$

Where $K_{f,i}$ is the Freundlich constant and n_f is the Freundlcih coefficient. In the case of the adsorbable components, instead of an individual q_i [M_{DOC}/M_{AC}], our model uses a lumped parameter q_T [M_{DOC}/M_{AC}] that represents the total adsorbed DOC concentration, equation P1.10 thus becomes:

$$\gamma_{ad} = k_{PFO}\left(q_{T,e} - q_{T,t}\right) \qquad \text{(P1.12)}$$

In order to calculate q_T a multicomponent isotherm has to be applied. For this purpose and according to the influent fractionation methodology, we selected the approach proposed by the IAS theory. q_T is given by single-component adsorbed concentrations (q_{i0}) calculated at a specific spreading pressure (φ [Mi/MAC]), which corresponds to the φ of the multicomponent system. Additionally, the mass fraction of the adsorbed components (z_i [-]) is also required. The original IAS theory defines zi as the molar fraction of the adsorbed components, however

in this work the mass fraction for the components are fictive and the exact molar mass is unknown. Equation P1.13 shows the expression used for calculating q_T.

$$q_T = \left[\sum_{i=1}^{N} \frac{z_i}{q_{i,B+U}^0}\right]^{-1} \qquad \text{(P1.13)}$$

In order to solve equation P1.13, the IAS theory has to be combined with the Freundlich isotherm (equation P1.11). Assuming a constant φ , and the same nf for all the single solute isotherms we obtain equation P1.14:

$$\varphi = \frac{1}{n_f}\left[\sum_{i=1}^{N} S_{i,B+U} K_{f.i}^{\frac{1}{n_f}}\right]^{n_f} \qquad \text{(P1.14)}$$

After calculating the spreading pressure, it is possible to compute the term zi as described in equation P1.15:

$$z_i = \frac{S_i}{\left(\frac{\varphi n_f}{K_{f,i}}\right)^{\frac{1}{n_f}}} \qquad \text{(P1.15)}$$

For calculating the multicomponent isotherm, both biodegradable and non-biodegradable components are treated as one according to their adsorbability (e.g $S_{G,B}$ and $S_{G,U}$ are considered as one fraction).

2.4. Desorption Kinetics

Analogous to the case of the adsorption kinetics a first order kinetic rate is applied for describing the desorption of adsorbed components back into the bulk phase as presented in Sutikno and Himmelstein (1983).

$$\gamma_{des} = k_{des} \frac{\varepsilon_p}{\rho_p}\left(\sum_{i=1}^{n} S_{i,e} - \sum_{i=1}^{n} S_{i,t}\right) \qquad \text{(P1.16)}$$

Where $S_{i,e}$ is the concentration of a component i at equilibrium and $S_{i,t}$ at a given time t. In correspondence to the lumped parameter q_T the algebraic summation of the dissolved components has to be used for the calculation of the desorption rate.

2.5. Biological Growth

The model assumes a simplified biofilm that is formed by only one microbial species, which is capable of degrading DOC using oxygen as electron acceptor. Biodegradation takes places within a multi-layer biofilm and follows a Monod type growth equation. Microbial growth and biodegradation in the bulk phase were neglected. Biomass decay follows a first order kinetic and biomass detaches according to the biofilm detachment approach implemented in the process unit “Trickling Filter” of the simulation software SUMO19 © (Dynamita 2020). Unlike

other conventional biofilm models, this approach assumes a constant biofilm thickness (L_f) during the whole operation period and let the biomass concentration increase until a maximal concentration ($X_{HB,SP}$) is reached. Afterwards detachment starts and so X_{HB} equals $X_{HB,SP}$ until the end of the operation. Equation P1.17 shows the mathematical description of the processes involved in the biological growth as implemented in SUMO19 ©.

$$\frac{\partial X_{HB}}{\partial t} = \left[\int_0^{L_f} \left(\mu_{max}\frac{S_{i,B}}{S_{i,B}+K_{aff,i}} - b_{HB}\right) dL_f - \left(k_{att} - \frac{r_{det}}{L_{BL}}\right)\right] A_{BF} \cdot X_{HB} \qquad \text{(P1.17)}$$

where: $r_{det} = \frac{1}{1+e^{(X_{HB}-X_{HB,SP})}}$

Although at the beginning of the operation GAC does not have biofilm on the surface, the model assumes that biofilm is present on the external GAC surface from t=0 onwards. The biodegradation rate presented in the mass balance of the dissolved components in the biofilm (equation P1.4) corresponds to the term associated to the consumption of S_i and thus equation P1.18 holds:

$$\gamma_{bio} = \mu_{max}\frac{S_{i,B}}{S_{i,B}+K_{aff,i}} \qquad \text{(P1.18)}$$

2.6. Stoichiometric Parameters

On the one hand, the stoichiometric coefficient $v_{i,bio}$ is the same for all the biodegradable components $S_{i,B}$ and links the microbial growth of the heterotrophic biomass X_{HB} with the consumption of DOC as electron donor and oxygen as electron acceptor.

$$v_{i,bio} = -\frac{1}{Y_{HB,i}} \qquad \text{(P1.19)}$$

On the other hand $v_{i,\mathrm{ad}}$ and $v_{i,\mathrm{ad,q}}$ link the concentration of the adsorbed components (q_T) with the concentration of the dissolved ones (S_i). As the model assumes, that the adsorption takes place in the pores of the GAC, for the transformation of q_T into Si the GAC material density (ρ_M) and its particle porosity (ε_P) are required. In addition to that, z_i is use for the allocation of the lumped adsorbed variable q_T to each individual S_i.

$$v_{i,ad} = -z_i\left[\rho_M\frac{(1-\varepsilon_P)}{\varepsilon_p}\right] \qquad \text{(P1.20)}$$

The parameter $v_{i,\mathrm{des}}$ can be similarly defined as $v_{i,\mathrm{ad}}$ in equation P1.20. However, $v_{i,\mathrm{des}}$must be positive, which indicates an increase in the dissolved concentration.

As $v_{i,\mathrm{ad,q}}$ and $v_{i,\mathrm{des,q}}$link q_T directly with itself, they equal one. However, $v_{i,\mathrm{des,q}}$ must be positive, which indicates a decrease in the adsorbed concentration.

2.7. ASM Framework Implementation

Analogous to an ASM model, the rates of all the transformation processes taking place in the system (equations P1.11, P1.15 and P1.17) can be summarized in a Petersen-Matrix as showed in Tables P1.1 and P1.2. Traditionally ASM models use COD as basic unit, however due to the low concentration that characterizes WWTP effluents Total Organic Carbon (TOC) is the preferred parameter for determining the organic matter content. Our model in consequence uses TOC instead of COD and follows the methodology proposed in Henze et al. (2006)

Table P1. 1. Petersen-Matrix for the model developed in this work Part I: Rates used in the stoichiometric model.

	RATE	UNITS
R1 ADSORPTION	$k_{PFO}\left(q_{T,e} - q_{T,t}\right)$	$\frac{\text{mgTOC}}{\text{g}_{\text{GAC}} \cdot \text{d}}$
R2 BIODEGRADATION	$\mu_{max} \frac{S_i}{S_i + K_{aff,i}} \frac{S_{O2}}{S_{O2} + K_{aff,O2}} X_{HB}$	$\frac{\text{mgTOCx}}{\text{m}^3 \cdot d}$
R3 DESORPTION	$k_{des} \frac{\varepsilon_p}{\rho_p} \left(\sum_{i=1}^{n} S_{i,e} - \sum_{i=1}^{n} S_{i,t} \right)$	$\frac{\text{mgTOC}}{\text{m}^3 \cdot \text{d}}$
R4 BIOMASS DECAY	$b_{HB} X_{HB}$	$\frac{\text{mgTOCx}}{\text{m}^3 \cdot d}$
R5 HYDROLYSIS OF ENTRAPPED ORGANICS	$k_h \frac{\frac{X_S}{X_{HB}}}{\left(K_X + \frac{X_S}{X_{HB}}\right)} X_{HB}$	$\frac{\text{mgTOC}}{\text{m}^3 \cdot d}$

Table P1. 2. Petersen-Matrix for the model developed in this work Part II: Stoichiometric parameters and elementary composition.

	S_i	S_{O2}	q_T	X_{HB}	X_I	X_S
	$\frac{mgDOC}{m^3}$	$\frac{mgDOC}{m^3}$	$\frac{mgDOC}{g_{GAC}}$	$\frac{mgTOCx}{m^3}$	$\frac{mgTOC}{m^3}$	$\frac{mgTOC}{m^3}$
R1	$-z_i\left[\rho_M\frac{(1-\varepsilon_P)}{\varepsilon_p}\right]$		1			
R2(*)	$-\frac{1}{Y_i}$	$\frac{(iCOD_x - iCOD_{Si})}{Y_i}$		1		
R3	$z_i\left[\rho_M\frac{(1-\varepsilon_P)}{\varepsilon_p}\right]$		-1			
R4				$-\frac{f_p iCOD_{Si}}{iCOD_{Si} - iCOD_X}$	f_p	$\frac{f_p iCOD_{Si}}{iCOD_{Si} - iCOD_X - f_P}$
R5	1(**)					-1
ELEMENTARY COMPOSITION						
TOC	1	$\frac{(1-Y_i)}{Y_i(iCOD_x - iCOD_{Si})}$	$\left[\rho_M\frac{(1-\varepsilon_P)}{\varepsilon_p}\right]$	1	1	1

(*) R2 is only relevant for all the $S_{i,B}$ components. In the cases of $S_{i,U}$ components all the stoichiometric parameters for R2 equal zero. (**) this stoichiometric parameter is only valid for $S_i = S_{N,B.}$ For all other Si components, this parameter equals zero.

3. Model Implementation

The model was implemented using the developing platform offered by SUMO19 © (Dynamita 2020). A new process model was generated based on the model's Petersen-Matrix presented in Tables P1.1 and P1.2.Additionally, the existing process unit "Trickling Filter" was modified, so it can be employed as a bGAC-filter.

In the original "Trickling Filter" process unit, the filter is divided into three compartments along the Y-axis and, likewise the biofilm is divided into an n number of layers (along the X-axis). For modeling the advective transport, the vertical compartmentalization was kept as in the original unit, whereas a further layer in the X-axis was added to represent the GAC. The GAC-layer acts as supporting material of the biofilm and only adsorption and desorption processes take place within. As mentioned in section 2.2, A_{GAC} and A_{BF} were differentiated and implemented in the corresponding mass transport processes. The biofilm model incorporated in the original process unit "Tricking Filter" was maintained. This section explains the basic principles of this particular biofilm model. Values of the biofilm parameters were, however, adapted to the specific simulated system. Table P1.3 summarizes the input parameters used in the modified process unit as showed in the SUMO19 © interface:

Table P1. 3. Parameters used in the modified process unit "Trickling Filter" in the simulation software SUMO19 ©

Symbol	Name	Units	Value	Reference
Filter Settings				
A_F	Transversal area of the filter	m²	0.02	(Fundneider 2020)
h_F	Filter bed depth	m	2.5	(Fundneider 2020)
LRT	Liquid residence time	min	Variable according to the EBCT	(Fundneider 2020)
Biofilm and media parameters				
$A_{GAC,s}$	GAC specific surface	m²/g	1199	(Fundneider 2020)
r_g	GAC grain radio	m	$7.25\ 10^{-4}$	(Fundneider 2020)
n	Number of biofilm layers	-	3	This work
L_{BL}	Boundary layer thickness	m	$6\ 10^{-5}$	This work
L_f	Biofilm thickness	m	$5.0\ 10^{-6}$	This work
$X_{HB,SP}$	X_{HB} concentration set point	mgTSS/m²	4000	(Dynamita 2020)
τ	GAC-tortuosity	m³/m³	6	(Sontheimer et al. 1987)
Mass transfer in biofilm				
D_{DOC}	Diffusivity of DOC	cm²/s	0.000056	(Kim and Pirbazari 1989)

A comprehensive description of the kinetic parameters and the process unit parameter used in the model as well as the characteristics of the GAC are available in Table P1.6 in the supplementary material.

4. Model Evaluation

Experimental data collected at the pilot plant described in Fundneider (2020) were used to evaluate the developed model. The pilot plant treated the effluent of a conventional municipal WWTP. The performance of the plant for advanced removal of DOC and organic micropollutants was tested over a period of approximately three years. The pilot plant consisted of six GAC-filters all of which showed evidence of biofilm formation and biological DOC removal. The filters operated with different GAC types, pretreatments and EBCTs. For the evaluation of the model, the data from the filter that operated with Hydraffin-AR (Donau Carbon), cloth

and membrane filtration (Mecana Umwelttechnik GmbH and Pall Corporation, respectively) as pretreatment and EBCT ranging between 6 and 33 min were selected.

As first step for this modeling exercise, the DOC of the WWTP effluent was fractionated into five fictive fractions using the adsorption analysis software AdsANA version 1.5 (Worch 2016). Table P1.4 summarizes the Freundlich coefficients selected for the fractionation and defines the DOC fractions implemented in the model.

Table P1. 4. Freundich isotherm parameters of the fictive fractions used in the DOC fractionation of the influent of the bGAC-filters using Hydrafin-AR. (Fundneider 2020)K_f is the Freundlich coefficient and n_f the Freundlich exponent. Fractionation was conducted using the adsorption analysis tool available in AdsANA.

Symbol	Classification (- Absorbable)	K_f $\left[\frac{mgDOC}{gGAC}\right]\left[\frac{mgDOC}{m^3}\right]^{-1}$	n_f [-]	DOC Fraction [%]
VG	Very Good	32	0.25	13
G	Good	18	0.25	37
M	Moderately	11	0.25	20
P	Poorly	3.6	0.25	10
N	Non	0.0	0.25	20

It is important to note, that the fractionation resulted from an isotherm analysis, and thereby it is specific not only for the wastewater but also for the GAC type used in the filter. In the same way, the biodegradable fraction was determined using the results delivered in the experiments conducted by Fundneider (2020). The author found that approximately 20% of the total WWTP effluent's DOC could be biologically removed by a pre-adapted biomass. Combining these result with those from the absorption analysis (Table P1.4) we obtained the fractionation for the WWTP effluent, i.e. the influent to the bGAC-filters as shown in Table P1.5

Table P1. 5 .DOC fractionation for the influent to the bGAC–Filter using Hydrafin-AR. The first subscript stand for the adsorbability of the fraction and the second one for its biodegradability. VG: Very Good, G:Good, M: Moderately, P:Poor, N:non, B: Biodegradable and U: Non-Biodegradable

	DOC Fraction [%]		DOC Fraction [%]
$S_{VG,B}$	2.6	$S_{VG,U}$	29.6
$S_{G,B}$	7.4	$S_{G,U}$	16.0
$S_{M,B}$	4.0	$S_{M,U}$	8.0
$S_{P,B}$	2.0	$S_{P,U}$	4.0
$S_{N,B}$	10.4	$S_{N,U}$	16.0

After fractionation, the model was tested with a bGAC-filter simulated as described in Table P1.3 with an EBCT of 24 min. The kinetic constants of both adsorption and desorption (k_{PFO} and k_{des}) processes were varied until a good qualitative agreement between the simulated and experimental data was obtained. To validate the fitted parameters, two further bGAC-fiterls were simulated with EBCTs of 12 and 33 min.

Figure P1.2 is a first visual inspection of the goodness of fit of the model, it compares the results delivered by the model at three different EBCTs. For EBCTs equal to 12 and 24 min, the simulated DOC concentration follows the trend of the experimental data, yet a difference between modeled and experimental data can be observed between days 30 and 120. The Root Mean Squared Error (RMSE) was 0.9 for these two EBCTs. For an EBCT of 33 min the deviation between experimental and modeling results during the starting phase becomes more severe. Nevertheless, afterwards a good fit is obtained. The poorer overall fit of the model for an EBCT of 33 min is reflected in a RMSE of 1.4. Given that L_f is a constant and biomass concentration is almost negligible at the beginning of the operation (see Figure P1.1 in the supplementary material), the observed deviations between simulated and measured data suggest an anomaly in the adsorptive removal modeling rather than in the modeling of the biological processes.

A possible explanation for this behavior is that the PFO kinetic model does not adequately describe the initial stage of the adsorption. It has been shown that for complex systems a mixed order model might better describe the adsorption kinetics rather than a simplified PFO model (Guo and Wang 2019). Moreover, a Pseudo Second Order kinetic model is believed to be more appropriate in periods when a rapid change in the concentration in the bulk phase due to the adsorption occurs, as for instance in the initial adsorption stages (Marczewski 2010). Likewise, Yao and Chen (2015) demonstrated for single solute systems that in the early stages the adsorption follows a PSO-like kinetic rate, whereas at the late stages a PFO-like kinetic rate applies. It was not possible in the analyzed pilot plant to differentiate between the adsorptive removed DOC and the biologically removed DOC. This makes the determination of suitable adsorption kinetics difficult. The determination of the adsorption kinetics had to be based on assumptions and relied on a fitting procedure. Thus, further research is required to improve the model performance during the initial adsorption stages.

For all the evaluated EBCTs, approximately 20% of the total DOC is removed neither by biological nor by adsorptive processes and it breaks through shortly after the beginning of the operation (first operation day). Subsequently, the concentration gradually increases and after a certain time (depending on the EBCT), it flattens out. Due to the biological activity, in both experimental and simulated data, the filters continue removing DOC even after the GAC is saturated. Figures P1.2d to P1.2f illustrate the effect of the EBCT on the DOC removal and the filter lifespan. The longer the EBCT the better the removal and the later the filters become saturated.

In order to prove the rationality of the model structure, the breakthrough curves of the individual fictive DOC fractions were analyzed. The ratio between the effluent concentration S_i and the initial concentration $S_{i,0}$ ($S_i/S_{i,0}$) was used for a better visualization of the results. Figures P1.3a to P1.3e depict the modelled $S_i/S_{i,0}$ for each DOC fraction at an exemplary EBCT of 24

min. Figure P1.3a shows the non-adsorbable DOC fractions ($S_{N,U}$ und $S_{N,B}$), it is clear that $S_{N,U}$ is completely inert and flows through the bGAC-filter intact. In contrast $S_{N,B}$ is not removed initially, but from approximately day 150 onwards, it starts being consumed by the biofilm. Day 150 corresponds to the time when the biomass concentration X_{HB} reaches the selected $X_{HB,SP}$ i.e. the biofilm reaches the steady state. Figure P2.6 in supplementary material shows the development of X_{HB} in the biofilm for all the evaluate EBCTs. The time at which the biofilm is fully developed ($X_{HB} = X_{HB,SP}$) for each EBCT can be clearly recognized in this figure.

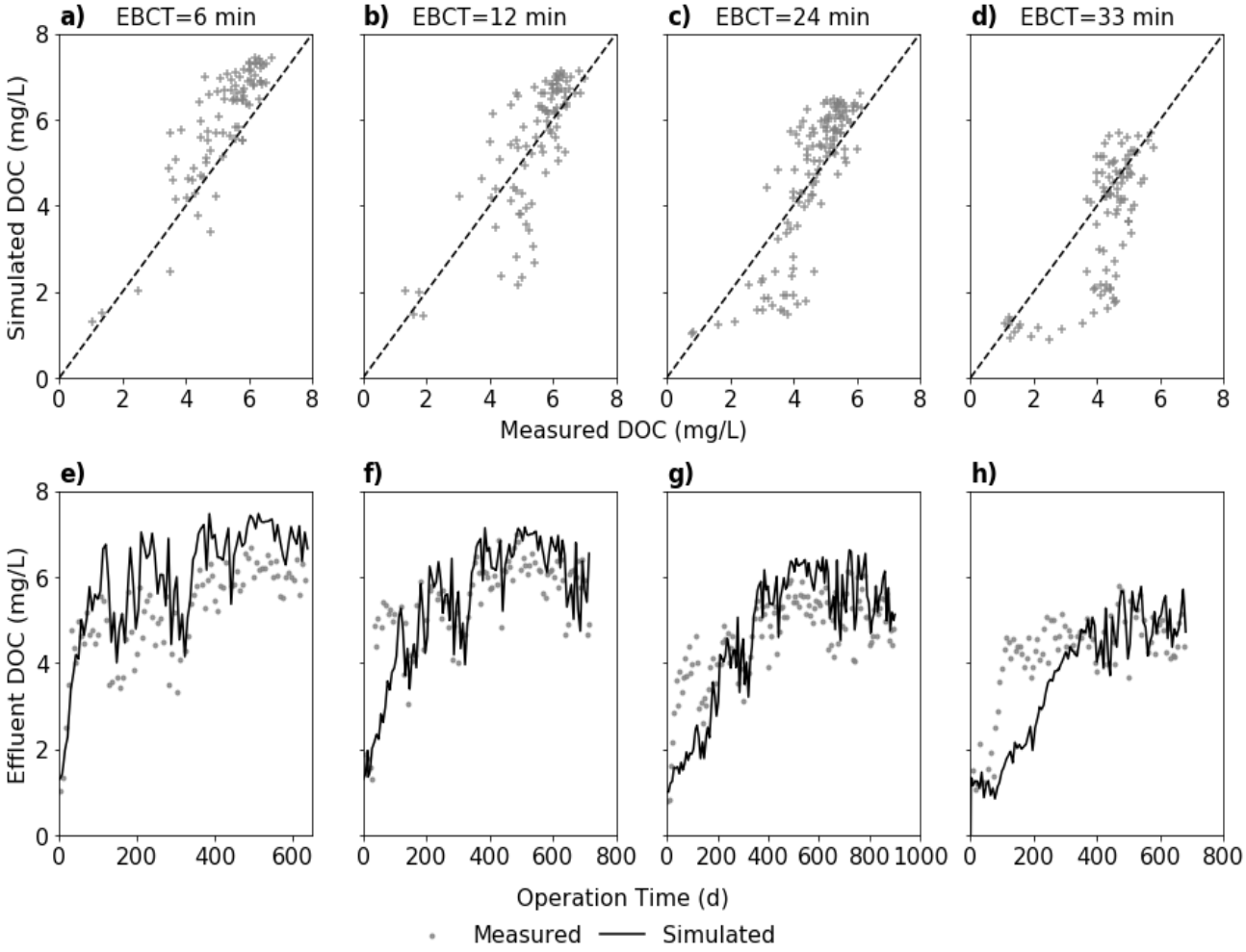

Figure P1. 2. Evaluation of the modeling results. a), b), c), d) direct comparison of the simulated and measured effluent DOC concentrations and e), f), g), h) comparison over the operation time of the simulated and measured DOC effluent concentrations, for EBCTs equal to 6, 12, 14 and 33 min respectively.

Figures P1.3b and P1.3c illustrate the poorly and moderately adsorbable fractions ($S_{P,U}$, $S_{P,B}$, $S_{M,U}$, $S_{M,B}$), and Figures P1.3d and P1.3e the good and very good adsorbable fractions ($S_{G,U}$, $S_{G,B}$, $S_{VG,U}$, $S_{VG,B}$). Similarly, to Figure P1.3a the point at which the biological removal starts can be recognized as well as the strong effect of the temperature on the biological removal. When the temperature decreases the biological removal decreases along with it. The occurrence of desorption is also recognizable in Figures P1.3a to P1.3e, when the S_i/S_{i0} ratio takes values higher than one. If the GAC is nearly saturated and the influent concentration decreases,

desorption will occur. As shown in the Petersen-Matrix (Tables P1.1 and P1.2) the desorption dynamics depend on the lumped adsorbed concentration (q_T), which results in an equal desorption rate for all the DOC fractions. However, desorption stoichiometry depends on the adsorbed mass fraction (z_i), which is particular for each DOC fraction. This in turn causes that the good adsorbable DOC fractions ($S_{VG,U}$, $S_{VG,B}$, $S_{G,U}$, $S_{G,B}$) tend to desorb more than the poorly adsorbable ones ($S_{M,U}$, $S_{M,B}$, $S_{P,U}$, $S_{P,B}$). The dependency on z_i also guarantees that the non-adsorbable DOC fractions do not desorb, as it is to be expected.

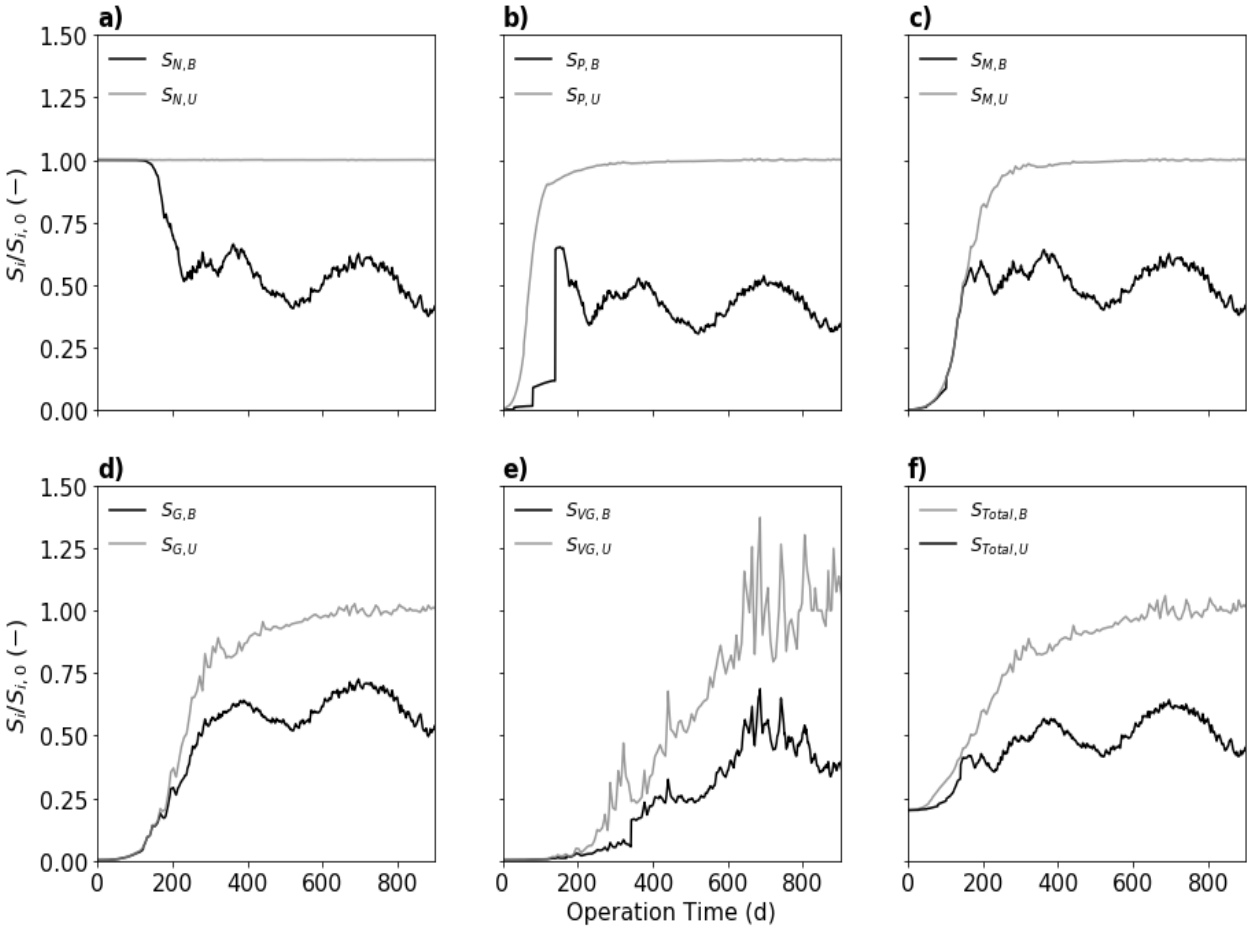

Figure P1. 3. Effluent concentration to influent concentration ratios (S_i/S_{i0}) for the fictive DOC fractions for an EBCT of 24 min. a) Non-adsorbable: biodegradable ($S_{N,B}$) and non-biodegradable ($S_{N,U}$) DOC fractions. b) Poorly adsorbable: biodegradable ($S_{P,B}$) and non-biodegradable ($S_{P,U}$) DOC fractions. c) Moderately adsorbable: biodegradable ($S_{M,B}$) and non-biodegradable ($S_{M,U}$) DOC fractions. d) Good adsorbable: biodegradable ($S_{G,B}$) and non-biodegradable ($S_{G,U}$) DOC fractions. e) Very good adsorbable: biodegradable ($S_{VG,B}$) and non-biodegradable ($S_{VG,U}$) DOC fraction and f) Total biodegradable ($S_{Total,B}$) and total non-biodegradable ($S_{Total,U}$) DOC fractions.

Finally, Figure P1.3f illustrates the breakthrough curves of the total biodegradable ($S_{Total,B}$) and the total non-biodegradable ($S_{Total,U}$) DOC fractions. For the simulated systems, Fundneider (2020) was able to experimentally observe the influence of the temperature on the removal of

biodegradable organic micropollutants, however temperature effect on the total DOC breakthrough curve was not as pronounced. This was also the case of the modeling results as Figure P1.3f displays.

Animation 1 shows the advective-diffusive fronts for the total DOC in the bGAC-filters operated at the EBCTs of 6, 12, 24 and 33 min. In the color maps shown in Figure P1.4a, the Y-axis corresponds to the filter depth and the X-axis to the model structure explained in Figure P1.1. The color at any (X,Y) coordinate in the plots indicates the ratio between the DOC concentration at this coordinate ($S_{DOC,x,y}$) and its corresponding influent concentration ($S_{DOC,0,x=0,y=0}$). Red represents a ratio of 1 (no DOC removal) while dark green a ratio of 0 (complete DOC removal). Additionally, Figures P1.4b and P1.4c show the progression of the DOC influent concentration and water temperature over an operation period of 700 days, respectively. These two plots help to visualize how sudden influent concentration and temperature changes affect the model behavior.

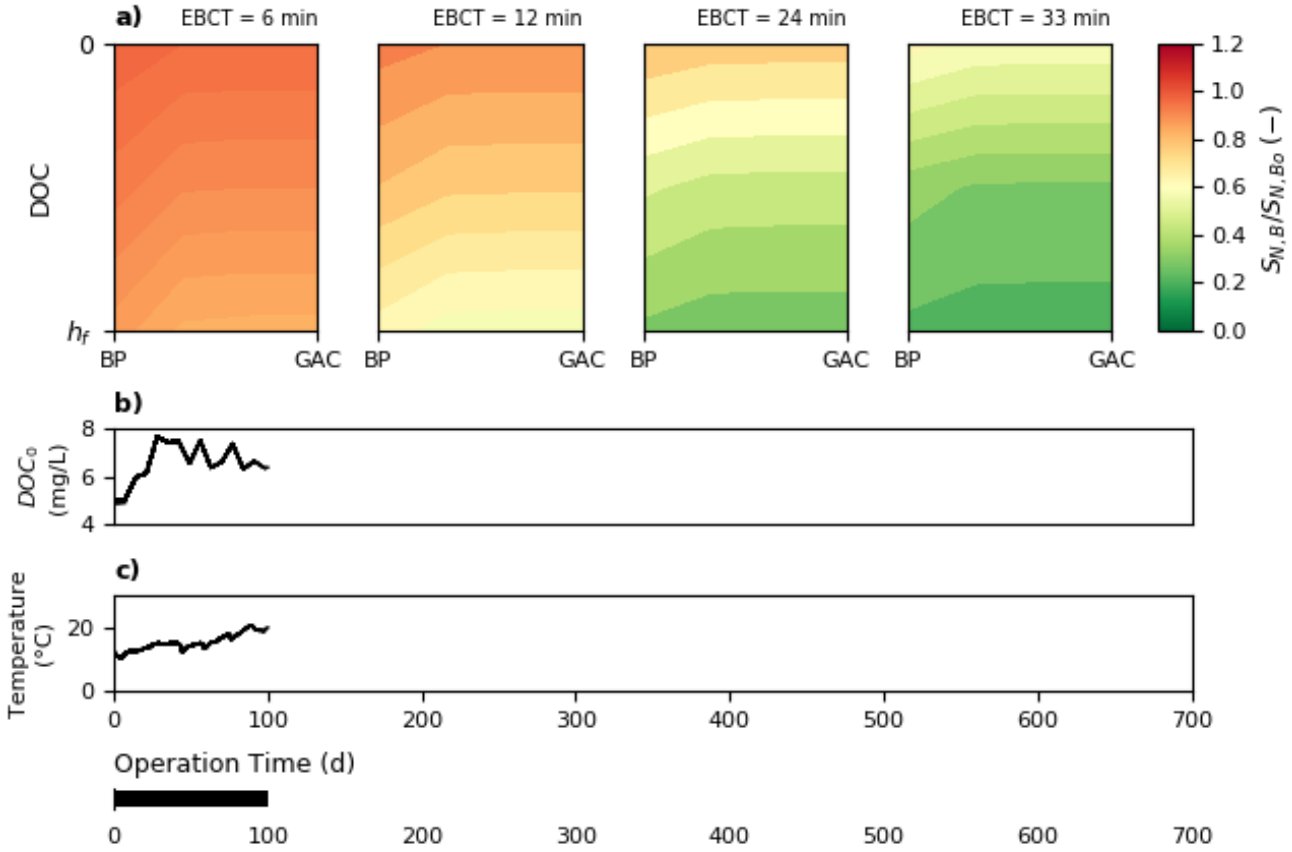

Figure P1. 4. Thumbnail of Animation 1. a) Advective fronts for the DOC at evaluated EBCTs: 6, 12, 24, 33 min. X-axis covers from the Bulk Phase (BP) until the Granular Activated Carbon (GAC).Y-axis is the filter depth with Y=0 as inlet and Y=hf as outlet. b) Time series for influent DOC concentration and c) water temperature.

Animation 2 is built in the same manner as animation 1 and serves as a complement to it. Animation 2 shows the advective-diffusive fronts of the non-adsorbable and biodegradable ($S_{N,B}$) and the very good adsorbable and non- biodegradable ($S_{VG,U}$) DOC fractions. In animation 2, for the $S_{N,B}$ fraction, it can be seen that regardless of the EBCT no removal occurs within

the filter and thus in every location $S_{N,B}/S_{N,B0}$ equals one. In contrast, once the biomass concentration in the biofilm reaches $X_{HB,SP}$ the biological removal begins and $S_{N,B}/S_{N,B0}$ starts decreasing. Animation 2 shows that, the shorter the EBCT, the earlier the biological removal starts, however after biofilm establishment, for the short EBCTs (6 and 12 min) higher $S_{N,B}/S_{N,B0}$ are observed than for the long EBCTs (24 and 33 min). Short EBCTs constrain the adsorptive removal and therefore more DOC is available for the biofilm formation in the early stages, however once the biofilm is fully developed the effect of the longer contact time between biofilm and substrate becomes dominating and causes a higher biological removal at longer EBCTs. This confirms the experimentally observed influence of the EBCT on the biological removal; a longer EBCT promotes biodegradation due to the longer exposure of the biofilm to the substrate (Terry and Summers 2018). This effect can be also observed for all the other biodegradable fractions ($S_{i,B}$), yet not as clearly as for the $S_{N,B}$ for which the effect of the adsorption is suppressed.

The advective-diffusive fronts for the $S_{VG,U}$ fraction showcase several other effects. Firstly, an EBCT equal to 6 min results in no further removal of this fraction once the adsorptive capacity of the carbon is depleted within the filter, as it is to be expected for a non-biodegradable DOC fraction. Secondly, as already described before, bGAC-filters operated at longer EBCTs (until a certain maximum EBCT) better utilize the GAC adsorption capacity and have therefore longer lifespans. Finally, and most interesting, desorption can be easily inspected. As mentioned before, desorption can be recognized by the increase of $S_i/S_{i,0}$ above one. When the DOC influent concentration (see Animation 1) abruptly decreases and again recovers, it forces the $S_i/S_{i,0}$ to become higher than one. This is due to the temporary reversion of the concentration profiles on the X-axis (between the bulk phase and the biofilm surface) and the consequent dissolution of already adsorbed DOC back into the bulk phase. Proportionally to this dissolution, q_T decreases and some adsorption capacity is virtually regained. Thus, immediately afterwards, $S_i/S_{i,0}$ decreases anew and the regained q_T is used. Animation 2 displays a precise example of this phenomenon for the bGAC-filter with an EBCT of 6 min in the period between day 120 and 160. It is important to highlight that experimentally desorption is a highly complex phenomenon, which depends on various parameters and processes that are not include in the present model. Nevertheless, the overall outcome of desorptive processes is well represented by the modeling approach described in this contribution.

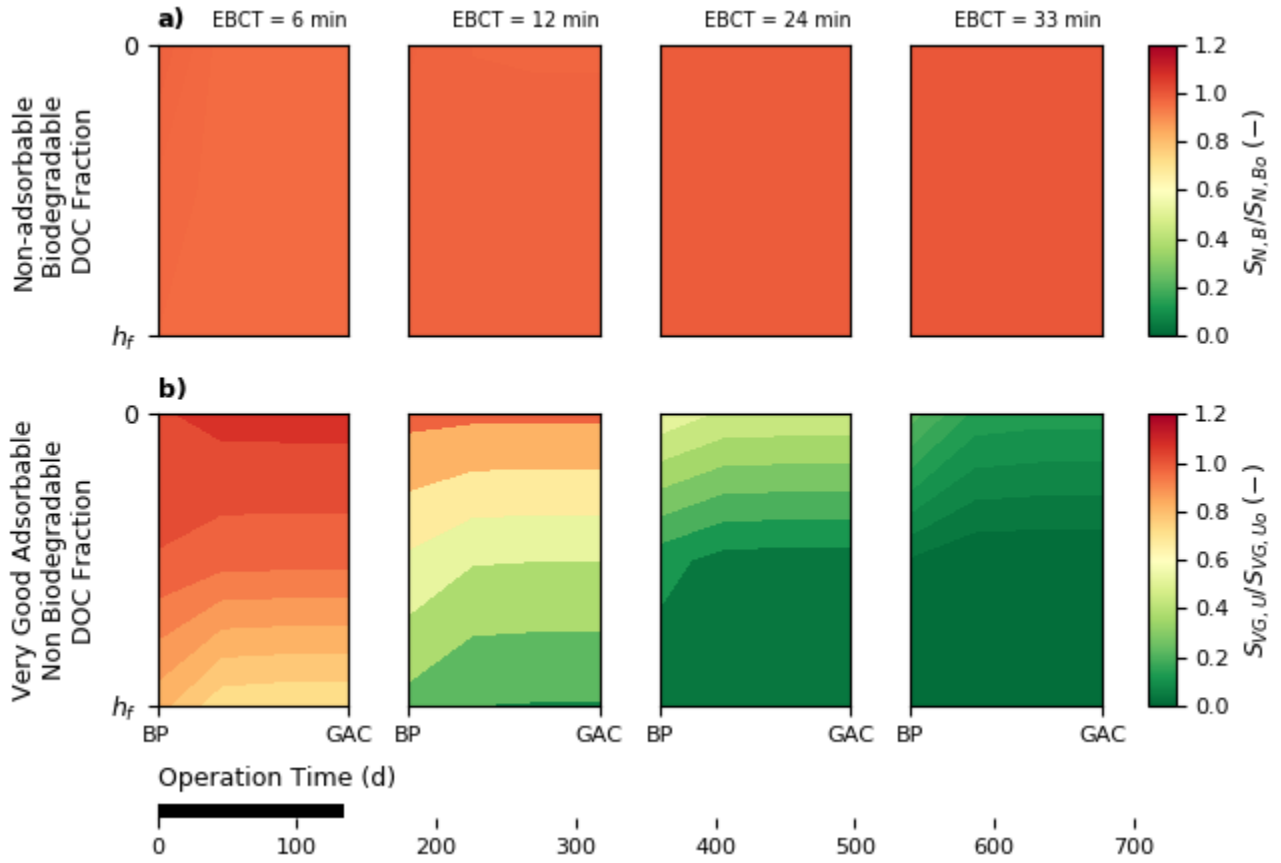

Figure P1. 5. Thumbnail of Animation 2. Advective fronts for the DOC Fractions a) SN,B and b) SVG,U at evaluated EBCTs: 6, 12, 24, 33 min. X-axis covers from the Bulk Phase (BP) until the Granular Activated Carbon (GAC).Y-axis is the filter depth with Y=0 as inlet and Y=hf as outlet.

The good agreement between the experimental and modeling results indicates that the assumptions made in regard of biofilm and adsorption dynamics, mass transfer processes, and DOC fractionation, are plausible and apply for the analyzed process conditions. Moreover, this model sets the basis for potential further extensions, which would be able to predict the removal of individual organic micropolluntants and other remaining macropollutants, as for instance NH_4^+, NO_2^- and NO_3^-.

5. Conclusions

The model presented in this contribution is the first attempt of implementing a multicomponent adsorption process in combination with biofilm degradation into the ASM-Framework. The developed model is capable of reproducing the DOC breakthrough curve of a bGAC-filter as advanced treatment for a WWTP effluent.

The fractionation of the influent according to its biodegradability and adsorbability makes the model more flexible and insightful. It also allows the future incorporation of specific fractions e.g individual organic micropollutants.

The implementation of the IAS theory along with the use of a lumped state variable (q_T) for the adsorbed components is a good approximation for modeling complex multicomponent mixtures, as in the case of WWTP effluents.

The simplified microbial community is able to accurately predict the DOC consumption.

The model accurately predicts the influence of the determinant parameter EBCT on the DOC breakthrough curves. Its effect on both adsorptive and biological removal is observed.

Further research regarding the adsorption kinetic rate, its implementation and parameters is still required.

6. Supplementary Material

Table P1. 6. Activated carbon, biological removal, adsorption dynamics and mass transfer parameters for the processes implemented in the model.

Symbol	Name	Units	Value	Reference
Activated Carbon Parameters				
ε_B	Bed porosity	-	0.51	(Fundneider 2020)
ε_P	Particle porosity	-	0.63	(Fundneider 2020)
ρ_B	Bed density	g/m³	400000	(Fundneider 2020)
ρ_M	Material density	g/m³	2223000	(Fundneider 2020)
ρ_P	Particle density	g/m³	822475	(Fundneider 2020)
Biological Removal Parameters				
L_f	Biofilm thickness	m	5e-6	This work
$K_{aff,DOC}$	Affinity constant of HB on DOC	mgDOC/m³	183	(Cecen and Aktaş 2011)
b_{HB}	Decay coefficient	1/d	0.001	(Tijhuis et al. 1993)
μ_{max} @12°C	Maximum growth rate of HB	1/d	0.025	(Velten et al. 2011)
$K_{aff,O2}$	Affinity constant of HB on O2	mgO2/m³	200	(Henze et al. 2006)
θ_{HB}	Temperature dependency coefficient HB	1/K	0.07	(Koch et al., 2000)

K_X	Hydrolysis half saturation constant	mgXBH·mgXS/d	3.4	(Henze et al. 2006)
k_h	Maximum specific hydrolysis rate	mgXBH/mgXS	1	(Henze et al. 2006)
Y_{HB}	Yield of Biomass on DOC	mgXBH/mgDOC	0.61	(Henze et al. 2006)
iCOD,x	Conversion factor for soluble TOC into COD	mgCOD/mgTOC	3.2	(Henze et al. 2006)
iCOD,Si	Conversion factor for Particulate TOC into COD	mgCOD/mgTOC	2.8	(Henze et al. 2006)
fp	Fraction of XI generated in biomass decay	-	0.08	(Henze et al. 2006)

Adsorption dynamics

k_{PFO}	Pseudo first order kinetic constant	1/d	0.1	This Work
k_{des}	Desorption kinetic constant	1/d	10000	This Work

Mass Transfer Parameters

D_{DOC}	Diffusivity of DOC	cm^2/s	0.000056	(Kim and Pirbazari 1989)

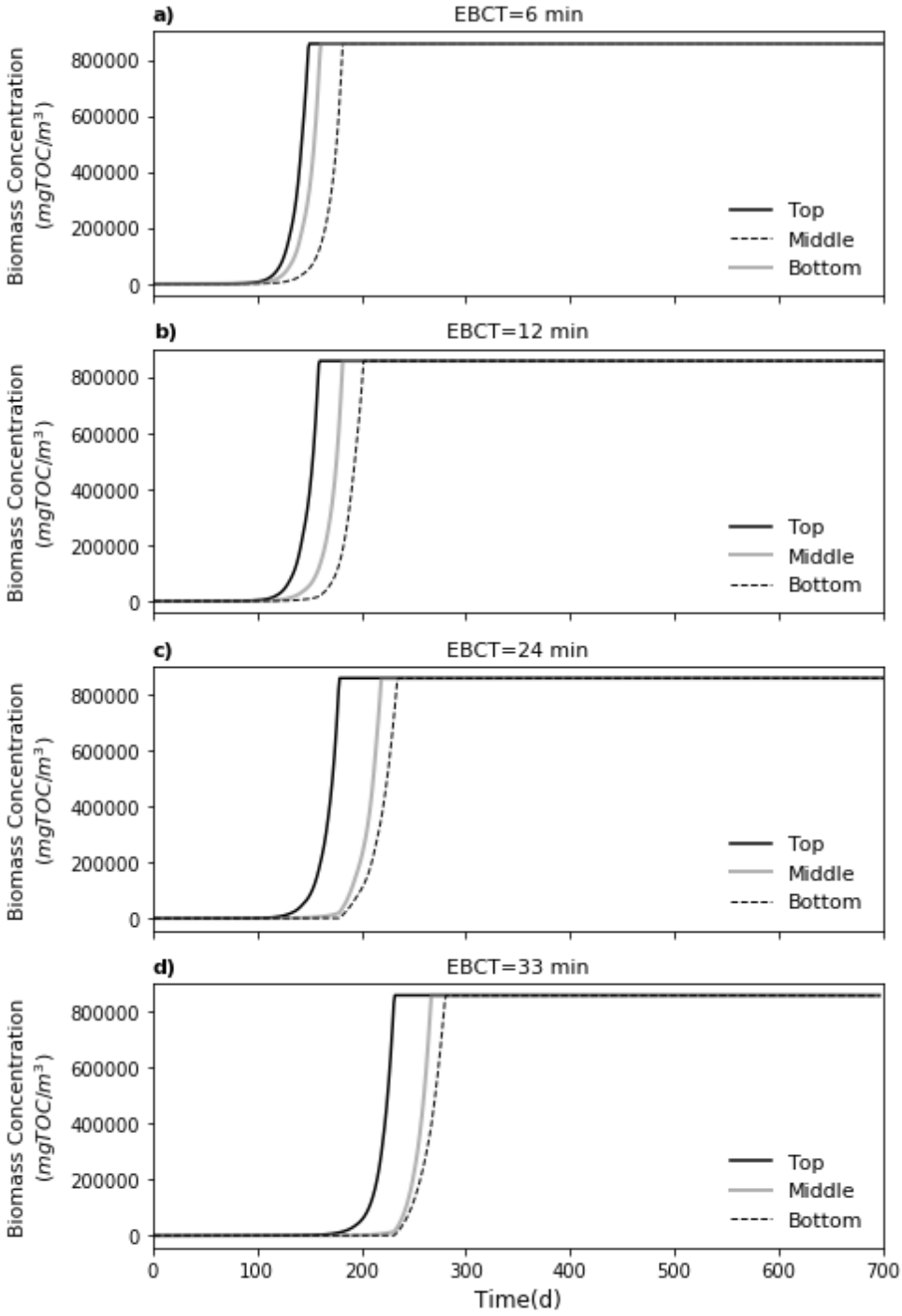

Figure P1. 6. Biomass concentration in the biofilm at three vertical compartments of the model: top, middle and bottom as programed in the original process unit "Trickling Filter" from SUMO19©. Here depicted for an EBCT of a) 6, b) 12, c) 24 and d) 33 min.

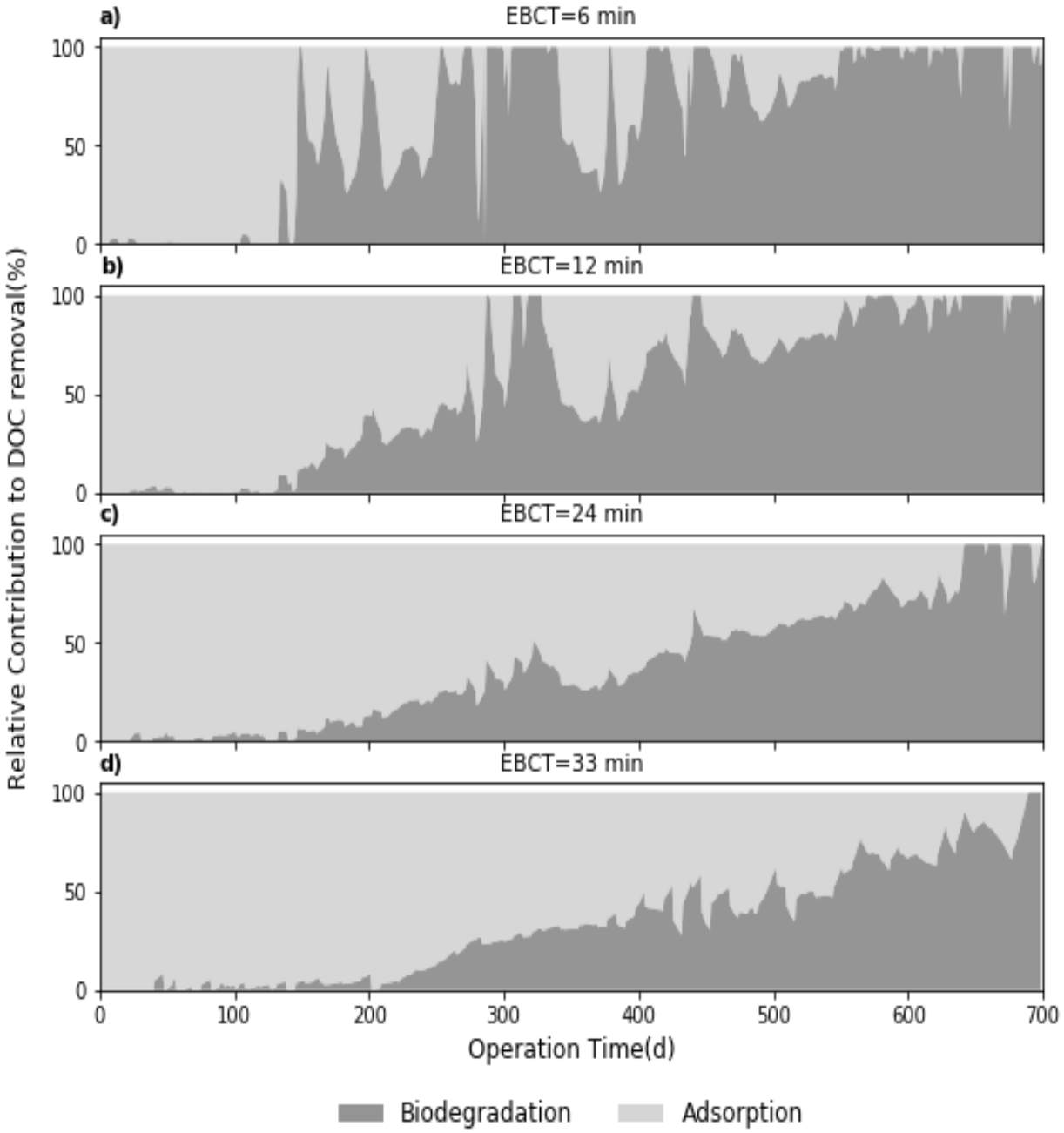

Figure P1. 7. Predicted relative contribution of adsorption and biodegradation to the overall observed DOC removal. Here depicted for an EBCT of a) 6, b) 12, c) 24 and d) 33 min.

References

Batstone, D.J., Amerlinck, Y., Ekama, G., Goel, R., Grau, P., Johnson, B., Kaya, I., Steyer, J.P., Tait, S., Takács, I., Vanrolleghem, P.A., Brouckaert, C.J. and Volcke, E. (2012) Towards a generalized physicochemical framework. Water Sci Technol 66(6), 1147-1161.

Cecen, F. and Aktaş, Ö. (2011) Activated Carbon for Water and Wastewater Treatment: Integration of Adsorption and Biological Treatment, 388 pages, ISBN: 978-3-527-32471-2, Wiley-VCH.

Chang, H.T. and Rittmann, B.E. (1987) Mathematical modeling of biofilm on activated carbon. Environmental Science & Technology 21(3), 273-280.

Dynamita (2020) SUMO19 ©. Engineering, D.P. (ed), Sigale, FRance.

Fundneider, T. (2020) Filtration und Aktivkohleadsorption zur weitergehenden Aufbereitung von kommunalem Abwasser – Phosphor- und Spurenstoffentfernung (Filtration and activated carbon adsorption for advanced treatment of municipal wastewater – phosphorus and micropollutants removal). Doctoral Thesis Technical University Darmstadt, Darmstadt.

Guo, X. and Wang, J. (2019) A general kinetic model for adsorption: Theoretical analysis and modeling. Journal of Molecular Liquids 288, 111100.

Henze, M., Gujer, W., Mino, T. and van Loosedrecht, M. (2006) Activated Sludge Models ASM1, ASM2, ASM2d and ASM3, IWA Publishing.

Johannsen, K. and Worch, E. (1994) Eine mathematische Methode zur Durchführung von Adsorptionsanalysen A Mathematical Method for Evaluation of Adsorption Analysis. Acta hydrochimica et hydrobiologica 22(5), 225-230.

Kim, S.H. and Min, B.M. (1993) Mathematical modeling of bio-physico chemical processes in activated carbon columns. Korean Journal of Chemical Engineering 10(1), 18-27.

Kim, S.H. and Pirbazari, M. (1989) Bioactive Adsorber Model for Industrial Wastewater Treatment. Journal of Environmental Engineering 115(6), 1235-1256.

Marczewski, A.W. (2010) Application of mixed order rate equations to adsorption of methylene blue on mesoporous carbons. Applied Surface Science 256(17), 5145-5152.

Nowotny, N., Epp, B., von Sonntag, C. and Fahlenkamp, H. (2007) Quantification and Modeling of the Elimination Behavior of Ecologically Problematic Wastewater Micropollutants by Adsorption on Powdered and Granulated Activated Carbon. Environmental Science & Technology 41(6), 2050-2055.

Pürschel, M., Ender, V. and Worch, E. (2014) Modelling the NOM uptake by anion exchange resins in drinking water plants. Desalination and Water Treatment 52(22-24), 4029-4039.

Radke, C.J. and Prausnitz, J.M. (1972) Thermodynamics of multi-solute adsorption from dilute liquid solutions. AIChE Journal 18(4), 761-768.

Schideman, L.C., Mariñas, B.J., Snoeyink, V.L. and Campos, C. (2006) Three-Component Competitive Adsorption Model for Fixed-Bed and Moving-Bed Granular Activated Carbon Adsorbers. Part I. Model Development. Environmental Science & Technology 40(21), 6805-6811.

Shim, W.G., Singh Chaudhary, D., Vigneswaran, S., Ngo, H.-H., Lee, J.W. and Moon, H. (2004) Mathematical modeling of granular activated carbon (GAC) biofiltration system. Korean Journal of Chemical Engineering 21(1), 212-220.

Simpson, D.R. (2008) Biofilm processes in biologically active carbon water purification. Water Research 42(12), 2839-2848.

Sontheimer, H., Frick, R., Fettig, J., Hörner, G., Hubele, C. and Zimmer, G. (1987) Adsorptionsverfahren zur Wasserreinigung. Karlsruhe, DVGW Forsch. stelle am Englet-Bunte-Inst. Univ. Karlsruhe, 1985, 640 S., 259 Abb., 73 Tab., DM 145–, ISBN 3-922671-11-X. Acta hydrochimica et hydrobiologica 15(6), 681-681.

Sutikno, T. and Himmelstein, K.J. (1983) Desorption of phenol from activated carbon by solvent regeneration. Industrial & Engineering Chemistry Fundamentals 22(4), 420-425.

Terry, L.G. and Summers, R.S. (2018) Biodegradable organic matter and rapid-rate biofilter performance: A review. Water Research 128, 234-245.
Tijhuis, L., Van Loosdrecht, M.C.M. and Heijnen, J.J. (1993) A thermodynamically based correlation for maintenance gibbs energy requirements in aerobic and anaerobic chemotrophic growth. Biotechnology and Bioengineering 42(4), 509-519.
Velten, S., Boller, M., Köster, O., Helbing, J., Weilenmann, H.-U. and Hammes, F. (2011) Development of biomass in a drinking water granular active carbon (GAC) filter. Water Research 45(19), 6347-6354.
Worch, E. (2010) Competitive adsorption of micropollutants and NOM onto activated carbon: comparison of different model approaches. Journal of Water Supply: Research and Technology-Aqua 59(5), 285-297.
Worch, E. (2016) AdsAna - Adsorption Analysis Software, Dresden, Germany.
Yao, C. and Chen, T. (2015) A new simplified method for estimating film mass transfer and surface diffusion coefficients from batch adsorption kinetic data. Chemical Engineering Journal 265, 93-99.
Yapsakli, K. and Çeçen, F. (2010) Effect of type of granular activated carbon on DOC biodegradation in biological activated carbon filters. Process Biochemistry 45(3), 355-362.

P2. Are K-Strategists Yield- Strategists in disguise? An example from autotrophic nitrogen removal

Vanessa Acevedo Alonso, Susanne Lackner. In: Biotechnology and Bioengineering, 1– 11

https://doi.org/10.1002/bit.28058

Abstract

The behavior of heterotrophic bacteria growing in systems with low or no external supply of COD has become more relevant within the wastewater context. Growth strategies help to clarify how bacteria behave and adapt to different environmental conditions. In the case of substrate limited conditions, research has been mainly focused on the k-strategy, whereas another important strategy: the yield strategy has not been explored intensely. Some authors have, however, demonstrated the implications of bacteria pursuing the yield strategy when living in structured environments and facing low substrate concentrations.

This work uses a one-dimensional biofilm model to study the influence of the affinity constant, the maximum growth rate and the growth yield on the heterotrophic formation of dinitrogen gas (N_2) in a completely autotrophic Partial Nitritation Anammox (PN/A) system. The effect of these parameters on the composition and the diversity of the heterotrophic community is also evaluated. In a first scenario heterotrophic bacteria are allowed to grow only on the COD produced by biomass decay. In a second step the competition with a second group of heterotrophs using external COD as electron donor is assessed. For both evaluated scenarios, the results suggest that the yield plays a crucial role in the heterotrophic biomass and dinitrogen gas formation.

Moreover in the case of the community diversity the yield seems to be the decisive parameter. Finally, we conceptually compared the K and the yield strategy and give some insight to the possibility of both either being closely related or even being the same strategy.

1. Introduction

Microbial communities in traditional biological treatment systems are traditional divided into two groups: autotrophic and heterotrophic bacteria. Experimental evidence has demonstrated that heterotrophic bacteria manage to survive in environments without external organic carbon or, in other words, that autotrophic bacteria are able to support heterotrophic growth. In the wastewater field, the experiments conducted by Rittmann and Brunner (1984) were one of the first hints towards the existence of HB in systems without any external carbon source. Further research proved the ability of autotrophic bacteria to synthetize complex organic molecules through carbon fixation. These complex organic compounds serve as carbon source for the HB present in such microbial communities (Barker and Stuckey 1999, Rittmann et al. 1994).

In the later years, the rise of molecular biology methods has helped to broaden the knowledge about the interactions between different bacteria within completely autotrophic biofilms.

Kindaichi et al. (2004) studied a nitrifying biofilm fed only with NH_4^+-N and found that approximately half of the biomass consisted of heterotrophs. Likewise, Nogueira et al. (2005) evaluated the biomass composition in nitrifying biofilms and found that heterotrophic bacteria accounted for 27% of the total biofilm. Matsumoto et al. (2010) were also able to find heterotrophs in nitrifying granules from a system operated without external carbon source. Such heterotrophic–autotrophic networks are also encountered in other than nitrifying systems. Their existence has also been observed in Partial Nitritation/Anammox (PN/A) systems (Agrawal et al. 2017) and enriched anammox and Nitrobacter cultures (Dapena-Mora et al. 2004, Ni et al. 2012, Vadivelu et al. 2006). The role of heterotrophic bacteria in fully autotrophic systems dedicated to nitrogen removal has not been completely elucidated yet. The traditional understanding of denitrification as carried out by HB has been expanded by the discovery of the role these bacteria play in the production and reduction of N2O, including reductive pathways outside the denitrification pathway (Conthe et al. 2019). In addition, recent research has demonstrate the potential of heterotrophs to perform dissimilatory nitrate ammonification, which constitutes an interesting alternative pathway for the reduction of NO_3^-/NO_2^- in both natural and engineered ecosystems. (van den Berg et al. 2017). Given the functional diversity of heterotrophic bacteria and the various ways in which these heterotrophs might impact fully autotrophic nitrogen removal processes, it is worthwhile to analyze those conditions under which their diversity becomes relevant to engineered systems and how this diversity can be used to even enhance such systems.

Studies that evaluate the importance of the growth strategies used by heterotrophic bacteria under substrate-limiting conditions are still lacking, as pointed out by Merkey et al. (2009) . In their study, they investigated heterotrophs that follow either the r- or K-strategy. Mathematically, this concept is represented through the affinity constant (K) and growth rate (μ). Organisms that behave like K-strategists have low K and μ; In contrast, organisms are considered as r-strategists when exhibiting high K and μ. The findings from Merkey et al. (2009) suggested that heterotrophs within a completely autotrophic biofilm are likely to be K-strategists; however, the results were not categorical. Besides the r/K-strategy, bacteria are believed to be able to pursue the yield strategy. An organism that undergoes the yield strategy uses substrate more efficiently for biomass production (higher biomass yield); however, as trade off the organism has to have a lower specific growth rate. Microorganism growing under substrate limiting conditions and in spatial structured environments are likely to select this kind of growth-strategy (Kreft and Bonhoeffer 2005a, Kreft 2004). Experimental evidence of microorganism undergoing the yield strategy has already been reported for different species such as yeast and Holophaga foetida (Kreft 2004, MacLean and Gudelj 2006). Lipson et al. (2009) were able to find a negative relationship between yield and growth rate in bacterial soil communities, however they only identified organisms pursuing the r-strategy, in this case high growth rates at cost of lower biomass yields.

Although the concept of K-strategy is established and well accepted in the wastewater modelling practice, several ecological studies do not completely support the K-strategy, as a sounding trade-off, which bacteria are subjected to (Aksnes and Cao 2011). The lack of a satisfactory mechanistic meaning of the affinity constant along with contradictory experimental observations, are the main reasons for challenging the current interpretation of the K-strategy. These

studies do not completely disregard the validity and utility of the K-strategy, they encourage instead an enhanced framework to understand the biological processes that underlay the different growth strategies or tradeoffs. In contrast, an exploration of the thermodynamic background of the yield-strategy has been conducted (Pfeiffer et al. 2001). According to the results of this study, it could be argued that the yield strategy has a stronger mechanistic foundation. Nevertheless, the conceptual implications of the yield strategy on the behavior of fully autotrophic systems has been largely overlooked in the wastewater field.

This paper uses a multi-species model for assessing the effect of the yield on the production of N_2 and heterotrophic biomass in a completely autotrophic PN/A system. We compare the influence of the yield, the maximum growth rate (μ) and the affinity constant (K) on the behavior and composition of a heterotrophic community growing solely on the COD produced due to biomass decay within a biofilm. The competition with another heterotrophic group capable of growing on external COD was explored as well. Lastly, we briefly compare the K- and yield strategies and the implications of the appropriate understanding of the growth strategies that bacteria pursue under substrate limiting conditions.

2. Methods

A one dimensional, multispecies, multicomponent model was implemented in AQUASIM (Reichert 1994). The kinetic model used in this study is an extension of the standard ASM1 model. It includes a two-step denitrification carried out by Ammonium Oxidizing Bacteria (AOB) and subsequently by Nitrite Oxidizing Bacteria (NOB). The model also considers the conversion of NH_4^+ and NO_2^- into dinitrogen gas by Anaerobic Ammonium Oxidizing Bacteria (AnAOB). The classification of the heterotrophic community was made based on the electron acceptors relevant to the global modelling results and intends to represent the functional diversity of HB present in the system. The heterotrophic community was then divided into three groups: HB1, HB2 and HB3, growing on different electron acceptors: O_2, NO_2- or NO_3^-, respectively. Separated state variables were introduced for tracking the dinitrogen gas produced by HB2 and HB3. All the three HB species were also allowed to grow on two different carbon sources: endogenous COD (COD_{BF}) and external COD (COD_{ex}). It has been observed that the traditional ASM hydrolysis term from the AMS1 model is not suitable for autotrophic biofilm systems with low to zero COD in the influent. Therefore an alternative approach is required (Lackner et al. 2008a, Wan et al. 2019). For simulating the COD that is produced during bacterial decay, the approach introduced by Wan et al. (2019) was applied. This approach neglects the hydrolysis of particulate/slowly biodegradable organics (X_S) and assumes that during decay, the biomass is directly converted into readily biodegradable organics (S_S), i.e. into COD_{BF} in this work. This method was selected to guarantee that sufficient CODBF was produced within the biofilm, at the location where it presumably happens. Thereby, the investigation of the behavior of HB when growing in biofilms without external COD supply (influenced by diffusion from the bulk liquid into the biofilm) could be specifically targeted. The Supplementary Information contains a comprehensive summary of the stoichiometric matrix, and model parameters.

A Moving Bed Biofilm Reactor (MBBR) was modeled based on the operational conditions described in Gilbert et al. (2014). The reactor's conditions are similar to those expected in a B-

stage reactor used within an A-B treatment scheme i.e. a reactor dedicated to the treatment of wastewater with high NH_4^+ concentration as well as low COD concentration (previously captured under anaerobic conditions in the A-stage)(Liu et al. 2020). The conceptual MBBR was modelled using the biofilm model provided in AQUASIM (Reichert 1994).The reactor had a volume of 0.01 m^3, a specific surface area of 800 m^2/m^3 and a maximal biofilm thickness of 1 mm. The influent flow was 0.02 m^3/d, the initial influent NH_4-N concentration was 100 gN/m^3 whereas the initial influent concentration of the NO_2-N and NO_3-N where set to be zero. The dissolved oxygen concentration in the bulk phase was selected to be 0.75 $gCOD/m^3$, the temperature was constant for all the experiments and set to 20 °C. These conditions ensured sufficient nitrogen removal and activity of both heterotrophic and autotrophic communities.

Two different scenarios regarding COD were evaluated. In the first one the external COD (coming with the influent) was selected to be 0 $gCOD_{Ex}/m^3$, in order to evaluate the behavior of the heterotrophic community when growing solely on limited endogenous COD (COD_{BF}). A second scenario was designed to evaluate the impact of potential fluctuations in the performance of pre-treatment stage that may result in external COD coming into the P/NA system. This second scenario assumed a concentration of external biodegradable COD (COD_{Ex}) equal to 50 $gCOD_{Ex}/m^3$ to analyze under which conditions bacteria growing on a scarce carbon source (CODBF) are able to equal or even outcompete bacteria growing on a relatively abundant carbon source. The initial concentration of the COD_{Ex} was selected so a COD_{BF}/COD_{EX} near to 0.5 was achieved and the competition over the two carbon sources was still observable. Table P2.1 summarizes parameters used in the studied scenarios.

Table P2. 1. Description of the modelling scenarios. Scenario 1 represents a situaion without externa COD supply, while Scenario 2 tries to mimic the competition between 2 heterotrophic groups when external COD is present

		HB growing on endogenous COD			HB growing on influent COD		
Scenario	Influent COD ($gCOD_{Ex}/m^3$)	$K_{HB,BF}$ $\left(\frac{gCOD_{BF}}{m^3}\right)$	$\mu_{HB,BF}$ (d^{-1})	$Y_{HB,BF}$ $\left(\frac{gCOD_x}{gCOD_{BF}}\right)$	$K_{HB,Ex}$ $\left(\frac{gCOD_{Ex}}{m^3}\right)$	$\mu_{HB,Ex}$ (d^{-1})	$Y_{HB,Ex}$ $\left(\frac{gCOD_x}{gCOD_{Ex}}\right)$
1	0	0.01,1,10	(0.5-10)	(0.1-0.7)	10	6	0.67
2	50	0.01,1,20	(0.5-10)	(0.1-0.7)	10	6	0.67

As shown in Table P2.1, several sets of combinations for $\mu_{HB,BF}$ and $Y_{HB,BF}$ of the HB growing on COD_{BF} were tested at three different substrate affinity constants K = 0.01, 1 and 10 $gCOD_{BF}/m^3$.In the scenario 2, the introduction of COD_{Ex} resulted in the increase of the total biomass within the system and an increment in the available COD_{BF}. In scenario 1 the ratio between COD_{BF} and K was always lesser than, to maintain this condition, in the second scenario the upper limit of K was set to 20 $gCOD_{BF}/m^3$, ensuring in doing so the comparability of the results obtained in both scenarios. The plausibility of the results was checked through the mass balances of dissolved COD and total nitrogen. Combinations of $\mu_{HB,BF}$ and $Y_{HB,BF}$ that led to inconsistent results in at least one scenario were discarded for all the scenarios. We

defined all combinations of $\mu_{HB,BF}$ and $Y_{HB,BF}$ as inconsistent, for which the results presented a deviation of more than 1% in the mass balances for either dissolved nitrogen or COD.

All the results presented in the figures refer to steady state conditions i.e. at the state when the biofilm is fully grown and has reached the maximal biofilm thickness (1 mm) and the state variables (concentrations) in both biofilm and liquid phase remain constant with time.

3. Results

3.1. Scenario 1: Fully Autotrophic Conditions

For tracking the activity of the heterotrophic community when growing on COD_{BF}, the production of nitrogen gas by each of the HB species was used as main indicator. Figure P2.1 depicts the fraction of the total nitrogen gas that was produced by the denitrifier community (HB2 and HB3) and the contributions of each single species. Figure P2.1 includes the results for the three evaluated K values and the minimum, maximum and the midpoint of the yield ($Y_{HB,BF}$) interval: 0.1, 0.35 and 0.7 $gCOD_x/gCOD_{BF}$, respectively.

Figure P2.1 shows that the yield has a stronger influence on the total nitrogen production than µ. Once a minimum growth velocity is reached, µ does not longer affect the nitrogen production by the denitrifiers, for K = 0.01 and 1 $gCOD_{BF}/m^3$. Nevertheless, when K takes the value of 10 $gCOD_{BF}/m^3$, µ does affect the nitrogen gas production to a certain extent, as is to be expected since the value of K is nearly the same as the available concentration of COD_{BF}, and therefore COD_{BF} is less available to the bacteria than in the other two cases (lower values of K). In the case of NO_2^- reduction to N_2 by HB2, only when the yield equals 0.7 $gCDO_x/gCOD_{BF}$ HB2 showed activity and were able to overcome the competition of HB3 over the electron donor (COD_{BF}). In the scenario where K equals 10 $gCOD_{BF}/m^3$, µ moderately affects the production of N_2 by HB2. HB2 compete not only over their electron donor but also compete with AnAOB and NOB over their electron acceptor (NO_2^-). Due to this double competition, the µ from which HB2 are able to grow is higher at K=10 $gCOD_{BF}/m^3$ than at the other values of K, where CODBF is more accessible and thus the competition over COD_{BF} is lesser.

For the reduction of NO_3^- to N_2 the influence of the yield on the N_2 production seems to be coupled with the value of the affinity constant K. At low values of the affinity constant (K= 0.01 $gCOD_{BF}/m^3$) the highest amount of N_2 is not produced at the maximum yield. Unlike the case with HB2 , N_2 production does not increase from a yield of 0.35 $gCOD_x/gCOD_{BF}$ onwards. In this case, the electron acceptor (NO_3^-) becomes the limiting factor and hence HB3 cannot profit from a more efficient utilization of COD_{BF}.

At the highest affinity constant (K=10$gCOD_{BF}/m^3$) and the maximum yield (0.7 $gCOD_x/gCOD_{BF}$), the N_2 production by HB3 increases with µ until a maximum and afterwards it drops back and remains constant. Here HB3 profit of the COD_{BF} scarcity, the unfeasible HB2 growth and the consequent abundance of NO_3^-. Once HB2 reach a µ from which they are able to grow, HB3 do not dominate the biofilm any longer and a sort of equilibrium between these bacterial groups is attained, allowing them to simultaneously grow. These results showcase the dominating influence of the yield on the heterotrophic grow within completely autotrophic biofilms.

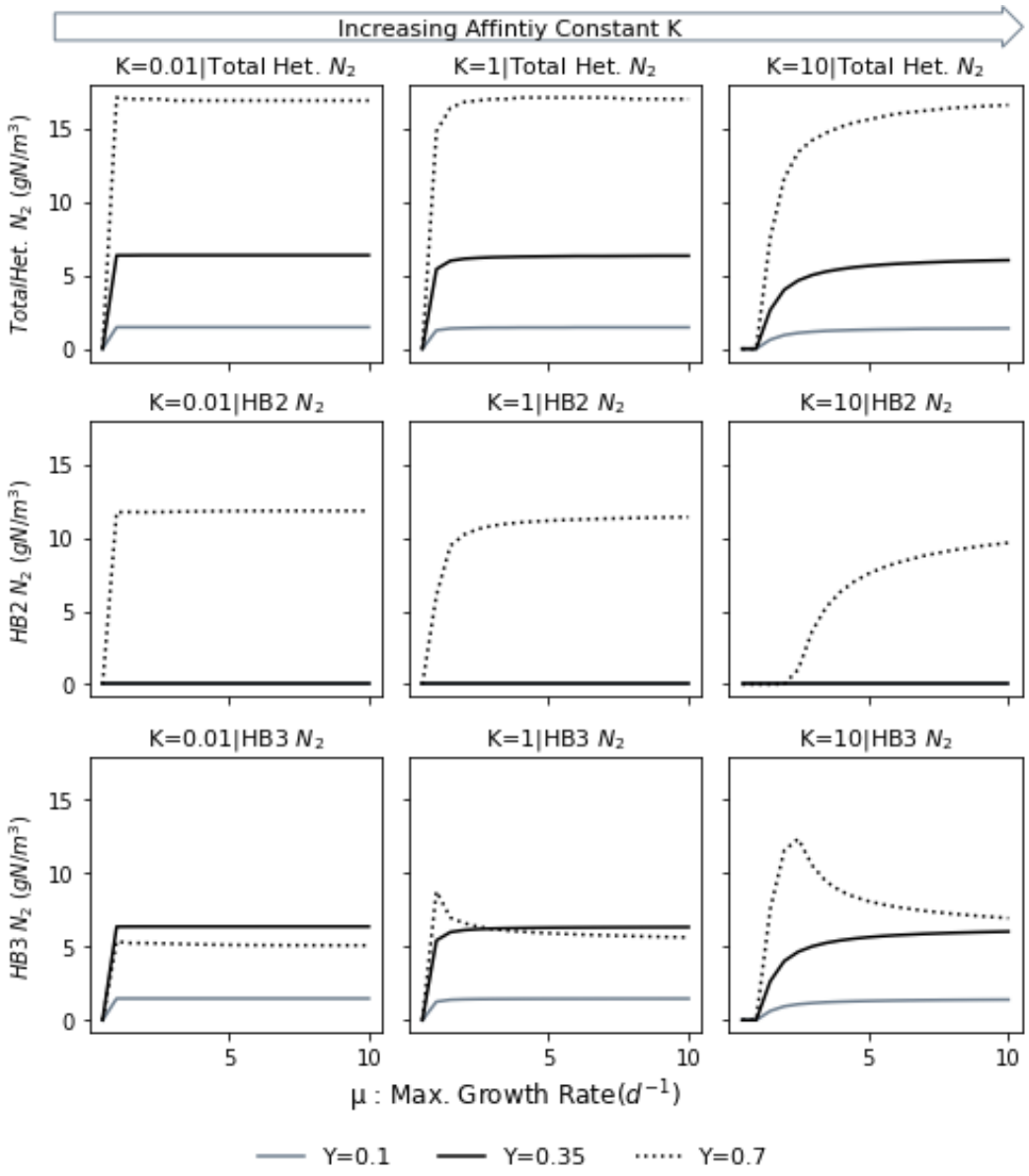

Figure P2. 1.Nitrogen gas production by the denitrifier community for the Scenario 1 (no external COD, COD_{Ex}=0) as a function of the affinity constant KHB,BF ($gCOD_{BF}/m^3$), the maximum growth velocity (d^{-1}) for 3 selected values of the growth yield ($gCODx/gCOD_{BF}$). HB2 uses NO_2^- as electron acceptor, while HB3 uses NO_3^- as electron acceptor.

Figure P2.2 depicts heterotrophic biomass over the biofilm thickness for the simulations with K=10 $gCOD_{BF}/m^3$ at different values of μ and Y. When μ has a value of 1.5 d^{-1}, HB3 are the only existent group of HB. This is in accordance with the results presented in Figure P2.1**Figure P2. 1**, where a minimum μ for HB2 is observed. Once this μ-threshold is passed and HB2 are able to grow, they do it exclusively at the highest yield value. Although HB2 profit from high values of μ, a high value of yield is still compulsory for HB2 to appear. A high yield is apparently a must for the heterotrophic community to be diverse, i.e. for all the bacterial groups to be present within the biofilm. A high biomass yield is characteristic of an efficient substrate utilization. In a bacterial community this trait is crucial for the survival of all the bacterial groups that share/ compete over a limited substrate. Our results show that the heterotrophic community is only able to develop in a diverse way, at the highest value of the yield. This

underlines the importance of the efficient utilization of a shared substrate (high yield) previously observed in other studies (Kreft and Bonhoeffer 2005a).

Although COD_{BF} is available along the whole biofilm thickness (in-situ production due to biomass decay), heterotrophic growth takes place mainly in the zone near to, but not directly at the biofilm surface i.e. at L_f between 0.7 and 0.9 mm. The presence of NO_3^-, NO_2^-, COD_{BF} in addition to low oxygen concentrations enable the growth of both HB2 and HB3. Interestingly, the aerobic heterotrophs (HB1) appeared only in extremely low quantities regardless of the values of μ, yield and K. This indicates a strong competition for oxygen with AOB and NOB as well as a strong competition for COD_{BF} and space with HB2 and HB3. Figure P2.6 in the supplementary information depicts the NO_3^- and NO_2^- profiles along the biofilm thickness and complements the information shown in this section. As mentioned before high values of the yield foster the denitrification activity and the diversity of the heterotrophic community. In the case of NO_3^- , the higher the growth yield the lower the concentration, due to the increased activity of HB3. As seen in the Figure P2.6 of the supplementary information, the NO_3^- concentration profile along the biofilm thickness is rather flat with a slight decrease at the biofilm surface (biofilm thickness = 1mm). This corresponds to the biomass profiles showed in Figure 2. In contrast, in the case of NO_2^- , the concentration remains nearly the same regardless of the yield's value. At higher yields the HB2 amount increases and so HB2 reduce the NO_2^- otherwise reduced by AnAOB (configuration with low yield values). Additionally, Figure P2.7in the supplementary information shows the corresponding COD_{BF} profiles. It can be seen that the growth rate does impact the COD_{BF} concentration. At high growth rates, COD_{BF} concentration is lower than at low growth rates. The shape of the profiles are in accordance to the biomass distribution showed in Figure P2.2, near to the biofilm surface a peak can be seen were the majority of the biomass is located (higher production of COD_{BF}), whereas directly at the surface a decrease is observed due to the lesser amount of biomass located at this point.

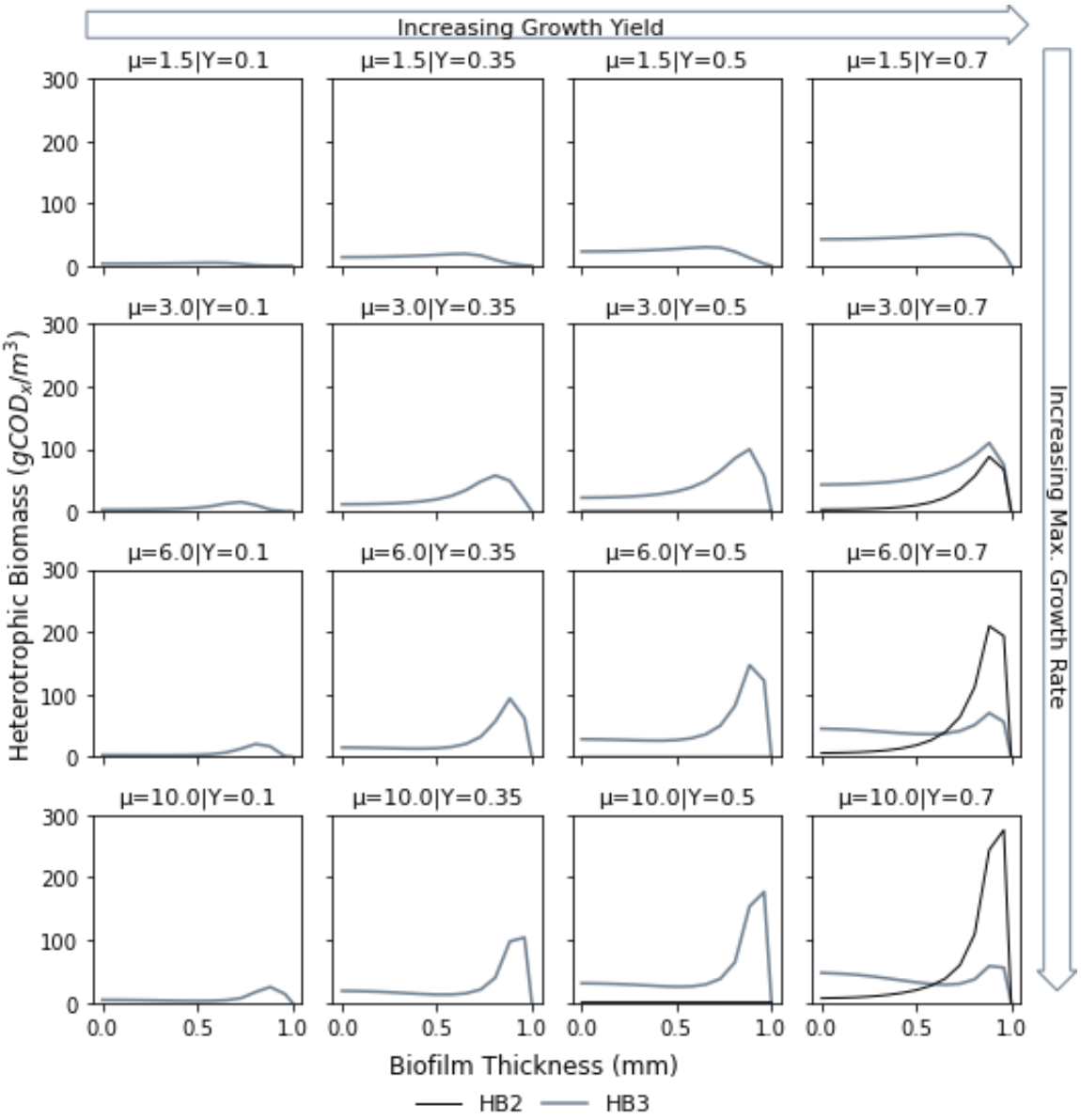

Figure P2. 2. Distribution of the heterotrophic biomass along the biofilm thickness for the Scenario 1 (no external COD, COD_{Ex}=0), for a selected affinity constant $K_{HB,BF}$ equal to 10 $gCOD_{BF}/m^3$ and different selected values of the maximum growth velocity (d^{-1}) and the growth yield (gCODx/gCODBF). HB2 uses NO_2^- as electron acceptor, while HB3 uses NO_3^- as electron acceptor.

Figure P2.3 further supports the hypothesis that the yield plays a decisive role in the heterotrophic biomass composition, while K and μ have only secondary roles. In terms of biomass quantity, the influence of the evaluated parameters remains the same. The heterotrophic biomass quantity only reaches 2% of the total active biomass. This does not correspond to the observations in autotrophic systems, in which the heterotrophic biomass accounts for at least 20% of the total active biomass (Agrawal et al. 2017, Kindaichi et al. 2004, Ni et al. 2012). The implementation of Extracellular Polymeric Substances (EPS) into the modelling has proved successful for better predicting the amount of heterotrophic biomass that occurs in autotrophic systems (Azari et al. 2018, Liu et al. 2016b), however the EPS production and all its related process were out of the scope of this work.

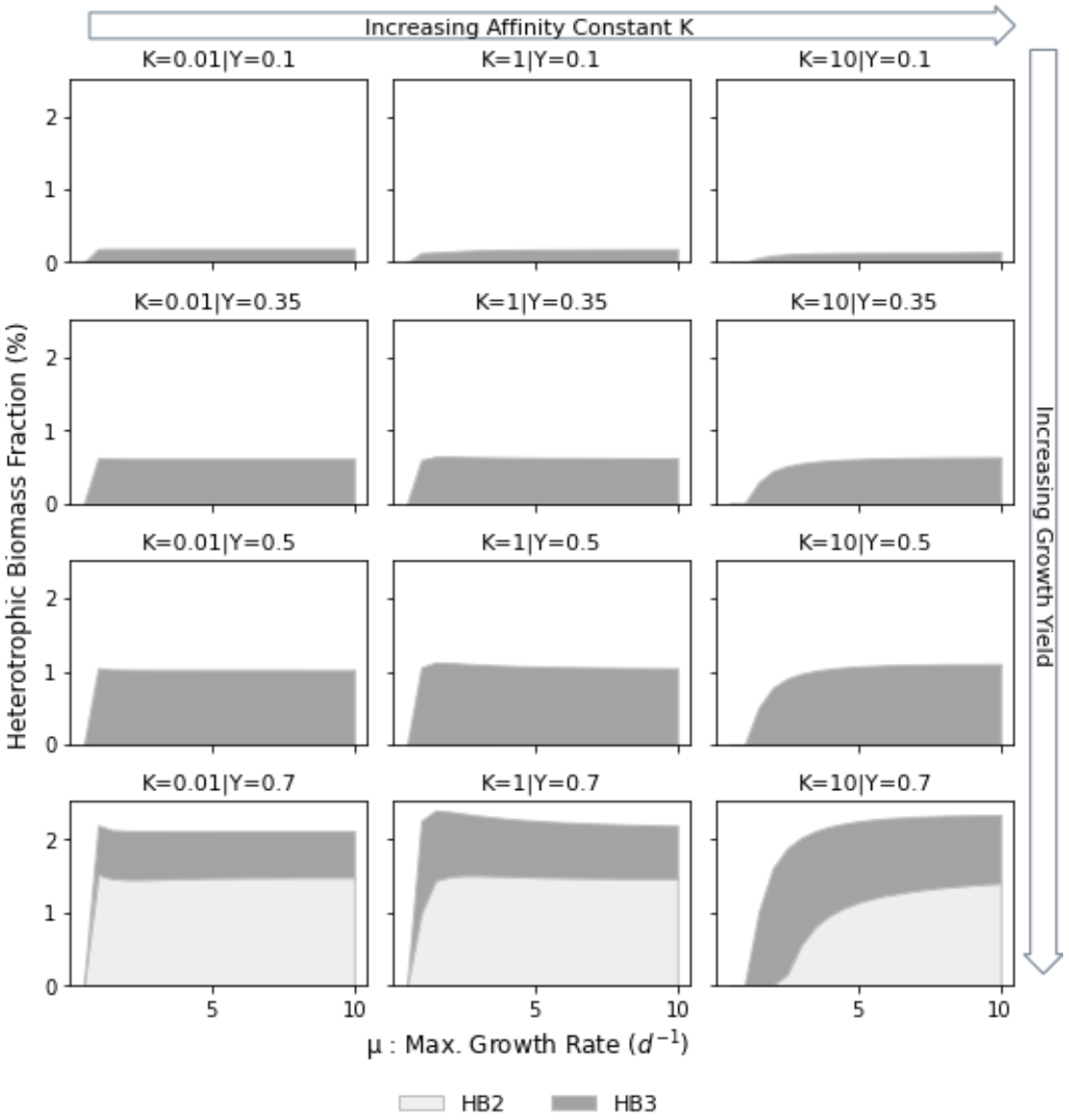

Figure P2. 3. Heterotrophic biomass quantity and composition for the Scenario 1. (no external COD, COD_{Ex}=0) as a function of the affinity constant KHB,BF ($gCOD_{BF}/m^3$), the maximum growth velocity (d^{-1}) and the growth yield ($gCOD_x/gCOD_{BF}$). HB2 uses NO_2^- as electron acceptor, while HB3 uses NO_3^- as electron acceptor.

When exploring the adaptation strategies of bacteria to substrate limiting conditions, the parameters of the Monod kinetics (μ and K) occupy a central role in wastewater modelling practice, whereas the yield is commonly believed to be rather constant and its influence is often disregarded. Merkey et al. (2009) already investigated the behavior of heterotrophic bacteria growing in purely autotrophic biofilms in terms of growth velocity and affinity constant. They found that when the values of K are sufficiently low, the utilization rate (analogous to μ) does not influence the heterotrophic biomass production, which points towards the heterotrophic bacteria pursuing a K-strategy to grow under substrate limiting conditions. Our study also predicted that at low values of K (0.01 and 1 $gCOD_{BF}/m^3$), the effect that μ has on both biomass and N2 production can be neglected. In contrast to the results from (Merkey et al. 2009), we highlighted the role of the yield and showed that even at low affinity constants, the yield is still

a decisive parameter for N_2 and biomass production. This major influence of the yield suggests that the heterotrophic community undergoes the so-called yield-strategy to thrive when sharing the scarce COD_{BF} as carbon resource. Bacteria that follow the yield-strategy convert substrate more efficiently into biomass at the cost of a reduced growth rate. At first glance, a negative relationship between yield and growth rate may be counterintuitive since a positive relationship between growth rate and yield is expected i.e. bacteria that grow faster are expected to use substrate more efficient and produce more biomass per unit of substrate (Henze et al. 2008). However, this is valid mostly for planktonic cells and it is subject to the metabolic state of the bacteria. A microorganism growing at high rates may attain an off-balance state between anabolism and catabolism, in which energy, that otherwise would be used in biomass production (high yield), is utilized for futile cycles/overflow metabolism.(Lipson 2015). There is a maximum growth rate from which the yield must necessarily decrease, so that bacteria are able to sustain rapid growth rates. Likewise, it has been demonstrated that in biofilms with limited substrate a trade-off between yield and growth rate exists. Kreft (2004) demonstrated through an individual-based model that spatially structured systems like biofilms provide the necessary conditions for a yield-strategist to survive. They also concluded that the concept of growth rate (μ) being a more crucial factor than yield is wrongfully carried over from observations in completely mixed reactors. In light of the results delivered by our modelling exercise, we hypothesize that under the studied conditions, the heterotrophic community is likely to pursue a yield-strategy, which allows HB to maximize N_2 and biomass production. Moreover, the use of a yield-strategy seems to be the only way to achieve diversity within the microbial community.

3.2. Scenario 2: Heterotrophic Community Behavior in the Presence of COD_{Ex}

The behavior of HB growing on the scarce COD_{BF} when facing competition by HB growing on a more abundant external source of COD were also evaluated. The heterotrophic bacteria growing on COD_{Ex} were intentionally modelled as rate-strategists using the parameters traditionally used in the ASM1 (Henze et al. 2006). The combinations of parameters under which the heterotrophic bacteria using COD_{BF} were able to overcome this competition were explored. Our results showed that the aerobic heterotrophs (HB1) using COD_{BF} were able to grow in small quantities in comparison with HB1 growing on COD_{Ex}. Given that oxygen and COD_{Ex} are supplied through the bulk phase, the zones close to the biofilm surface are rich in both substrates, and thus, HB1 using COD_{Ex} have an advantage and deplete the oxygen, leaving HB1 growing on COD_{BF} with fewer chances of survival.

In contrast, the denitrifiers (HB2 and HB3) growing on COD_{BF} were able to survive and compete with their counterparts growing on COD_{Ex}. Figure P2.4 shows the amount of N_2 produced by the heterotrophs when growing on COD_{BF} and when growing on COD_{Ex} at different yield levels for a $K = 20\ gCOD_{BF}/m^3$ and a $\mu = 6\ d^{-1}$. From Figure P2.4 is clear that the amount of N_2 produced by the HB growing on COD_{BF} is determined by the yield, as seen in the previous section. High yield leads to a high N_2 production regardless of the values of μ and K. As to be expected, the denitrifiers growing on COD_{Ex} were better off in the scenarios that were not suitable for the denitrifiers dependent of COD_{BF} (low value of yield $Y_{HB,BF}$). When both HB groups have the approximately the same yield ($Y_{HB,BF} = 0.7\ gCOD_x/gCOD_{BF}$ and $Y_{HB,Ex} = 0.67$

$gCOD_x/gCOD_{Ex}$), denitrifiers that use COD_{BF} produced more N_2 than the ones growing on $COD_{Ex.}$ Here the location of the COD sources comes once again into play, COD_{BF} is supplied in-situ through biomass decay while the COD_{Ex} comes with the influent and needs to diffuse from the bulk liquid into the biofilm. At the biofilm surface, oxygen and COD_{Ex} are both available and thus heterotrophic bacteria using oxygen as electron acceptor (HB1) and COD_{Ex} as electron donor are in advantage. The majority of the external COD is consumed by HB1 before getting through the biofilm and reaching the location at which all the required conditions for the denitrifiers to grow are guaranteed; namely absence of oxygen and presence of NO_3^-/NO_2^- This indicates that the spatial structure of the biofilm is an essential feature for the survival of HB growing on COD_{BF} i.e. the yield strategist. Without the biofilm structure and the diffusion processes taking place within it, HB with low μ would not stand a chance again HB growing on a more abundant carbon source and having a faster μ.

The composition of the heterotrophic community as well as its quantity are severely affected by the presence of external COD. COD_{Ex} favours the growth of HB1 (aerobic heterotrophic bacteria) and increases the amount of heterotrophic bacteria present in the biofilm up to 10% of the total biomass. Independently of the value of all the evaluated parameters (μ,Y and K), HB using COD_{Ex} as electron donor are able to grow. Nevertheless, at high values of yield (Y) the amount of denitrifiers (HB2 and HB3) slightly decreases. In the case of the heterotrophic community using COD_{BF} as electron donor, the composition of the community is strongly influenced by the value of yield, as expected. With increasing yield, the amount of HB2 increases and as result HB3 decrease, while HB1 remain relatively constant. As seen in the previous scenario, the three heterotrophic groups are able to co-exist only at high values of yield. If the diversity is defined as both heterotrophic groups growing simultaneously (the group using COD_{BF} and the groups using COD_{Ex}), it can also be stated that the only way to obtain a diverse community is when the bacteria growing on the scarce source COD_{BF} undergo the yield strategy i.e at high values of yield regardless of μ.

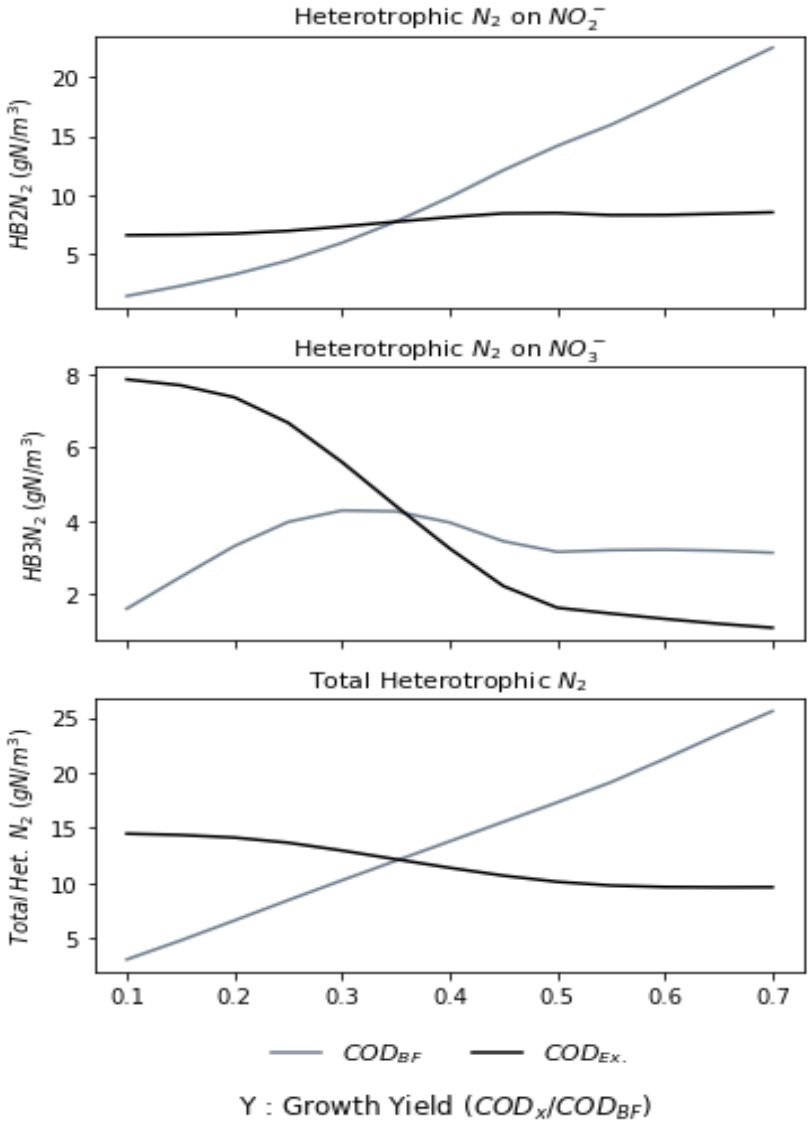

Figure P2. 4. Comparison of the nitrogen production by the denitrifier communities in the Scenario 2 (with external COD supply, COD_{Ex}= 50 $gCOD_{Ex}/m^3$) as a function of the growth yield ($gCOD_x/gCOD_{BF}$). For a for a selected affinity constant equal to 20 $gCOD_{BF}/m^3$ and maximum growth velocity equal to 6 d^{-1}. HB2 uses NO^{2-} as electron acceptor, while HB3 uses NO_3^- as electron acceptor.

3.3. k-Strategy vs Yield Strategy

The r/K-strategy is widely known and accepted as explanation for the microbial adaptation to substrate-limiting conditions. K-strategists are believed to have a very low K in combination with a relatively low μ, which makes them capable of surviving by scavenging substrate even at very low concentrations. In contrast r-strategist have a high μ and as consequence they are not able to grow at low concentrations due to their high values of K. Andrews and Harris (1986) originally defined a K-strategist in the microbiological context as an organism that efficiently extract energy from an environment with high population density i.e. limited resources. They mathematically demonstrated that when bacteria are faced with low substrate environments, a low affinity constant as trade-off for a high growth rate is a determinant trait to the K-strategy.

They also demonstrate that more efficient use of the energy is also central to the survival of microorganism under substrate limiting conditions and thus a high yield could be also characteristic of a K-strategy. This suggests that K- and yield strategies are closely related and if bacteria pursue any of these strategies, they would be pursuing most probably both of them. Traditionally, K- and yield strategy are regarded as independent approaches that bacteria may select, depending on the environmental conditions (Beardmore et al. 2011). However, if the yield and the affinity constant were dependent on each other, then both strategies would be two sides of the same coin. Recently Ugalde-Salas et al. (2020) demonstrated, based on the microbial transition state theory, that the affinity constant (K) from the Monod equation may be written as a function of the yield as presented in equation P2.1:

$$K = \frac{1}{Y \cdot V_H} \qquad \text{(P2.1)}$$

V_H is called the harvesting volume and is defined as the volume that bacteria can access to obtain substrate during their doubling period. A closer look to equation 1 shows that for a constant V_H, low yields (Y) lead to high affinity constants (K); whereas high yields result in low affinity constants. Equation 1 can also be interpreted as follows: if VH decreases and less substrate is available to the bacteria, they might be subjected to a selection pressure for the most efficient use of the scarce substrate instead of the fastest growth rate ("wasteful" use of the substrate). This pressure might lead to the selection of a metabolic state with a higher yield but a lower growth rate (Wortel et al. 2018), and in accordance to Equation 1, a lower affinity constant.

Based on this inverse relation of the yield and the affinity constant, we hypothesized that what we observe and we know as a k-strategy may in fact be a yield-strategy. Using the results delivered by the developed model, we cannot prove for certain that there is a relationship between the yield and the K strategy. However, we can conclude that in our model at low growth rates a diverse heterotrophic community can only be obtained using a combination of low K and high growth yield. Figure P2.5 presents the biomass profiles along the biofilm thickness for different combinations of yield and affinity constants at a fixed low growth rate of 1.5 d^{-1}. It can be observed that HB2 and HB3 coexist only in the cases where the affinity constant takes a low value and the growth yield is rather high. The subplots corresponding to these conditions are highlighted with a blue square in Figure P2.5. In the cases with higher growth rates (data not shown), this tendency remains, however, the affinity constant is less influential as the growth rate increases.

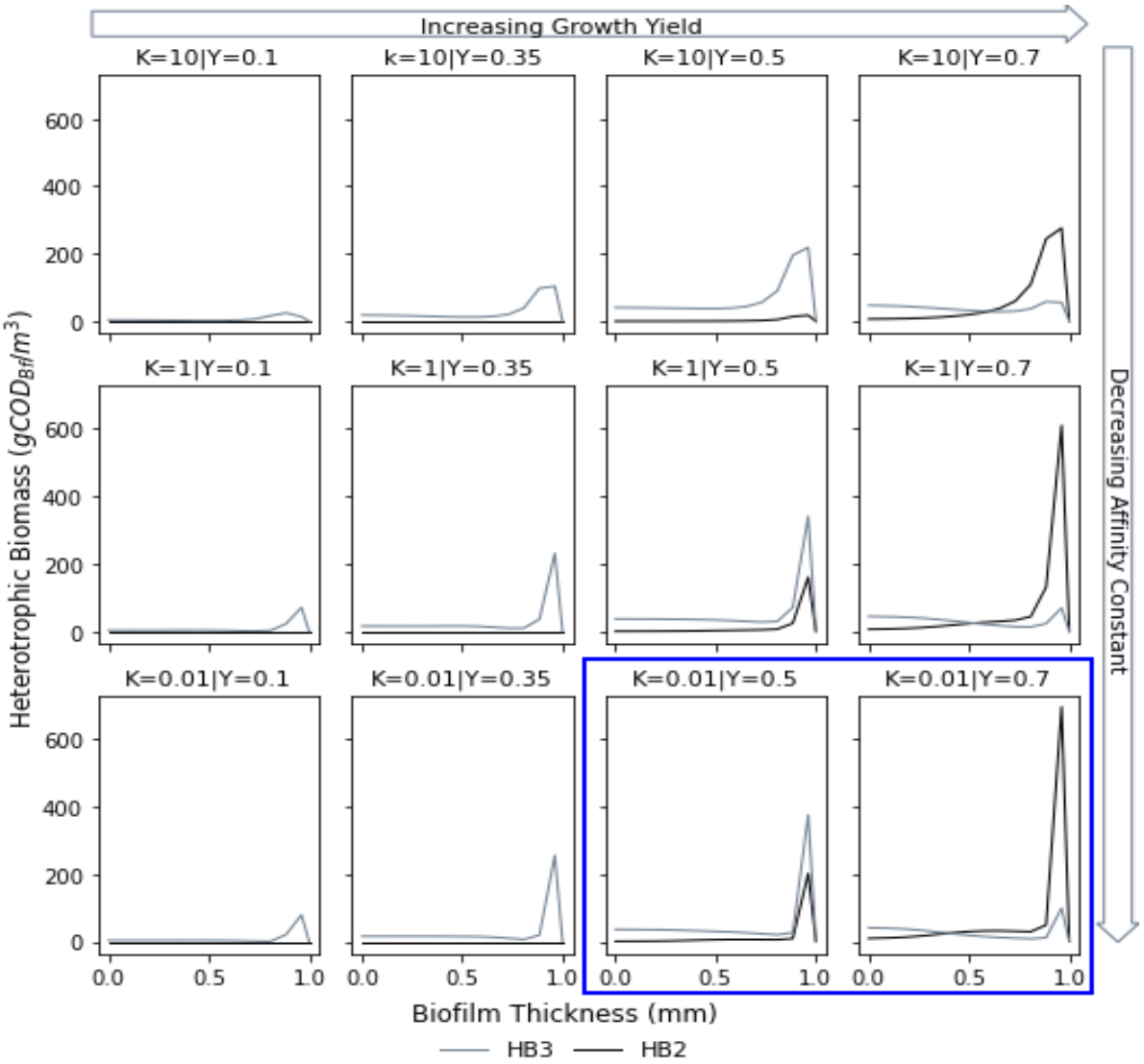

Figure P2. 5. Distribution of the heterotrophic biomass along the biofilm thickness for Scenario 1 (no external COD, COD_{Ex}=0), for a selected growth rate equal to 1.5 d^{-1} and different selected values of the affinity constant and growth yield ($gCOD_x/gCOD_{BF}$). HB2 uses NO_2^- as electron acceptor, while HB3 uses NO_3^- as electron acceptor.

Some authors challenge the mechanistic meaning of the affinity constant (K) and argue that although measurements of K provide valuable experimental information about the affinity of the bacteria to a certain substrate, it does not have a strict mechanistic interpretation (Kiørboe and Andersen 2019). Liu (2007) showed in his review that despite the many efforts of mechanistically defining K, no consensus has been reached and no intrinsic meaning can be attributed to the affinity constant of the Monod equation. In addition, Fiksen et al. (2013) even question the existence of a tradeoff between the affinity constant and the growth rate, especially in situations where diffusion plays an important role in the substrate transfer as for example environments with low substrate concentration and biofilms. Those works also claim that a proper understanding of the microbial traits is crucial to elucidate the possible tradeoffs and growth strategies that bacteria undergo depending on the specific conditions of their environment.

Within such a mechanistic framework the yield-strategy may be more suitable for the description of the behavior of bacteria under substrate limiting conditions or at least should take a prominent place alongside the K-strategy.

The results of this work show that the yield plays an important role when modelling the behavior of HB in biofilms under substrate limiting conditions and suggest that more attention has to be paid to this specific parameter and its relation to the traditional kinetics parameters μ and K. The harvesting volume arises as interesting parameter that relates both affinity constant and growth yield in a simple manner. It should be explored in more depth to elucidate the relationship between K- and yield strategy. Although, heterotrophic bacteria in conventional activated sludge systems are modeled with fast growth rates and high growth yields, our results suggest that this may not be the case in biofilm systems and under substrate-limiting conditions. In such systems the yield may be more determinant for the behavior of HB than the growth rate and a closer look to the experimental determination of the yield and its implications is worthwhile. Finally acknowledging that HB may prefer the yield strategy when growing in fully autotrophic systems such as PN/A reactors could help to also focus on isolation, cultivation and analysis of species that cannot be found in conventional laboratory settings where fast-growing bacteria are favored and yield strategists may be outgrown.

4. Conclusions

Between the evaluated parameters: Affinity constant (K), maximum growth rate (μ) and yield, the yield showed the strongest influence on the production of N_2 by the heterotrophic community in the two evaluated scenarios.

The diversity of the community is determined to a large extent by the yield, where high yield values are more advantageous to diverse communities. The composition and the diversity of the heterotrophic community is highly dependent on the value of the yield. When HB grow solely on COD_{BF}, HB2 and HB3 coexist only at high yield values, regardless on the values of K and μ. Likewise, when external COD is available, the HB community composition fluctuates with the yield, but it remains nearly constant with μ and K.

If the postulates of the microbial transition state theory are sound and K and yield are dependent, it could be that what we know as a k-strategy is a form of a yield strategy.

5. Supplementary Material

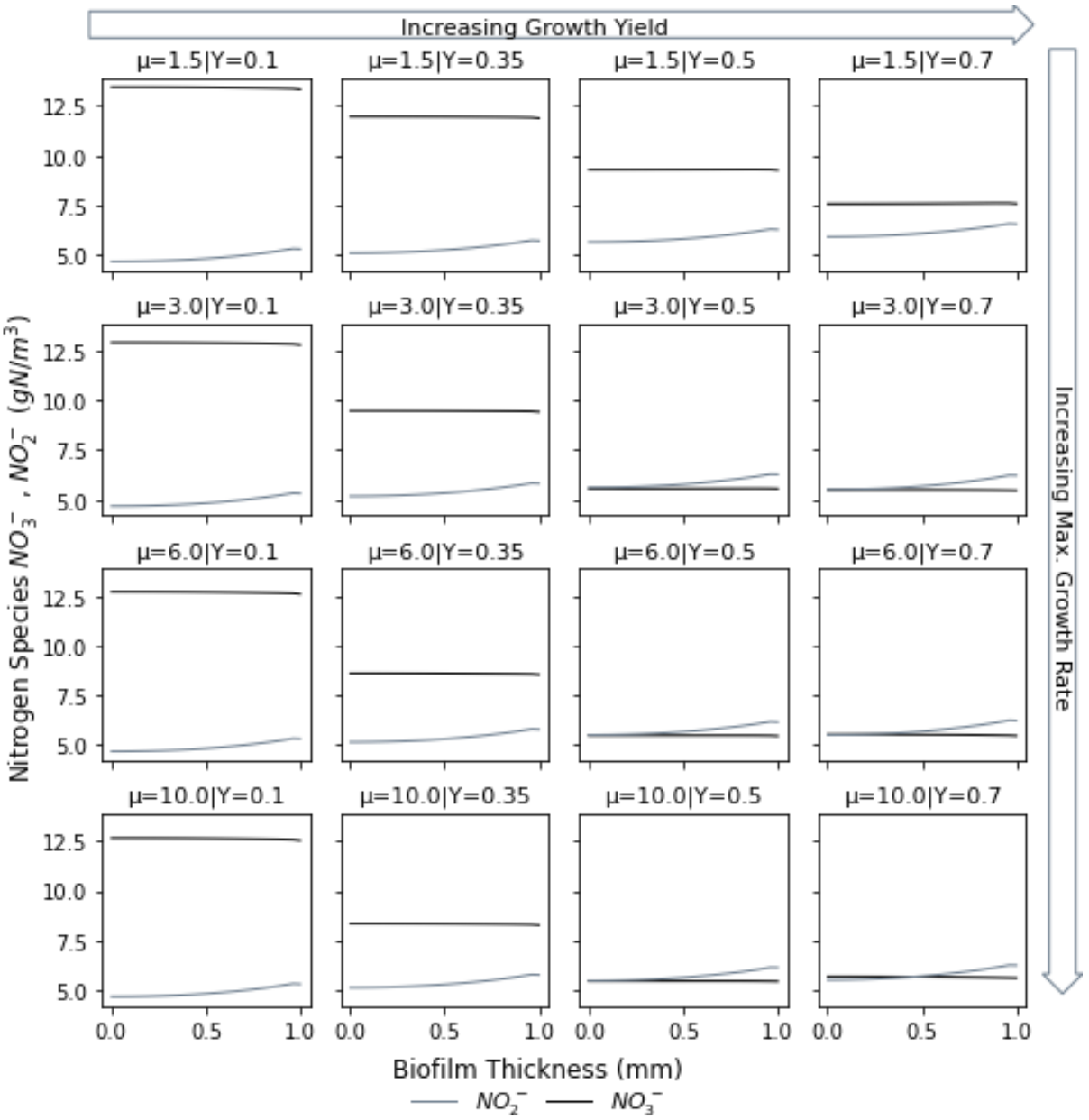

Figure P2. 6. Distribution of the NO2- and NO3- concentrations along the biofilm thickness for Scenario 1 (no external COD, CODEx=0), for a selected affinity constant equal to 10 gCODBF/m^3 and different selected values of the maximum growth velocity (d-1) and of the growth yield (gCODx/gCODBF).

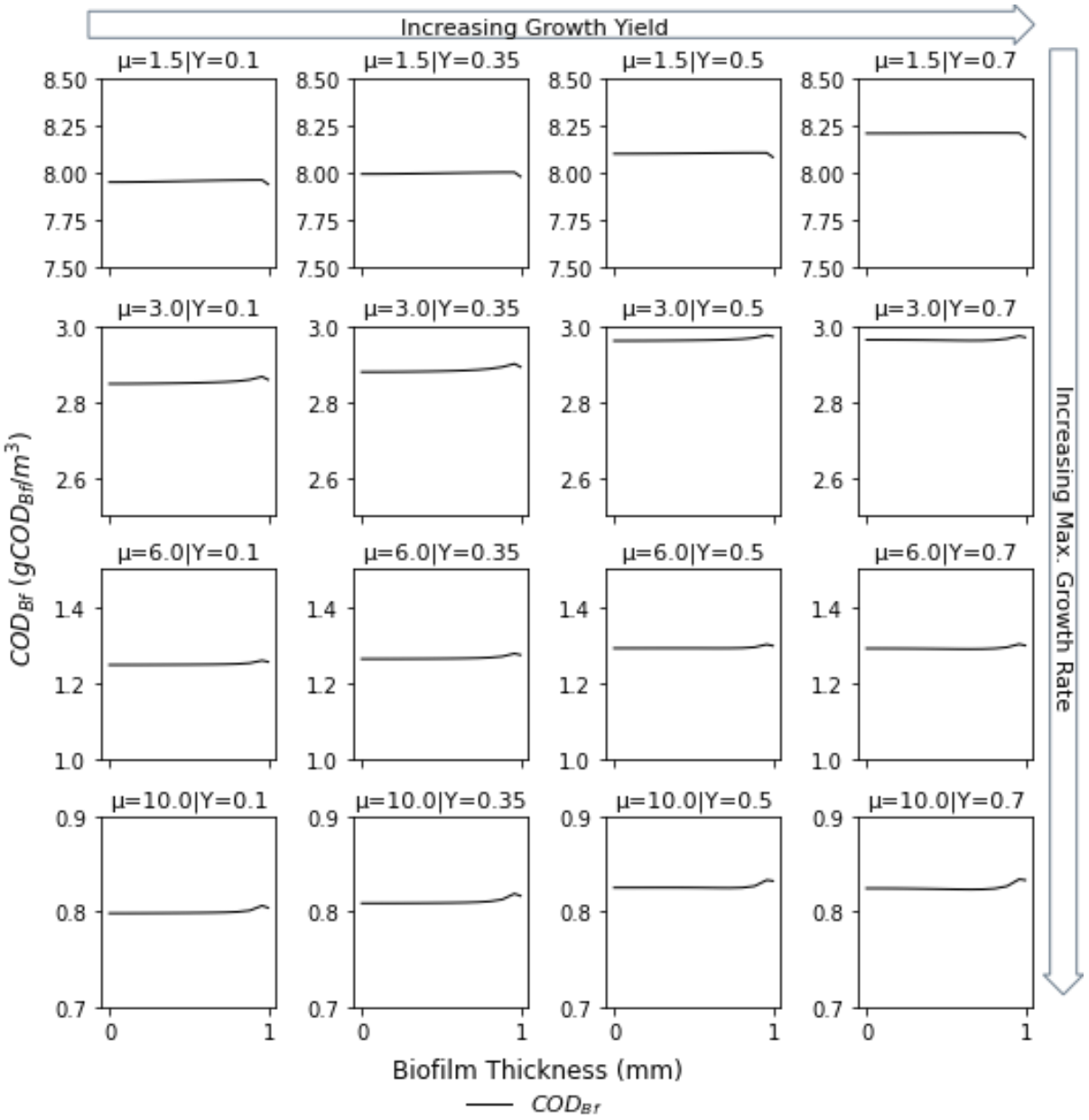

Figure P2. 7. Distribution of the COD_{BF} concentration along the biofilm thickness for Scenario 1 (no external COD, COD_{Ex}=0), for a selected affinity constant equal to 10 $gCOD_{BF}/m^3$ and different selected values of the maximum growth velocity (d^{-1}) and of the growth yield ($gCOD_x/gCOD_{BF}$).

Table P2. 2. Peterson matrix: soluble variables

	S_{CODBf}	S_{CODEx}	S_{NH4}	S_{O2}	S_{NO2}	S_{NO3}	S_{N2}
	mgCOD_{Bf}/l	mgCOD_{Ex}/l	mg-N/l	mg-N/l	mg-N/l	mg-N/l	mg-N/l
Growth of AOB	-	-	$-i_{NXB}-1/Y_{AOB}$	$-\frac{3.43-Y_{AOB}}{Y_{AOB}}$	$1/Y_{AOB}$	-	-
Growth of NOB	-	-	$-i_{NXB}$	$-\frac{1.14-Y_{NOB}}{Y_{NOB}}$	$-1/Y_{NOB}$	$1/Y_{NOB}$	-
Growth of AnAOB	-	-	$-i_{NXB}-1/Y_{AnAOB}$	-	$-\frac{1}{1.14}-\frac{1}{Y_{AnAOB}}$	1/1.14	$2/Y_{AnAOB}$
Aerobic Growth of HB	$-1/Y_{HB1}$	-	$-i_{NXB}$	$-\frac{1-Y_{HB1}}{Y_{HB1}}$	-	-	-
Growth of HB on NO_2^-	$-1/Y_{HB2}$	-	$-i_{NXB}$	-	$-\frac{1-Y_{HB2}}{1.71Y_{HB2}}$	-	$\frac{1-Y_{HB2}}{1.71Y_{HB2}}$
Growth of HB NO_3^-	$-1/Y_{HB3}$	-	$-i_{NXB}$	-	-	$-\frac{1-Y_{HB3}}{2.86Y_{HB3}}$	$\frac{1-Y_{HB3}}{2.86Y_{HB3}}$
Aerobic Growth of HB on COD_{Ex}	-	$-1/Y_{HB1,\ CODEx}$	$-i_{NXB}$	$-\frac{1-Y_{HB1,CODex}}{Y_{HB1,SB}}$	-	-	-
Growth of HB on NO_2^- and COD_{Ex}	-	$-1/Y_{HB2,\ CODEx}$	$-i_{NXB}$	-	$-\frac{1-Y_{HB2,CODex}}{1.71Y_{HB2,CODEx}}$	-	$\frac{1-Y_{HB2,CODEx}}{1.71Y_{HB2,CODEx}}$
Growth of HB NO_3^- on COD_{Ex}	-	$-1/Y_{HB3,\ CODEx}$	$-i_{NXB}$	-		$-\frac{1-Y_{HB3,CODEx}}{2.86Y_{HB3,CODEx}}$	$\frac{1-Y_{HB3,CODEx}}{2.86Y_{HB3,CODEx}}$
Decay AOB	$1-f_i$	-	-	-	-	-	-
Decay NOB	$1-f_i$	-	-	-	-	-	-
Decay AnAOB	$1-f_i$	-	-	-	-	-	-
Decay HB1	$1-f_i$	-	-	-	-	-	-
Decay HB2	$1-f_i$	-	-	-	-	-	-
Decay HB3	$1-f_i$	-	-	-	-	-	-
Decay HB1, COD_{Ex}	$1-f_i$	-	-	-	-	-	-
Decay HB2, COD_{Ex}	$1-f_i$	-	-	-	-	-	-
Decay HB3, COD_{Ex}	$1-f_i$	-	-	-	-	-	-

Table P2. 3. Peterson matrix : particulate variables

	X_I	X_{AOB}	X_{NOB}	X_{AnAOB}	X_{HB1}	X_{HB2}	X_{HB3}	X_{HB1} CODEx	X_{HB2} CODEx	X_{HB3} CODEx
	mgCOD/l	$mgCOD_B/l$	$mgCOD_B/l$	$mgCOD_B/l$	$mgCOD_B/l$	$mgCOD_B/l$	$mgCOD_B/l$	$mgCOD_B/l$	$mgCOD_B/l$	$mgCOD_B/l$
Growth of AOB	-	1	-	-	-	-	-	-	-	-
Growth of NOB	-	-	1	-	-	-	-	-	-	-
Growth of AnAOB	-	-	-	1	-	-	-	-	-	-
Aerobic Growth of HB	-	-	-	-	1	-	-	-	-	-
Growth of HB on NO_2^-	-	-	-	-	-	1	-	-	-	-
Growth of HB NO_3^-	-	-	-	-	-	-	1	-	-	-
Aerobic Growth of HB, COD_{Ex}	-	-	-	-	-	-	-	1	-	-
Growth of HB on NO2- ,CODEx	-	-	-	-	-	-	-	-	1	-
Growth of HB NO3- CODEx	-	-	-	-	-	-	-	-	-	1
Decay AOB	f_i	-1	-	-	-		-	-	-	-
Decay NOB	f_i	-	-1	-	-		-	-	-	-
Decay AnAOB	f_i	-	-	-1	-		-	-	-	-
Decay HB1	f_i	-	-	-	-1	-	-	-	-	-
Decay HB2	f_i	-	-	-	-	-1	-	-	-	-

Decay HB3	f_i	-	-	-	-	-	-1	-	-	-
Decay HB1, CODEx	f_i	-	-	-	-	-	-	-1	-	-
Decay HB2, CODEx	f_i	-	-	-	-	-	-	-	-1	-
Decay HB3, CODEx	f_i	-	-	-	-	-	-	-	-	-1

Table P2. 4. Peterson matrix : rate formulations

Rate / Process	
Growth of AOB	$\mu_{\mathrm{AOB}} \mathrm{X}_{\mathrm{AOB}} \frac{\mathrm{S}_{\mathrm{NH4}}}{\mathrm{K}_{\mathrm{NH4,AOB}} + \mathrm{S}_{NH4}} \frac{S_{O2}}{K_{O2,AOB} + S_{O2}}$
Growth of NOB	$\mu_{\mathrm{NOB}} \mathrm{X}_{\mathrm{NOB}} \frac{\mathrm{S}_{\mathrm{NO2}}}{\mathrm{K}_{\mathrm{NO2,NOB}} + \mathrm{S}_{NO2}} \frac{S_{O2}}{K_{O2,NOB} + S_{O2}}$
Growth of AnAOB	$\mu_{\mathrm{AnAOB}} \mathrm{X}_{\mathrm{AnAOB}} \frac{\mathrm{S}_{\mathrm{NH4}}}{\mathrm{K}_{\mathrm{NH4,AnAOB}} + \mathrm{S}_{NH4}} \frac{S_{NO2}}{K_{NO2,AnAOB} + S_{NO2}} \frac{K_{O2,AnAOB}}{K_{O2,AnAOB} + S_{NO2}}$
Aerobic Growth of HB1	$\mu_{\mathrm{HB1},CODBf} \mathrm{X}_{\mathrm{HB1}} \frac{\mathrm{S}_{CODBf}}{\mathrm{K}_{\mathrm{HB1},CODBf} + \mathrm{S}_{CODBf}} \frac{S_{O2}}{K_{O2,HB1} + S_{O2}}$
Growth of HB2 on NO_2^-	$\mu_{\mathrm{HB2},CODBf} \mathrm{X}_{\mathrm{HB2}} \eta_{\mathrm{anox}} \frac{\mathrm{S}_{CODBf}}{\mathrm{K}_{\mathrm{HB2},CODBf} + \mathrm{S}_{CODBf}} \frac{S_{NO2}}{K_{NO2,HB2} + S_{NO2}}$
Growth of HB3 NO_3^-	$\mu_{\mathrm{HB3},CODBf} \mathrm{X}_{\mathrm{HB3}} \eta_{\mathrm{anox}} \frac{\mathrm{S}_{CODBf}}{\mathrm{K}_{\mathrm{HB3},CODBf} + \mathrm{S}_{CODBf}} \frac{S_{NO3}}{K_{NO3,HB3} + S_{NO3}}$
Aerobic Growth of HB1 on S_B	$\mu_{\mathrm{HB1,CODEx}} \mathrm{X}_{\mathrm{HB,CODEx}} \frac{\mathrm{S}_{\mathrm{CODEx}}}{\mathrm{K}_{\mathrm{HB1,CODEx}} + \mathrm{S}_{\mathrm{CODEx}}} \frac{S_{O2}}{K_{O2,HB1} + S_{O2}}$
Growth of HB2 on NO_2^- and on	$\mu_{\mathrm{HB2,CODEx}} \mathrm{X}_{\mathrm{HB2,CODEx}} \eta_{\mathrm{anox}} \frac{\mathrm{S}_{\mathrm{CODEx}}}{\mathrm{K}_{\mathrm{HB2,CODEx}} + \mathrm{S}_{\mathrm{CODEx}}} \frac{S_{NO2}}{K_{NO2,HB2} + S_{NO2}}$
Growth of HB3 NO_3^- and on S_B	$\mu_{\mathrm{HB3,CODEx}} \mathrm{X}_{\mathrm{HB3,CODEx}} \eta_{\mathrm{anox}} \frac{\mathrm{S}_{,\mathrm{CODEx}}}{\mathrm{K}_{\mathrm{HB3,CODEx}} + \mathrm{S}_{,\mathrm{CODEx}}} \frac{S_{NO3}}{K_{NO3,HB3} + S_{NO3}}$
Decay AOB	$b_{\mathrm{AOB}} \mathrm{X}_{\mathrm{AOB}}$
Decay NOB	$b_{\mathrm{NOB}} \mathrm{X}_{\mathrm{NOB}}$
Decay AnAOB	$b_{\mathrm{AnAOB}} \mathrm{X}_{\mathrm{AnAOB}}$
Decay HB1	$b_{\mathrm{HB1}} \mathrm{X}_{\mathrm{HB1}}$
Decay HB2	$b_{\mathrm{HB2}} \mathrm{X}_{\mathrm{HB2}}$
Decay HB3	$b_{\mathrm{HB3}} \mathrm{X}_{\mathrm{HB3}}$
Decay HB1, COD_{Ex}	$b_{\mathrm{HB1}} \mathrm{X}_{\mathrm{HB1,CODEx}}$
Decay HB2, COD_{Ex}	$b_{\mathrm{HB2}} \mathrm{X}_{\mathrm{HB2,CODEx}}$
Decay HB3, COD_{Ex}	$b_{\mathrm{HB3}} \mathrm{X}_{\mathrm{HB3,CODEx}}$

Table P2. 5 Kinetic and stoichiometric parameters for the implemented processes .

Symbol	Unit	Description	Value	Reference
μ_{AOB}	d^{-1}	Maximum specific growth rate of AOB	2.05	(Wiesmann 1994)
$K_{NH4,AOB}$	$g\text{-}N/m^3$	Affinity constant NH_4^+ for AOB	2.4	(Wiesmann 1994)
$K_{O2,AOB}$	$g\text{-}COD/m^3$	Affinity constant O_2 for AOB	0.6	(Wiesmann 1994)
b_{AOB}	d^{-1}	Decay rate for AOB	0.13	(Wiesmann 1994)
μ_{NOB}	d^{-1}	Maximum specific growth rate of NOB	1.45	(Wiesmann 1994)
$K_{NO2,NOB}$	$g\text{-}N/m^3$	Affinity constant NO_2^- for NOB	5.5	(Koch et al. 2000)
$K_{O2,NOB}$	$g\text{-}COD/m^3$	Affinity constant O_2 for NOB	2.2	(Wiesmann 1994)
b_{NOB}	d^{-1}	Decay rate for NOB	0.06	(Wiesmann 1994)
μ_{AnAOB}	d^{-1}	Maximum specific growth rate of AnAOB	0.08	(Koch et al. 2000)
$K_{NH4,AnAOB}$	$g\text{-}N/m^3$	Affinity constant NH_4^+ for AnAOB	0.07	(Strous et al. 1998)
$K_{NO2,AnAOB}$	$g\text{-}N/m^3$	Affinity constant NO_2^- for AnAOB	0.04	(Hao, 2002)
$K_{O2,AnAOB}$	$g\text{-}COD/m^3$	Inhibition constant O_2 for AnAOB	0.01	(Strous et al. 1998)
b_{AnAOB}	d^{-1}	Decay rate for AnAOB	0.003	(Hao et al. 2002b)

Heterotrophic Bacteria (HB)

$\mu_{HB1,CODEx}$ $\mu_{HB2,CODEx}$ $\mu_{HB3,CODEx}$	d^{-1}	Maximum specific growth rate of HB on COD_{Ex}	6	(Henze et al. 2000)
$\mu_{HB1,CODBf}$ $\mu_{HB2,CODBf}$ $\mu_{HB3,CODBf}$	d^{-1}	Maximum specific growth rate of HB growing on COD_{Bf}	Variable	---
$K_{O2,HB1}$	$g\text{-}COD/m^3$	Affinity constant O_2 for HB1	0.2	(Henze et al. 2000)
$K_{HB1,CODBf}$ $K_{HB2,CODBf}$	$g\text{-}CODBf/m^3$	Affinity constant COD for HB1, HB2, HB3 on ,COD_{Bf}	Variable	---

$K_{HB3,CODBf}$				
$K_{HB1,CODEx}$ $K_{HB2,CODEx}$ $K_{HB3,CODEx}$	g-COD_{Ex}/m^3	Affinity constant S_B for HB1, HB2, HB3 on COD_{Ex}	10	(Henze et al. 2000)
$K_{NO2,HB2}$	g-N/m^3	Affinity constant NO_2^- for HB2	0.3	(Alpkvist et al. 2006)
$K_{NO3,HB3}$	g-N/m^3	Affinity constant NO_3^- for HB3	0.3	(Alpkvist et al. 2006)
b_{HB1} b_{HB2} b_{HB3}	d^{-1}	Decay rate for HB1, HB2,HB3	0.62	(Henze et al. 2000)
η_{anox}	-	Anoxic reduction factor for growth	0.8	(Henze et al. 2000)

Stiochometric parameters

Y_{AOB}	g-COD_B/g-N	Growth yield for AOB	0.15	(Wiesmann 1994)
Y_{NOB}	g-COD_B/g-N	Growth yield for NOB	0.041	(Wiesmann 1994)
Y_{AnAOB}	g-COD_B/g-N	Growth yield for AnAOB	0.159	(Strous et al. 1998)
$Y_{HB1,CODBf}$ $Y_{HB2,CODBf}$ $Y_{HB3,CODBf}$	g-COD_B/g-COD	Growth yield for HB1, HB2 and HB3 on COD_{Bf}	Variable	---
$Y_{HB1,CODEx}$ $Y_{HB2,CODEx}$ $Y_{HB3,CODEx}$	g-COD_B/g-COD_{Ex}	Growth yield for HB1, HB2 and HB3 on COD_{Ex}	0.67	(Henze et al. 2000)
i_{NXB}	g-N/g-COD_B	Nitrogen content in biomass	0.086	(Henze et al. 2000)
i_{NXI}	g-N/g-COD	Nitrogen content in X_i	0.06	(Henze et al. 2000)
f_i	-	Fraction of biomass into particulate inert material	0.08	(Henze et al. 2000)

References

Agrawal, S., Karst, S.M., Gilbert, E.M., Horn, H., Nielsen, P.H. and Lackner, S. (2017) The role of inoculum and reactor configuration for microbial community composition and dynamics in mainstream partial nitritation anammox reactors. MicrobiologyOpen 6(4), e00456.

Aksnes, D.L. and Cao, F.J. (2011) Inherent and apparent traits in microbial nutrient uptake. Marine Ecology Progress Series 440, 41-51.

Alpkvist, E., Picioreanu, C., van Loosdrecht, M.C.M. and Heyden, A. (2006) Three-dimensional biofilm model with individual cells and continuum EPS matrix. Biotechnol Bioeng 94(5), 961-979.

Andrews, J.H. and Harris, R.F. (1986) r-and K-selection and microbial ecology. Advances in microbial ecology, 99-147.

Azari, M., Le, A.V., Lübken, M. and Denecke, M. (2018) Model-based analysis of microbial consortia and microbial products in an anammox biofilm reactor. Water Science and Technology 77(7), 1951-1959.

Barker, D.J. and Stuckey, D.C. (1999) A review of soluble microbial products (SMP) in wastewater treatment systems. Water Research 33(14), 3063-3082.

Beardmore, R.E., Gudelj, I., Lipson, D.A. and Hurst, L.D. (2011) Metabolic trade-offs and the maintenance of the fittest and the flattest. Nature 472(7343), 342-346.

Conthe, M., Lycus, P., Arntzen, M.Ø., Ramos da Silva, A., Frostegård, Å., Bakken, L.R., Kleerebezem, R. and van Loosdrecht, M.C.M. (2019) Denitrification as an N2O sink. Water research 151, 381-387.

Dapena-Mora, A., Van Hulle, S.W., Luis Campos, J., Méndez, R., Vanrolleghem, P.A. and Jetten, M. (2004) Enrichment of Anammox biomass from municipal activated sludge: experimental and modelling results. 79(12), 1421-1428.

Fiksen, Ø., Follows, M.J. and Aksnes, D.L. (2013) Trait-based models of nutrient uptake in microbes extend the Michaelis-Menten framework. Limnology and Oceanography 58(1), 193-202.

Gilbert, E.M., Agrawal, S., Karst, S.M., Horn, H., Nielsen, P.H. and Lackner, S. (2014) Low Temperature Partial Nitritation/Anammox in a Moving Bed Biofilm Reactor Treating Low Strength Wastewater. Environmental Science & Technology 48(15), 8784-8792.

Hao, X., Heijnen, J.J. and van Loosdrecht, M.C.M. (2002b) Sensitivity analysis of a biofilm model describing a one-stage completely autotrophic nitrogen removal (CANON) process. Biotechnol Bioeng 77(3), 266-277.

Henze, M., Gujer, W., Mino, T. and van Loosedrecht, M. (2000) Activated Sludge Models ASM1, ASM2, ASM2d and ASM3.

Henze, M., Gujer, W., Mino, T. and van Loosedrecht, M. (2006) Activated Sludge Models ASM1, ASM2, ASM2d and ASM3, IWA Publishing.

Kindaichi, T., Ito, T. and Okabe, S. (2004) Ecophysiological Interaction between Nitrifying Bacteria and Heterotrophic Bacteria in Autotrophic Nitrifying Biofilms as Determined by Microautoradiography-Fluorescence In Situ Hybridization. Applied and Environmental Microbiology 70(3), 1641-1650.

Kiørboe, T. and Andersen, K.H. (2019) Nutrient affinity, half-saturation constants and the cost of toxin production in dinoflagellates. Ecology Letters 22(3), 558-560.

Koch, G., Egli, K., Van der Meer, J.R. and Siegrist, H. (2000) Mathematical modeling of autotrophic denitrification in a nitrifying biofilm of a rotating biological contactor. Water Science and Technology 41(4-5), 191-198.

Kreft, J.-U. and Bonhoeffer, S. (2005a) The evolution of groups of cooperating bacteria and the growth rate versus yield trade-off. Microbiology 151(3), 637-641.

Kreft, J.U. (2004) Biofilms promote altruism. Microbiology (Reading) 150(Pt 8), 2751-2760.

Lackner, S., Terada, A. and Smets, B.F. (2008a) Heterotrophic activity compromises autotrophic nitrogen removal in membrane-aerated biofilms: results of a modeling study. Water Res 42(4-5), 1102-1112.
Lipson, D.A., Monson, R.K., Schmidt, S.K. and Weintraub, M.N. (2009) The trade-off between growth rate and yield in microbial communities and the consequences for under-snow soil respiration in a high elevation coniferous forest. Biogeochemistry 95(1), 23-35.
Liu, Y. (2007) Overview of some theoretical approaches for derivation of the Monod equation. Appl Microbiol Biotechnol 73(6), 1241-1250.
Liu, Y., Gu, J. and Zhang, M. (2020) A-B Processes: Towards Energy Self-sufficient Municipal Wastewater Treatment, IWA Publishing.
Liu, Y., Sun, J., Peng, L., Wang, D., Dai, X. and Ni, B.-J. (2016b) Assessment of Heterotrophic Growth Supported by Soluble Microbial Products in Anammox Biofilm using Multidimensional Modeling. Scientific Reports 6(1), 27576.
MacLean, R.C. and Gudelj, I. (2006) Resource competition and social conflict in experimental populations of yeast. Nature 441(7092), 498-501.
Matsumoto, S., Katoku, M., Saeki, G., Terada, A., Aoi, Y., Tsuneda, S., Picioreanu, C. and Van Loosdrecht, M.C.M. (2010) Microbial community structure in autotrophic nitrifying granules characterized by experimental and simulation analyses. 12(1), 192-206.
Merkey, B.V., Rittmann, B.E. and Chopp, D.L. (2009) Modeling how soluble microbial products (SMP) support heterotrophic bacteria in autotroph-based biofilms. J Theor Biol 259(4), 670-683.
Ni, B.-J., Ruscalleda, M. and Smets, B.F. (2012) Evaluation on the microbial interactions of anaerobic ammonium oxidizers and heterotrophs in Anammox biofilm. Water Research 46(15), 4645-4652.
Nogueira, R., Elenter, D., Brito, A., Melo, L.F., Wagner, M. and Morgenroth, E. (2005) Evaluating heterotrophic growth in a nitrifying biofilm reactor using fluorescence in situ hybridization and mathematical modeling. Water Science and Technology 52(7), 135-141.
Pfeiffer, T., Schuster, S. and Bonhoeffer, S. (2001) Cooperation and Competition in the Evolution of ATP-Producing Pathways. Science 292(5516), 504-507.
Reichert, P. (1994) AQUASIM – A TOOL FOR SIMULATION AND DATA ANALYSIS OF AQUATIC SYSTEMS. Water Science and Technology 30(2), 21-30.
Rittmann, B.E. and Brunner, C.W. (1984) The Nonsteady-State-Biofilm Process for Advanced Organics Removal. Journal (Water Pollution Control Federation) 56(7), 874-880.
Rittmann, B.E., Regan, J.M. and Stahl, D.A. (1994) Nitrification as a source of soluble organic substrate in biological treatment. Water Science and Technology 30(6), 1-8.
Strous, M., Heijnen, J.J., Kuenen, J.G. and Jetten, M.S.M. (1998) The sequencing batch reactor as a powerful tool for the study of slowly growing anaerobic ammonium-oxidizing microorganisms. Appl Microbiol Biotechnol 50(5), 589-596.
Ugalde-Salas, P., Desmond-Le Quéméner, E., Harmand, J., Rapaport, A. and Bouchez, T. (2020) Insights from Microbial Transition State Theory on Monod's Affinity Constant. Scientific Reports 10(1), 5323.
Vadivelu, V.M., Yuan, Z., Fux, C. and Keller, J. (2006) Stoichiometric and kinetic characterisation of Nitrobacter in mixed culture by decoupling the growth and energy generation processes. 94(6), 1176-1188.
van den Berg, E.M., Elisário, M.P., Kuenen, J.G., Kleerebezem, R. and van Loosdrecht, M. (2017) Fermentative bacteria influence the competition between denitrifiers and DNRA bacteria. Frontiers in Microbiology 8, 1684.
Wan, X., Baeten, J.E. and Volcke, E.I.P. (2019) Effect of operating conditions on N2O emissions from one-stage partial nitritation-anammox reactors. Biochemical Engineering Journal 143, 24-33.
Wiesmann, U. (1994) Biotechnics/Wastewater, pp. 113-154, Springer Berlin Heidelberg, Berlin, Heidelberg.

Wortel, M.T., Noor, E., Ferris, M., Bruggeman, F.J. and Liebermeister, W. (2018) Metabolic enzyme cost explains variable trade-offs between microbial growth rate and yield. PLOS Computational Biology 14(2), e1006010.

P3. Membrane Aerated Biofilm Reactors -How longitudinal gradients influence nitrogen removal – A conceptual study

Vanessa Acevedo Alonso, Susanne Lackner.
In: Water Research, Volume 166, 12 September 2019, 115060.
https://doi.org/10.1016/j.watres.2019.115060

Abstract

Membrane-aerated biofilm reactors are becoming more important for nitrogen removal in the wastewater sector. One-dimensional (1D) models are widely used to study the performance of such systems; however, 1D models are not able to simulate the longitudinal gradients that exist in the reactor. Although there is experimental evidence that points to the existence of longitudinal gradients simple modeling approaches that consider these gradients are not yet developed. This study proposes a novel multi-compartment model that simulates the longitudinal substrate and oxygen gradients. It assesses the effects of temperature, biofilm thickness, number of compartments, and flow configuration (liquid and gas phase) on the modeling results. Additionally, it compares the capabilities of a traditional 1D model with those of the novel multi-compartment model. Our results show that a classical 1D model predicts a lower total dissolved nitrogen concentration (TDN) in the effluent in contrast to the predictions of the multi-compartment model. In the worst-case scenario, the TDN predicted by the traditional 1D model was three times lower than the prediction of the multi-compartment model. The results delivered by the models differ also in the axial gradients. The traditional 1D model, for example, predicted an oxygen concentration at the membrane surface of 0.4 mg-O2/l while the multi-compartment model predicted a concentration of 2.9 mg-O2/l. Finally, the results of this study show that the longitudinal oxygen gradient has an important effect on both, biomass distribution and effluent TDN, whereas the longitudinal substrate exclusively affected the effluent TDN.

1. Introduction

Current research is moving towards the implementation of deammonification processes in the mainstream. One of the main goals is to develop strategies to overcome frequently encountered operational challenges, such as low temperatures (around 10°C), relatively low NH_4^+ concentrations, biomass retention and high C:N ratios (Xu et al. 2015).

One of the most widespread strategies to deal with those problems is a two-stage configuration. In the first stage COD is removed until an adequate C:N ratio is achieved. The effluent produced in this first stage is further treated in a subsequent stage through autotrophic deammonification (Han et al. 2016, Xu et al. 2015). Several processes have been tested for the second stage (Gilbert et al. 2015, Hu et al. 2013, Lotti et al. 2015a, Wang et al. 2016) among them also Membrane Aerated Biofilm Reactors (MABRs) and hybrid MABRs seem to be promising technologies (Peeters et al. 2016).

Therefore, MABRs lately regained significance in wastewater treatment. In contrast to traditional biofilm reactors, which use a co-diffusion geometry, i.e. both, electron donor and acceptor are supplied via the liquid phase, MABRs use a counter-diffusion geometry, i.e. the electron

acceptor is supplied through the membrane via the gas phase, whereas the electron donor is supplied through the liquid phase (Casey et al. 1999b).

In the case of nitrogen removal from wastewater, the diffusion of oxygen and substrates from different sides of the biofilm (membrane and bulk liquid, respectively) creates a uniquely stratified biofilm, that is capable of achieving several processes simultaneously (e.g. nitrification and denitrification or partial nitrification and anammox). The supply of oxygen from the biofilm base presents several advantages, easier oxygen control (Ni et al. 2013) and less N_2O emissions (Kinh et al., 2017) being two examples. In addition, the resistance of the diffusion layer affects the overall mass transfer less in comparison to the co-diffusion geometry (Nerenberg, 2016).

Modeling has proven to be a powerful tool for studying MABRs. Several research groups have already evaluated the influence of different factors on the performance of MABRs and their microbial communities. These studies mainly focused on the axial gradients (perpendicular to the membrane surface), the optimization of aeration patterns and the behavior of the different geometries (co- and counter-diffusion) (Lackner and Smets 2012, Liu et al. 2016a, Ni et al. 2013, Shanahan and Semmens 2004, Terada et al. 2007). Conceptual studies on MABRs use multispecies, one-dimensional models (1D) to analyze the reactor performance under the conditions of interest. Although these models predict the axial characteristics of the biofilm and the axial profiles within it, they do not include the ones occurring longitudinally (along the length of the reactor, resp. the membrane).

There is experimental evidence that oxygen and substrate concentrations change not only in the axial direction but also in the longitudinal direction. It has been reported that, depending on reactor (presence or absence of recirculation) and membrane configuration (dead-end, flow through), longitudinal substrate and oxygen profiles may appear (Hibiya et al. 2003, Martin and Nerenberg 2012, Pankhania et al. 1999, Shanahan and Semmens 2006).

The limitations of the traditional 1D models together with the experimental evidence confirming the occurrence of longitudinal substrate and oxygen gradients, disclose an important knowledge gap. The impact of longitudinal gradients on the reactor performance remains, to our knowledge, largely unexplored. Moreover, a simple method to introduce longitudinal gradients into conventional models is still missing.

This study developed a multi-compartment model for completely autotrophic nitrogen removal in AQUASIM 2.1 (Reichert 1998). It introduced longitudinal substrate and oxygen gradients, allowing the analysis of biofilm characteristics along the length of the reactor as well. The model simulated the longitudinal gradients by combining multiple single 1D models with the assumption that mass transfer is perpendicular between membrane and biofilm (IWA 2006).

In order to compare a 1D model with our multi-compartment model, different scenarios were proposed. Temperature, airflow (G_{in}), maximum biofilm thickness (L_{fmax}) and the number of compartments (n) took different values in the proposed scenarios. Additionally, several flow configurations (counter- and co-current flow) were evaluated to assess the influence of the direction of flow. The relative effect of the single inclusion of longitudinal gradients of either oxygen or substrates was also analyzed.

2. Methodology

A MABR for completely autotrophic nitrogen removal was modeled in AQUASIM 2.1 (Reichert 1998). A novel *multi-compartment model* was developed to evaluate the effect of longitudinal gradients for substrates and oxygen. Such gradients were implemented through the division of the biofilm reactor and the membrane lumen in several compartments. The Total Dissolved Nitrogen concentration (TDN) in the effluent and the biomass distribution obtained from the *multi-compartment model* and the traditional 1D models were compared and evaluated.

2.1. Model Set-Up

A multi-species model including AOB, NOB, AnAOB and HB was considered. Depending on the electron donor, the HB were divided into three groups: aerobic, NO_2^- reducing and nitrate NO_3^- reducing bacteria. Monod kinetics were applied for modelling growth and substrate conversion by the respective microorganisms. The rates were a function of the specific yield, biomass and substrate concentrations. Biomass decay was simulated using a first order kinetic expression and hydrolysis rates for organic matter and nitrogen were modelled using a simplified rate (equation P3.1) as previously suggested in Lackner et al. (2008b)

$$\frac{dX_S}{dt} = k_H \frac{X_S}{K_x} \; ; \; \frac{dX_N}{dt} = k_H \frac{X_N}{K_x} \qquad \text{(P3.1)}$$

where X_S and X_N are the particulate fractions of organics and nitrogen, respectively, k_H is the hydrolysis rate and Kx the half saturation coefficient for the hydrolysis. The supplementary material includes a comprehensive summary of all the processes and rates. The model used the kinetic parameters according to Lackner and Smets (2012).

Both compartments, biofilm reactor and membrane lumen, were represented as ideally mixed reactors, a diffusive link at the biofilm base connected both compartments. The oxygen flux (J_{O2}), represented by the diffusive link, was calculated according to equation P3.2 as proposed in Casey et al. (2000b):

$$J_{O2} = k_{tot}\left(\frac{S_{O2m}}{H} - S_{O2Bf}\right) \qquad \text{(P3.2)}$$

where k_{tot} is the total mass transfer coefficient for oxygen, S_{O2m} and S_{O2Bf} are the oxygen concentrations at the membrane and biofilm interface respectively.

The target TDN in the effluent was set to 20 g-N/m³. The reactor volume and surface area were selected in order to meet this target. At 30 and 20 °C the volume was 7.5 m³ and the specific surface area was 200 m^{-1}, for the scenarios at 10°C the volume was 20 m³ and the specific surface area 250 m-1. The inflow was set to 20 m3/d with an ammonium concentration of 100 g-N/m³ and 0 g/m3 for NO_2^--N, NO_3^--N and COD, respectively. The pH was assumed to remain constant in both axial and longitudinal directions. The COD required for the heterotrophic growth was exclusively provided by biomass decay. The influent composition was selected to represent a two-stage reactor configuration that employed carbon removal as first stage providing the effluent for the deammonification system in the second stage similar to Xu et al. (2015).

2.2. Scenarios

For the conceptual analysis of the *multi-compartment model*, different configurations and scenarios were studied. The variables and values for these scenarios were as follows:

L_{fmax}: 0.2, 0.5 and 1 mm

G_{in}: varied between 0 and 50 m^3/d

Temperature: 10, 20 and 30 °C

2.3. Temperature Dependency

The temperature dependency of the growth, decay and hydrolysis rates was modeled with an Arrhenius expression with θ being the temperature coefficient. Several studies have shown that AnAOB growth has different θ values within the temperature range of this study (Lotti et al. 2015b). Therefore, at 30 and 20 °C θ took the value of 0.096 as reported in Hao et al. (2002a), and for the simulations run at 10°C, θ took the value of 0.14. The later θ value was calculated from the activation energy reported in Lotti et al. (2015b). The temperature dependency for the diffusivity coefficients was modeled as suggested in Perry (1997). Supplementary material contains the values for the mass transfer coefficients used in the model.

2.4. Model Configurations

Five configurations were investigated and they are shown in Figure P3.1.Configuration number 1 corresponded to the traditional modeling approach with one single compartment for biofilm reactor and membrane lumen. The multi-compartment model was implemented through the division of both biofilm reactor and membrane lumen into n number of compartments (in this study, n took values of 3 and 5), that were connected by advective links.

The multi-compartment model used a recirculation Q_R when the simulation of an ideally mixed reactor (CSTR) was required. The recirculation was introduced through the artificial diffusion approach reported in Baeten et al. (2017). In their work, the authors suggest, that for a better representation of completely mixed systems in AQUASIM, the different reactors should be connected through diffusive links instead of adjective links. By doing so, numerical problems regarding the mass balance are avoided.

The multi-compartment model allowed the simulation of several configurations by deliberately inducing longitudinal substrate gradients in the biofilm reactor and longitudinal oxygen gradients in the membrane lumen Table P3.1 and Figure P3.1 summarize the configurations that were modeled.

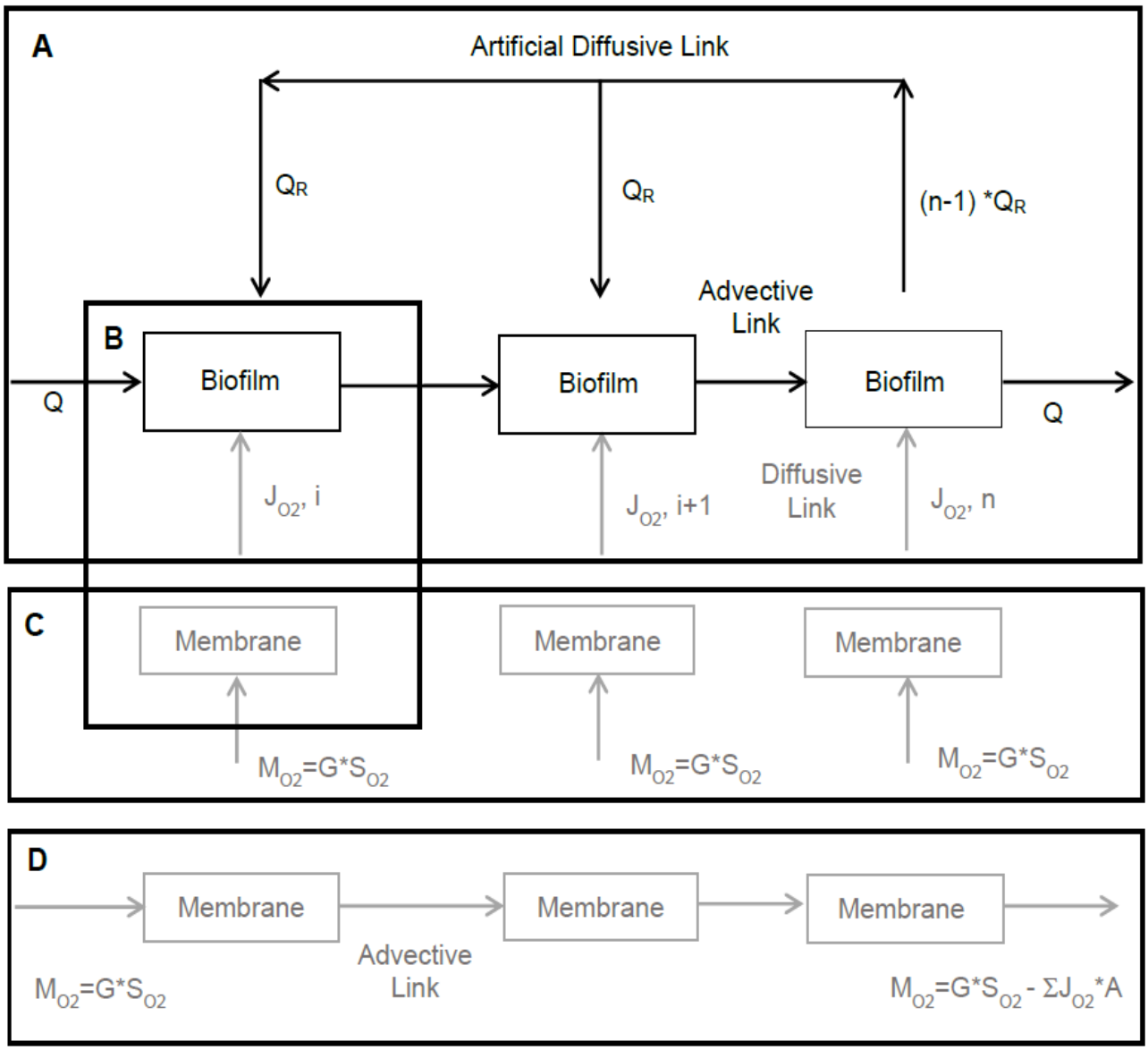

Figure P3. 1. Traditional and multi-compartment modeling approaches. Where MO2 is the mass of oxygen, G the airflow entering the system, SO2 is the concentration of oxygen in the inlet, A is the total membrane area, Q is the wastewater inflow, JO2 is the oxygen flux trough the membrane, QR is the recirculation flow, i is the compartment number and n the total number of compartments. Figure P3.1B shows the traditional approach with one compartment for both biofilm reactor and membrane lumen.

Figure P3.1B and Figure P3.1A with Q_R =0, show the configuration for modeling a MABR with substrate gradient and no oxygen gradient along the length. Figure P3.1C shows the membrane lumen configuration for modeling an MABR with oxygen gradient along the reactor´s length; in combination with Figure P3.1A: if QR > 0 the model includes the substrate gradient, if Q_R=0 the model does not include the substrate gradient.

Table P3. 1. Description of the configurations used for simulating the different combinations of oxygen and substrate longitudinal gradients. All the described configurations included axial gradients for both oxygen and substrate.

Configuration Number	Biofilm Reactor	Membrane Lumen	Schematic representation
1 (Traditional modeling approach)	One compartment as CSTR (no longitudinal substrate gradient)	One compartment as CSTR (no longitudinal oxygen gradient)	Figure P3.1B
2	n compartments as CSTR (no substrate gradient)	n compartments as plug flow (PFR) (with oxygen gradient)	Figure P3.1A + Figure P3.1D with $Q_R > 0$
3	n compartments as PFR (with substrate gradient)	n compartments as PFR (with oxygen gradient)	Figure P3.1A + Figure P3.1D with $Q_R = 0$ and co-current flow of air and wastewater
4	n compartments as PFR (with substrate gradient)	n compartments as PFR (with oxygen gradient)	Figure P3.1A + Figure P3.1D with $Q_R = 0$ and counter-current flow of air and wastewater
5	n compartments as PFR (with substrate gradient)	n compartments as CSTR (no oxygen gradient)	Figure P3.1A + Figure P3.1C with $Q_R = 0$ and

3. Results and Discussion

3.1. Optimal Airflow

The airflow is one of the key operating parameters of MABRs. Thus, finding the optimal airflow for the desired biological processes and effluent quality was the first exercise. All the configurations (Table P3.1) had their optimal airflow rate at G_{in} = 5 m³/d. This optimum corresponded to the minimal achievable TDN under the specific conditions for the respective configuration and also to the theoretical optimal ratio of oxygen flux to NH_4^+-N load (J_{O2}/L_{NH4+-N}) of 1.75 g-O_2/g-N reported in Terada et al. (2007), as can be seen in the Figures P3.8 and P3.9 the supplementary information.

The scenario at 30 °C with L_{fmax} = 0.5 mm was chosen as main example to underline our findings, because it clearly illustrates the differences between configurations and the existence of an optimum Gin. Figure P3.2 illustrates the dependency between TDN and the ratio J_{O2}/ L_{NH4+-N} for the example scenario.

Figure P3.2 shows a clear optimum for all the configurations except of configuration 4. In that configuration, the axial and longitudinal concentrations of oxygen and substrate in the biofilm did not match the optimal growth requirements of any species of the desired microbial community: the locations where oxygen was present NH_4^+-N was not and vice versa. This resulted in insufficient biomass activity which led to an inadequate performance of the reactor. Such disadvantages of using counter-current configurations have also been observed in other studies (Perez-Calleja et al. 2017). This configuration was thus of no further interest due to its restricted nitrogen removal.

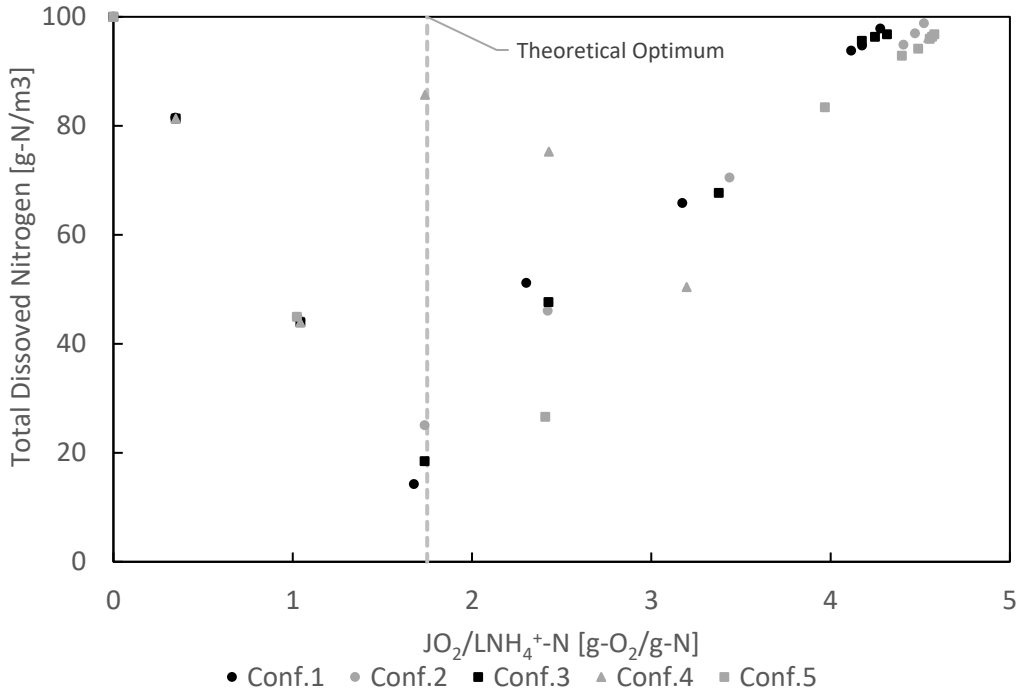

Figure P3. 2. Dependency between TDN and JO2/LNH4+-N and selected example for scenario at 30°C, Lf,max = 0.5 mm, airflow ranging from 1 to 50 m3/d and n=3. The theoretical point is 1.75 g-O2/g-N as reported in(Terada et al. 2007).

3.2. Optimal Biofilm Thickness

A comprehensive analysis was conducted for all the configurations, using the optimal Gin described in the previous section, Figure P3.3 shows the performance for each configuration at each studied temperature and $L_{f,max}$.

It has been demonstrated already experimentally, that the performance of an MABR system largely depends on the biofilm thickness (Ahmadi Motlagh et al. 2006, Martin and Nerenberg 2012, Matsumoto et al. 2007). A thicker biofilm promotes the substrate flux from the liquid. However, due to the counter-diffusion of both substrates (in case of this study NH4+-N and oxygen), there is a maximum biofilm thickness above which the NH4+-N flux stops increasing because oxygen becomes limiting and inactive layers appear (Semmens and Essila 2001, Terada et al. 2007). In addition, the mass transfer resistances increment with the biofilm thickness, so from the transport point of view an optimal biofilm thickness is also expected (Casey

et al. 2000a, b). Figure P3.3A gives an example on how a further increase in the biofilm thickness does not necessarily improve the performance of the reactor i.e. a lower TDN can be reached. This scenario at 30 °C revealed that the optimal biofilm thickness was 0.5 mm for all configurations and both thinner and thicker biofilms exhibited higher TDN concentrations in the effluent.

However, decreasing the temperature from 30°C, where the optimum biofilm thickness was 0.5 mm, showed that at 20 and 10 °C the optimum shifted to 1.0 mm (Figure P3.3). The activity of all the microbial species decreases with the temperature (Hao et al. 2002b). This decrease in activity also means a slower substrate consumption, and that more biomass is required to treat the same substrate load. As consequence, at lower temperatures an MABR requires a thicker biofilm to reach the performance of a reactor operating at higher temperatures as reflected by the results of this study.

At temperatures of 10 and 20 °C, the configurations that had a biofilm thickness of 0.2 mm showed a poor performance. The studied systems required a minimal biofilm thickness, which then comprised the required autotrophic microbial community. In the case of autotrophic nitrogen removal, it is of vital importance that the microbial community includes AnAOB. Figure P3.11 revealed how at 30°C the autotrophic microbial community was present, whereas at 20 and 10°C the biofilm consisted mainly of AOB and therefore almost no overall nitrogen removal was observed.

At 10°C, even the thickest biofilm (0.5 mm) had a poor performance. It reached TDN effluent concentrations of 60 mg/l. Experimental results from Lotti et al. (2015b) showed that temperatures lower than 15 °C have a stronger effect on AnAOB than on the other members of the microbial community. Thus, when the temperature drops below 15°C, significantly thicker biofilms are required to sustain a microbial community capable of performing complete autotrophic nitrogen removal that is biofilm that contains sufficient AnAOB.

The majority of the AnAOB was located in the outer layer of the biofilm where the oxygen concentration is nearly zero. Thinner biofilms reduce in consequence the amount of AnAOB within the biofilm, and lead to less efficient nitrogen removal. Figure P3.10 shows the axial distribution of the biomass where AnAOB were located in the more external part of the biofilm.

For configuration 5 (Table P3.1) the number of the compartments (n) did not greatly influence the TDN predictions, independently of the biofilm thickness. On the other hand, in configurations 2 and 3, the number of compartments (n) did have a significant effect on the performance of the MABR. More compartments resulted in a higher oxygen flux in the first part of the reactor (See section 3.3) and thus, depending on the specific configuration conditions, a different TDN concentration was obtained.

For the same temperature, all the model configurations predicted the same optimal biofilm thickness as the traditional model (configuration 1). Yet, configuration 1 predicted a lower TDN concentration than the configurations with a longitudinal oxygen gradient (configurations 2 and 3). It, however, predicted nearly the same TDN concentration than configuration 5.

The results discussed in this section are a first indication that neglecting longitudinal gradients may lead to underestimation of effluent TDN levels. Additionally, similar predictions between the traditional 1D model and the configuration 5 (only substrate gradient) in combination with

the negligible influence of the number of compartments (n) for this configuration, suggest, that the longitudinal oxygen gradient affects the TDN more than the longitudinal substrate gradient.

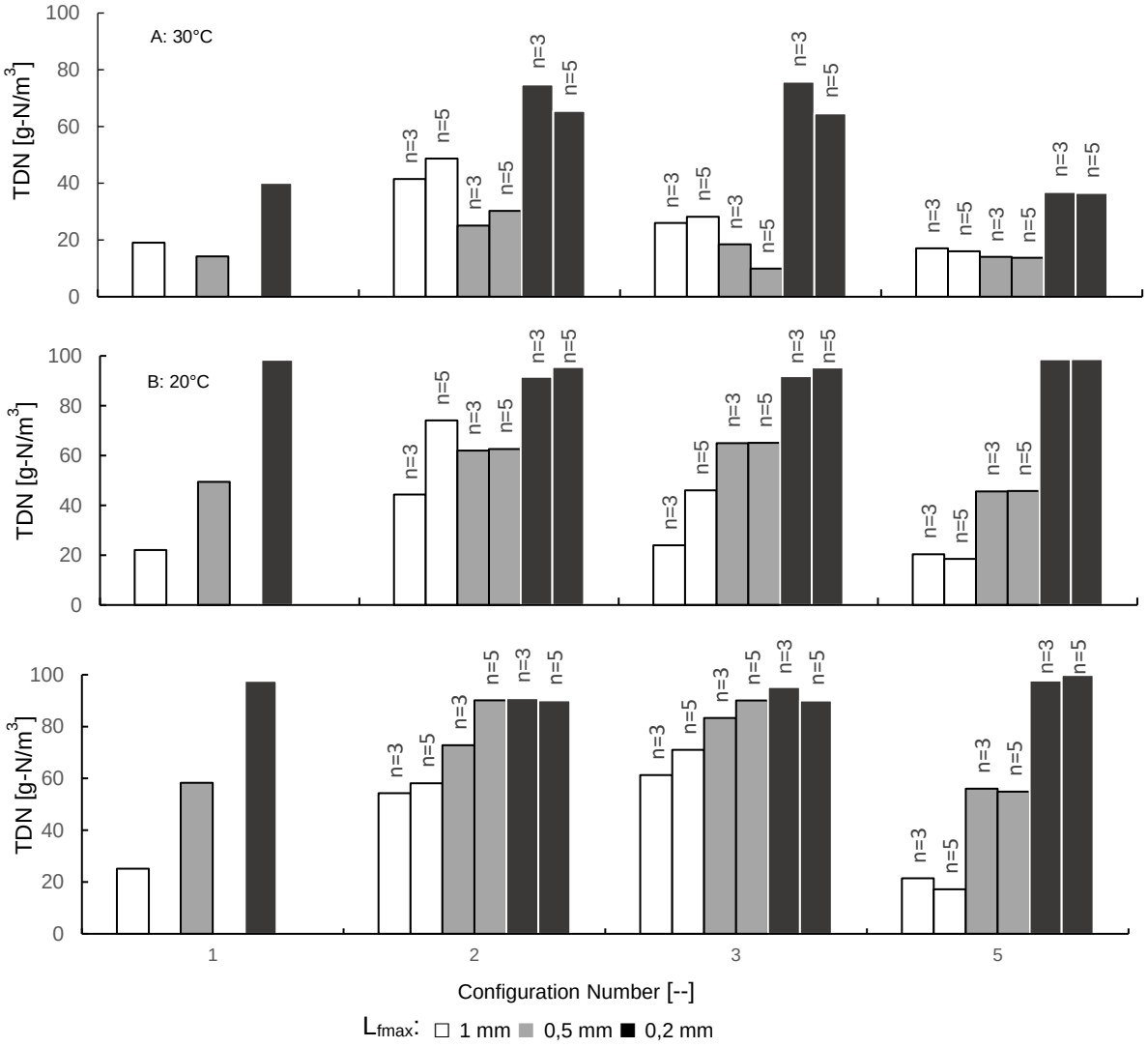

Figure P3. 3. Total dissolved nitrogen (TDN) effluent concentrations or all the configurations at each temperature and L_{fmax}, at G_{in}= 5 m^3/d.

3.3. Substrate and Oxygen Gradients

For highlighting the differences between the multi-compartment model and the traditional modelling approach, the scenario at 30 °C with Lfmax = 0.5 mm, was also selected in this section.Figure P3.4 presents the longitudinal gradients for Jo2 and the concentrations of all nitrogen species (NH_4^+-N, NO_2^--N, NO_3^--N) for the selected example scenario with the optimal airflow Gin= 5 m^3/d. Figure P3.4A shows the longitudinal oxygen gradients for all the configurations and both values of n.

Despite the evident differences in the substrate gradients (Figure P3.4C to H), configurations 2 and 3 did have nearly identical longitudinal oxygen gradients. Figure P3.4-A shows the similarities for n=3 and Figure P3.4Bf or n=5, respectively.

In contrast, the use of more compartments resulted in steeper longitudinal oxygen gradients. The differences between the number of compartments can be seen in Figures P3.4-A and P3.4-B. J_{O2} was higher in the first compartment and lower in the last compartments for n=5 (Figure P3.4-B) than in the case with n=3 (Figure P3.4-A). The steepness of the longitudinal oxygen gradient is important for a better representation of potential reactor configurations as demonstrated by the experiments conducted by Shanahan and Semmens (2006). The authors showed that steeper or flatter J_{O2} gradients could occur experimentally depending on the flow velocity of the bulk phase and the development stage of the biofilm. Other experiments have also shown that longitudinal profiles of J_{O2} take place when dead end configurations are used on the membrane side (Pankhania et al. 1999).

Figure P3.4B, Figure P3.4C and Figure P3.4D go into detail and illustrate the longitudinal NH_4^+-N, NO_2^--N and NO_3^--N concentration gradients and the influence of the number of compartments n. For configuration 2 (only longitudinal oxygen gradient), n had no significant influence on the NH_4^+-N concentration, it remained the same for both values of n. However, a steeper oxygen gradient resulted in lower NO_2^--N concentrations and conversely higher NO_3^--N concentrations. The higher J_{O2} in the first compartment for the scenarios with n=5 led to the emergence of NOB (as confirmed afterwards in Figure P3.6). Hence, more NO_2^--N was converted into NO_3^--N than into dinitrogen gas.

Configuration 3 (including both, substrate and oxygen gradients) exhibited a continuous decline of NH_4^+-N and NO_2^--N along the length. For the simulations with n=5 the values of those species in the effluent were lower than in simulations with n=3. The steeper oxygen gradient combined with the right availability of substrates were responsible for the improved performance. Almost fully anoxic zones appeared at the end of the reactor, fostering the growth of AnAOB, as shown in Figure P3.6. In configuration 3, NO_3^--N increased accordingly with the length and was slightly higher for n=5 than for n=3, due to its production by AnAOB.

In configuration 5 (only substrate gradient), n did not have an important influence on the nitrogen species. For both values of n, NH_4^+-N oxidized continuously along the length, no significant NO_2^--N accumulation was observed and NO_3^--N increased along the reactor as a result of the anammox reaction. This confirms once again the weak effect of the substrate gradient on the TDN.

The number of compartments (n) was expected to be an indicator of the steepness of the gradients. In the case of the oxygen gradient, more compartments resulted in a steeper gradient. On the contrary, the use of more compartments did not clearly change the steepness for the substrate gradients. Configurations with a substrate gradient (3 and 5) presented differences in the magnitude of the concentrations of nitrogen species for n=3 and n=5. However, these differences were rather a consequence of the difference in J_{O2} than an effect of the number of compartments.

The results of the present study indicate that the oxygen gradient may subordinate the substrate gradient. Similarly, other models have predicted a strong dependence of the nitrogen species fluxes with the oxygen concentration/flux (Downing and Nerenberg 2008). Other studies focusing on COD removal showed, how the presence of longitudinal oxygen gradients (dead-end MABR) negatively affect the COD flux, the biofilm formation and thus the reactor performance (Perez-Calleja et al. 2017). Although our findings cannot be directly compared with those results, a tendency is recognized: Oxygen concentration/flux give shape to the microbial

community and therefore the substrate tends to follow the oxygen concentrations, depending on the specific conditions of the systems.

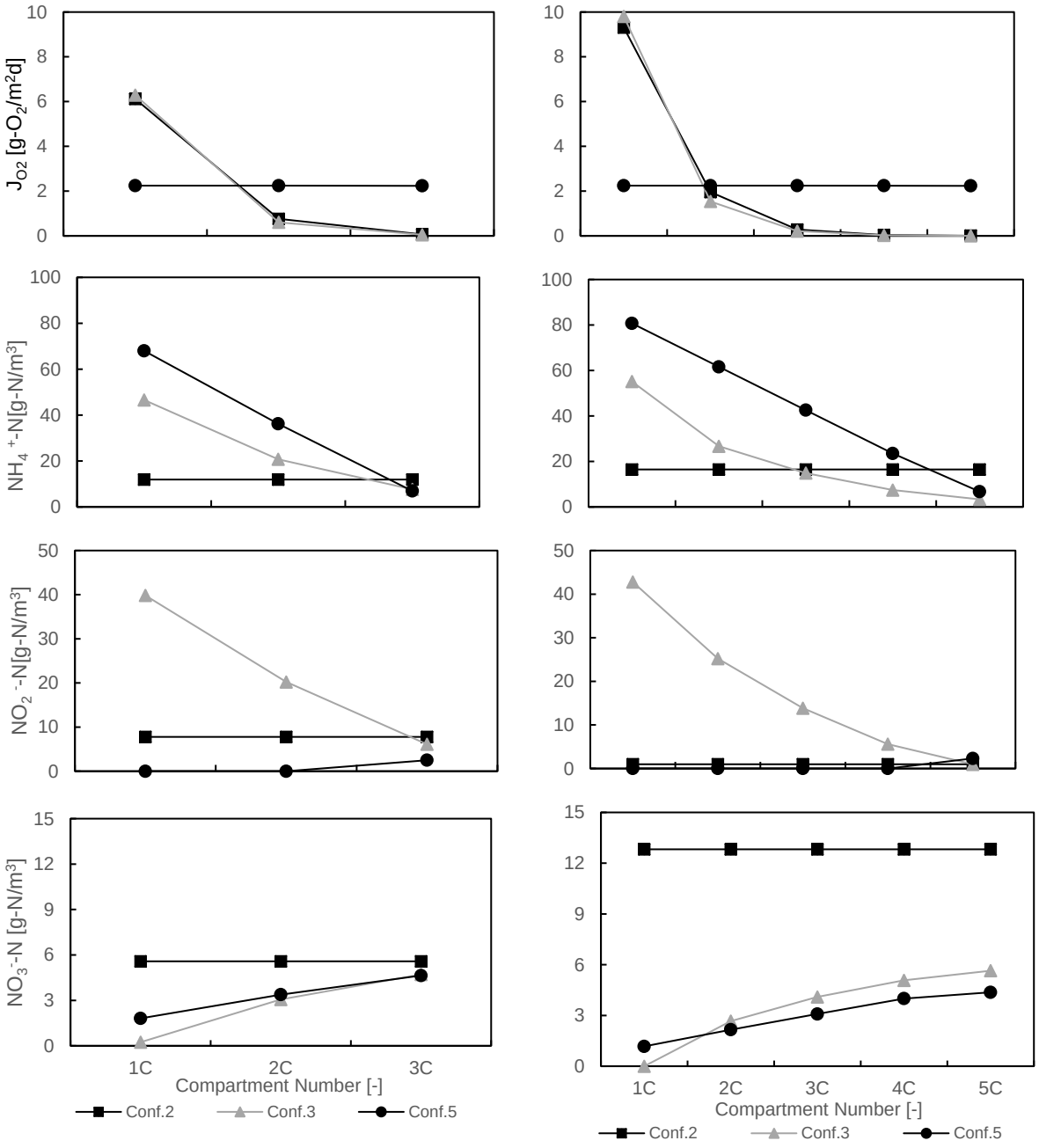

Figure P3. 4. Longitudinal profiles for the example scenario (T=30°C and L_{fmax}= 0.5mm, Gin= 5 m^3/d) for the configurations 2, 3 and 5. A and B oxygen flux profiles; C and D NH_4^+-N profiles; E and F NO_2^--N profiles; H and I NO_3^--N profiles (in all the cases for n= 3 and n=5 respectively).

3.4. Biomass Stratification

Figure P3.5 revealed that, when considering the reactor as one unit, the overall biomass distribution was comparable for all the configurations. The multi-compartment model predicted larger amounts of AnAOB biomass and less inert matter in comparison to the traditional model. The number of compartments (n) did not show a relevant influence on the overall biomass composition.

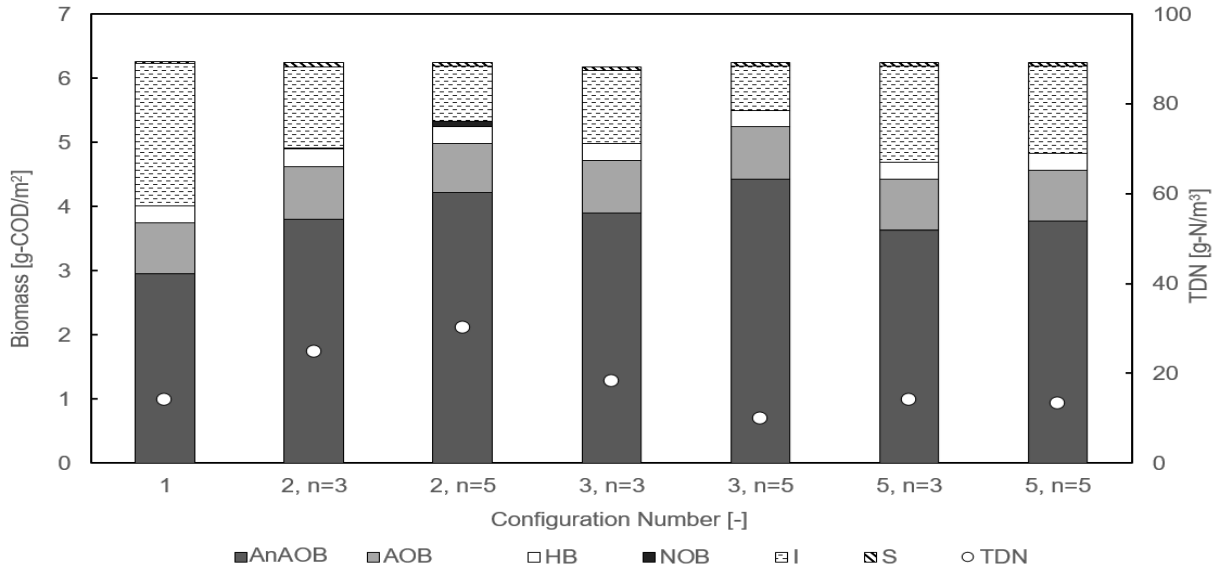

Figure P3. 5. Comparison of the global simulations results delivered by the traditional model and our multi-compartment model. Distribution of the biomass for the example scenario (T=30°C and Lfmax = 0.5mm), for the configurations 1, 2, 3 and 5, for both number of compartments (n=3 and n=5) using the optimal airflow Gin= 5 m^3/d.

The majority of related work has focused on the stratification of biomass over the biofilm depth (Boltz et al. 2017, Liu et al. 2016a, Terada et al. 2007). Longitudinal stratification has only been identified and observed in rather few studies (Gilmore et al. 2013, Pankhania et al. 1999, Röske et al. 1998, Shanahan and Semmens 2006). The traditional modelling approach neglects such stratifications, whereas the proposed multi-compartment model allows its prediction. Figure P3.6 shows the predicted biomass stratification along the length of the reactor for the example scenario. Configurations with longitudinal oxygen gradients (2 and 3) had a similar longitudinal distribution of biomass despite the differences in the substrate gradient as shown in Figure P3.6A to P3.6-D. For configuration 5 (Figure P3.6E and P3.6F), the biofilm composition was nearly the same in all the compartments. Additionally, its composition was similar to the one of configuration 1 (Figure P3.5). This suggests that the longitudinal oxygen gradient is the main driving force for biofilm composition. In configurations 2 and 3 (Figure P3.6A to P3.6D), the longitudinal oxygen gradients created a clear longitudinal stratification of the biomass. AOB appeared only in the first compartment, whereas AnAOB appeared almost exclusively in the last compartments. The first compartment had a high J_{O2}, in turn, the J_{O2} in the last compartments was close to zero and therefore such stratifications occurred. Despite the fact that configurations 2 and 3 presented the same J_{O2} in the first compartment (Figure P3.4A

and P3.4B), the biomass composition of the first compartment was different for both configurations as shown in Figure P3.6. Particularly for n=3, configuration 2 (Figure P3.6A) did not hold AnAOB, while they did appear in configuration 3 (Figure P3.6C). Likewise, for n=5, configuration 2 had NOB (Figure P3.6B), whereas in configuration 3 NOB did not appear (Figure P3.6D).

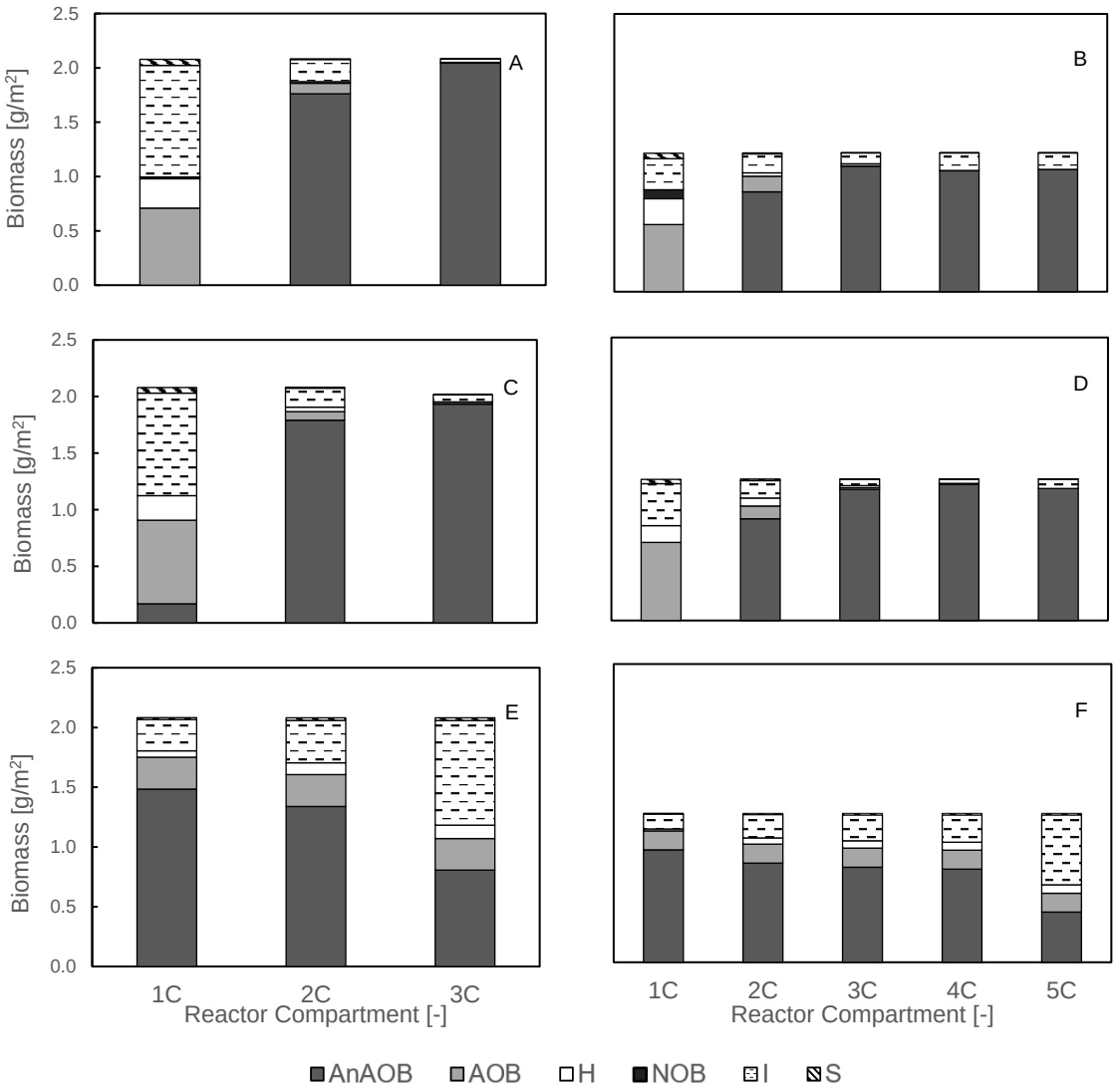

Figure P3. 6. Stratification of the biomass along the reactor's length for the example scenario (T=30°C and Lfmax=0.5mm) using the optimal airflow Gin= 5 m^3/d. A: Configuration 2 with n=3. B: Configuration 2 with n=5. C: Configuration 3 with n=3. D: Configuration 3 with n=5. E: Configuration 5 with n=3. F: Configuration 5 with n=5Comparison of the global simulations results delivered by the traditional model and our multi-compartment model. Distribution of the biomass for the example scenario (T=30°C and Lfmax = 0.5mm), for the configurations 1, 2,3 and 5, for both number of compartments (n=3 and n=5) using the optimal airflow Gin= 5 m^3/d.

Figure P3.7 provides a closer examination of the oxygen gradients of the first compartment in the axial direction which exhibited significant differences. The oxygen penetration depth varied depending on the configuration (Figure P3.7). In configuration 2, oxygen penetrated the biofilm deeper than in configuration 3. As a result, the oxygen concentration in configuration 2 never reached a value lower than 0.01 mg-O_2/l, but for configuration 3 it tended to zero from

0.06 mm onwards. The model included an oxygen-inhibition term for AnAOB according to the experimental evidence reported in Strous et al. (1997). The model used an inhibition constant of 0.01 mg/l. Therefore, no AnAOB occurred in the first compartment of configuration 2, in contrast to configuration 3, where AnAOB already appeared in the first compartment.

The axial oxygen gradient also explains the observed differences regarding NOB. Oxygen concentrations at the biofilm base were higher in configuration 2 than in configuration 3 (2.8 vs 1.7 mg-O_2/l). This study used an oxygen affinity constant for NOB equal to 2.2 mg-O_2/l, which caused the appearance of NOB in configuration 2 but not in configuration 3. Neither configuration 1 nor configuration 5 exhibited NOB within the biofilm and had similarly low values of oxygen at the biofilm base (0.44 and 0.35 mg-O_2/l, respectively). These results agree with experimental studies that demonstrated the dependency of NOB abundance on oxygen concentration at the biofilm base: values larger than 2 mg-O_2/l proved to benefit NOB (Downing and Nerenberg 2008, Pellicer-Nàcher et al. 2014).

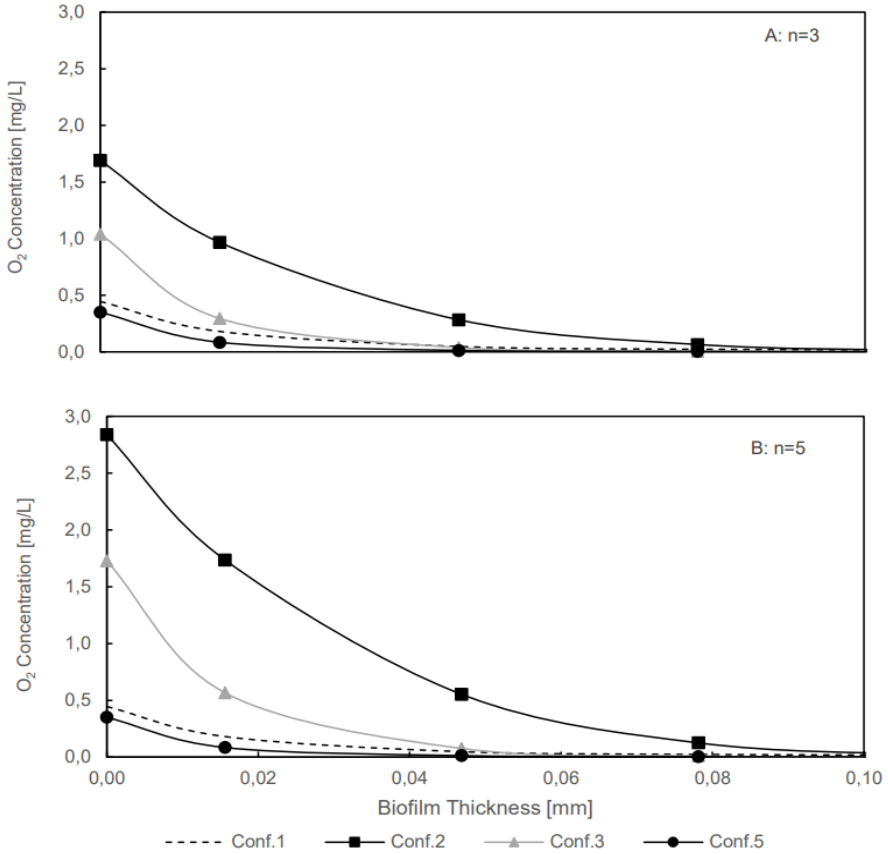

Figure P3. 7. Comparison of the local simulations results delivered by the traditional model and our multi-compartment model. Axial oxygen gradient in the first compartment, for the example scenario (T=30°C and Lfmax=0.5mm), for the configurations 1,2,3 and 5, for both number of compartments (n=3 and n=5) using the optimal airflow Gin= 5 m^3/d

According to the results of this study, the longitudinal oxygen gradient is the main driving force for both, the longitudinal and axial distribution of the biomass. Nevertheless, the substrate gradients slightly affected the axial gradients of oxygen and thus had an indirect influence on the biomass distribution. The inclusion of longitudinal gradients in the model may thus be a better representation of the system and can help finding better strategies for targeted suppression or fostering of bacterial groups within the microbial community.

4. Conclusion

The results delivered by the traditional MABR model for complete autotrophic nitrogen removal differ greatly from the results obtained with the multi-compartment model. The traditional model predicted lower effluent TDN concentrations than the new model.

The simulations indicated that longitudinal gradients of both, oxygen and substrate, significantly affected the global modelling results. Both gradients simultaneously influenced nitrogen removal, whereas the oxygen gradient considerably affected the composition and distribution of the microbial community.

Our multi-compartment model predicted oxygen gradients along the biofilm depth that differed greatly from the ones obtained when using the traditional modelling approach. In this work, we showed that the biomass stratification also differed between these two modeling approaches.

The implementation of more compartments in a multi-compartment model resulted in a steeper oxygen gradient. Both TDN concentrations and the microbial community distribution changed depending on the selected number of compartments.

5. Sumplementary Material

Table P3. 2. Stoichiometric matrix for the model, dissolved components

Component / Process	S_S	S_{NH4}	S_{O2}	S_{NO2}	S_{NO3}	S_{N2}
AOB Growth	-	$-i_{NXB}-1/Y_{AOB}$	$-\frac{3.43-Y_{AOB}}{Y_{AOB}}$	$1/Y_{AOB}$		
NOB Growth	-	$-i_{NXB}$	$-\frac{1.14-Y_{NOB}}{Y_{NOB}}$	$-1/Y_{NOB}$	$1/Y_{NOB}$	
AnAOB Growth	-	$-i_{NXB}-1/Y_{An-AOB}$		$-\frac{1}{1.14}-\frac{1}{Y_{AnAOB}}$	1/1.14	$2/Y_{AnAOB}$
Aerobic Growth HB	$-1/Y_{HB}$	$-i_{NXB}$	$-\frac{1-Y_{HB}}{Y_{HB}}$			
HB Growth of on NO_2^-	$-1/Y_{HB}$	$-i_{NXB}$		$-\frac{1-Y_{HB}}{1.71Y_{HB}}$		$\frac{1-Y_{HB}}{1.71Y_{HB}}$
Growth of AOB NO_3^-	$-1/Y_{HB}$	$-i_{NXB}$			$-\frac{1-Y_{HB}}{2.86Y_{HB}}$	$\frac{1-Y_{HB}}{2.86Y_{HB}}$
Hydrolysis organic matter	1	-	-	-	-	-
Hydrolysis nitrogen compounds	-	1	-	-	-	-
Decay AOB	-	-	-	-	-	-
Decay NOB	-	-	-	-	-	-

Decay AnAOB	-	-	-	-	-	-
Decay HB	-	-	-	-	-	-

Table P3. 3. Stoichiometric matrix for the model, particulate components

Component / Process	X_S	X_N	X_I	X_{AOB}	X_{NOB}	X_{AnAOB}	X_{HB}
AOB Growth		-	-	1	-	-	-
NOB Growth		-	-	-	1	-	-
AnAOB Growth		-	-	-	-	1	-
Aerobic Growth HB		-	-	-	-	-	1
HB Growth of on NO2-		-	-	-	-	-	1
Growth of AOB NO3-		-	-	-	-	-	1
Hydrolysis organic matter	-1	-	-	-	-	-	-
Hydrolysis nitrogen compounds	-	-1	-	-	-	-	-
Decay AOB	1-fi	iNXB-iNXI· fi	fi	-1	-	-	-
Decay NOB	1-fi	iNXB-iNXI· fi	fi	-	-1	-	-
Decay AnAOB	1-fi	iNXB-iNXI· fi	fi	-	-	-1	-
Decay HB	1-fi	iNXB-iNXI· fi	fi	-	-	-	-1

Table P3. 4. Tranformation processes for the model

Rate / Process	
Growth of AOB	$\mu_{\mathrm{AOB}} \mathrm{X}_{\mathrm{AOB}} \frac{\mathrm{S}_{\mathrm{NH4}}}{\mathrm{K}_{\mathrm{NH4,AOB}} + \mathrm{S}_{NH4}} \frac{S_{O2}}{K_{O2,AOB} + S_{O2}}$
Growth of NOB	$\mu_{\mathrm{NOB}} \mathrm{X}_{\mathrm{NOB}} \frac{\mathrm{S}_{\mathrm{NO2}}}{\mathrm{K}_{\mathrm{NO2,NOB}} + \mathrm{S}_{NO2}} \frac{S_{O2}}{K_{O2,NOB} + S_{O2}}$
Growth of AnAOB	$\mu_{\mathrm{AnAOB}} \mathrm{X}_{\mathrm{AnAOB}} \frac{\mathrm{S}_{\mathrm{NH4}}}{\mathrm{K}_{\mathrm{NH4,AnAOB}} + \mathrm{S}_{NH4}} \frac{S_{NO2}}{K_{NO2,AnAOB} + S_{NO2}} \frac{K_{O2,AnAOB}}{K_{O2,AnAOB} + S_{O2}}$
Aerobic Growth of HB	$\mu_{\mathrm{HB}} \mathrm{X}_{\mathrm{HB}} \frac{\mathrm{S}_{\mathrm{S}}}{\mathrm{K}_{\mathrm{S,HB}} + \mathrm{S}_{S}} \frac{S_{O2}}{K_{O2,HB} + S_{O2}}$
Growth of HB on NO2-	$\mu_{\mathrm{HB}} \mathrm{X}_{\mathrm{HB}} \eta_{\mathrm{anox}} \frac{\mathrm{S}_{\mathrm{S}}}{\mathrm{K}_{\mathrm{S,HB}} + \mathrm{S}_{S}} \frac{S_{NO2}}{K_{NO2,HB} + S_{NO2}}$
Growth of HB NO3-	$\mu_{\mathrm{HB}} \mathrm{X}_{\mathrm{HB}} \eta_{\mathrm{anox}} \frac{\mathrm{S}_{\mathrm{S}}}{\mathrm{K}_{\mathrm{S,HB}} + \mathrm{S}_{S}} \frac{S_{NO3}}{K_{NO3,HB} + S_{NO3}}$

Hydrolysis organic matter	$k_H \frac{X_S}{\mathrm{K}_X}$
Hydrolysis nitrogen compounds	$k_H \frac{X_N}{\mathrm{K}_X}$

Decay AOB	$b_{\mathrm{AOB}} \mathrm{X}_{\mathrm{AOB}}$
Decay NOB	$b_{\mathrm{NOB}} \mathrm{X}_{\mathrm{NOB}}$
Decay AnAOB	$b_{\mathrm{AnAOB}} \mathrm{X}_{\mathrm{AnAOB}}$
Decay HB	$b_{\mathrm{HB}} \mathrm{X}_{\mathrm{HB}}$

Table P3. 5. Kinetic, stoichiometric and mass transfer parameters for the processes implemented in the model. All values at a reference temperature of 30°C.

Symbol	Unit	Description	Value	Reference
Ammonia Oxidizing Bacteria (AOB)				
μ_{AOB}	d^{-1}	Maximum specific growth rate	2.05	(Wiesmann 1994)
$K_{NH4,AOB}$	$g\text{-}N/m^3$	Affinity constant NH_4^+ for AOB	2.4	(Wiesmann 1994)
$K_{O2,AOB}$	$g\text{-}COD/m^3$	Affinity constant O_2 for AOB	0.6	(Wiesmann 1994)
b_{AOB}	d^{-1}	Decay rate for AOB	0.13	(Wiesmann 1994)
Nitrite Oxidizing Bacteria (NOB)				
μ_{NOB}	d^{-1}	Maximum specific growth rate	1.45	(Wiesmann 1994)
$K_{NO2,NOB}$	$g\text{-}N/m^3$	Affinity constant NO_2^- for NOB	5.5	(Koch et al. 2000)
$K_{O2,NOB}$	$g\text{-}COD/m^3$	Affinity constant O_2 for NOB	2.2	(Wiesmann 1994)
b_{NOB}	d^{-1}	Decay rate for NOB	0.06	(Wiesmann 1994)
Anammox Bacteria (AnAOB)				
μ_{AnAOB}	d^{-1}	Maximum specific growth rate	0.08	(Koch et al. 2000)
$K_{NH4,AnAOB}$	$g\text{-}N/m^3$	Affinity constant NH_4^+ for AnAOB	0.07	(Strous et al. 1998)
$K_{NO2,AnAOB}$	$g\text{-}N/m^3$	Affinity constant NO_2^- for AnAOB	0.04	(Hao, 2002)
$K_{O2,AnAOB}$	$g\text{-}COD/m^3$	Inhibition constant O_2 for AnAOB	0.01	(Strous et al. 1998)
b_{AnAOB}	d^{-1}	Decay rate for AnAOB	0.003	(Hao et al. 2002b)
Heterotrophic Bacteria (HB)				
μ_{HB}	d^{-1}	Maximum specific growth rate	6	(Henze et al. 2000)
$K_{O2,HB}$	$g\text{-}COD/m^3$	Affinity constant O_2 for HB	0.2	(Henze et al. 2000)
$K_{s,HB}$	$g\text{-}COD/m^3$	Affinity constant COD for HB	20	(Henze et al. 2000)
$K_{NO2,HB}$	$g\text{-}N/m^3$	Affinity constant NO_2^- for HB	0.3	(Alpkvist et al. 2006)
$K_{NO3,HB}$	$g\text{-}N/m^3$	Affinity constant NO_3^- for HB	0.3	(Alpkvist et al. 2006)
b_{HB}	d^{-1}	Decay rate for HB	0.62	(Henze et al. 2000)
η_{anox}	-	Anoxic reduction factor for growth	0.8	(Henze et al. 2000)

Hydrolysis

k_H	g-COD/g-COD_B ·d	Hydrolysis rate	3	(Henze et al. 2000)
K_x	g-COD/g-COD_B	Half saturation constant for hydrolysis	0.3	(Henze et al. 2000)

Stiochometric parameters

Y_{AOB}	g-COD_B/g-N	Growth yield for AOB	0.15	(Wiesmann 1994)
Y_{NOB}	g-COD_B/g-N	Growth yield for NOB	0.041	(Wiesmann 1994)
Y_{AnAOB}	g-COD_B/g-N	Growth yield for AnAOB	0.159	(Strous et al. 1998)
Y_{HB}	g-COD_B/g-COD	Growth yield for HB	0.67	(Henze et al. 2000)
i_{NXB}	g-N/g-COD_B	Nitrogen content in biomass	0.086	(Henze et al. 2000)
i_{NXI}	g-N/g-COD	Nitrogen content in X_i	0.06	(Henze et al. 2000)
f_i	-	Fraction of biomass into particulate inert material	0.08	(Henze et al. 2000)

Mass transfer Parameters

D_{NH4}	m^2/d	Diffusivity in water of NH_4^+	1.5 10^{-4}	(Williamson and McCarty, 1976)
D_{NO2}	m^2/d	Diffusivity in water of NO_2^-	1.4 10^{-4}	(Williamson and McCarty, 1976)
D_{NO3}	m^2/d	Diffusivity in water of NO_3^-	1.4 10^{-4}	(Williamson and McCarty, 1976)
D_{N2}	m^2/d	Diffusivity in water of N_2	2.2 10^{-4}	(Picioreanu et al. 1997)
D_S	m^2/d	Diffusivity in water of COD	1.0 10^{-4}	(Hao, 2004)
D_{O2}	m^2/d	Diffusivity in water of O_2	2.2 10^{-4}	(Picioreanu et al. 1997)

Temperature dependency

θ_{AOB}	1/K	Temperature dependency coefficient AOB	0.094	(Hao et al. 2002a)
θ_{NOB}	1/K	Temperature dependency coefficient NOB	0.061	(Hao et al. 2002a)
θ_{AnAOB}	1/K	Temperature dependency coefficient AnAOB @10°C	0.140	(Lotti, 2015)
θ_{AnAOB}	1/K	Temperature dependency coefficient AnAOB (30-20°C)	0.096	(Hao et al. 2002a)

θ_{HB}	1/K	Temperature dependency coefficient HB	0.07	(Koch et al., 2000)
θ_{HB}	1/K	Temperature dependency coefficient Hydrolisis	0.04	(Koch et al., 2000)

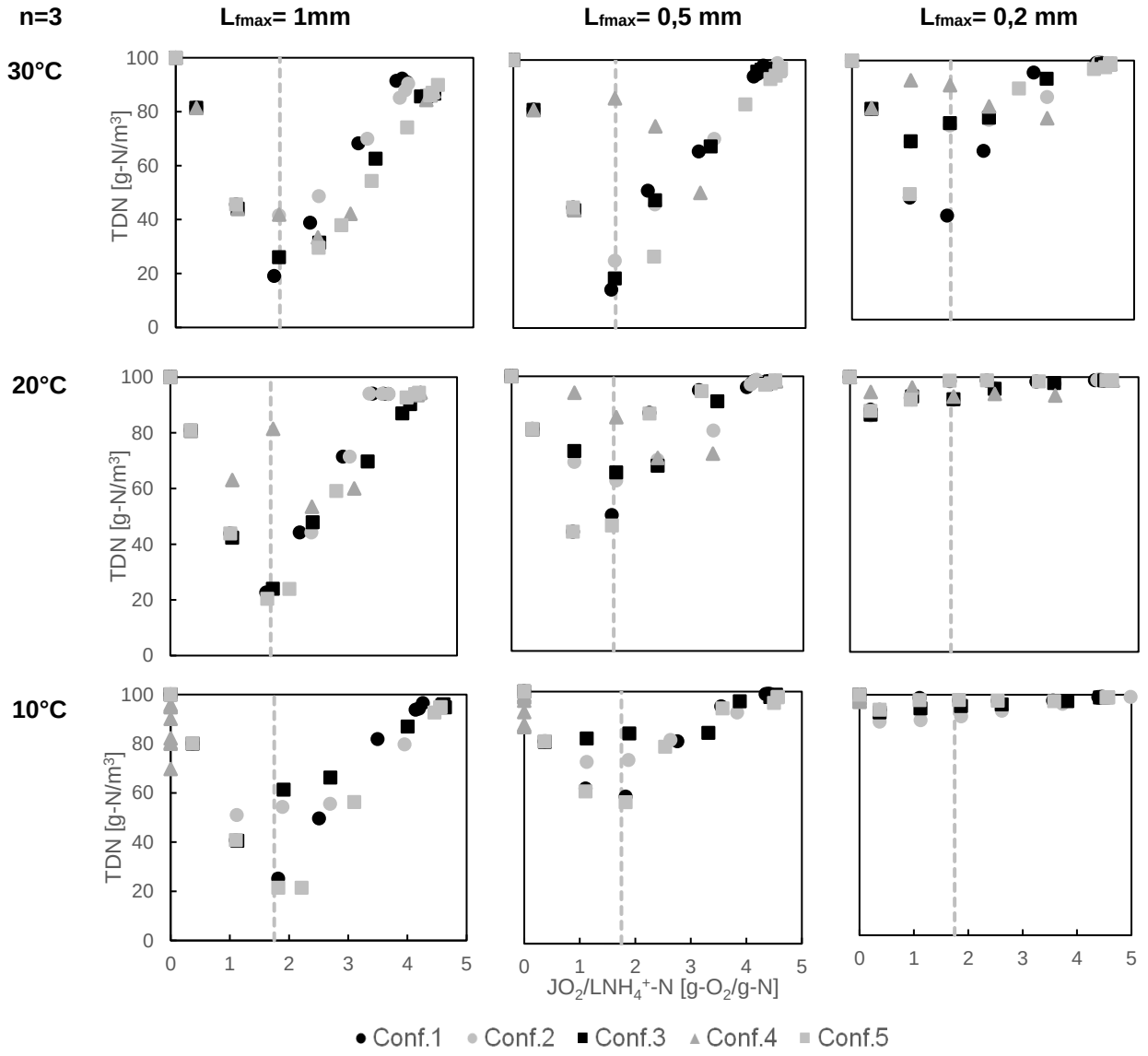

Figure P3. 8. Dependency between TDN and J_{O2}/LNH_4^+-N for all the scenarios with 3 compartments and with airflow ranging from 1 to 50 m3/d. The theoretical point is 1.75 g-O2/g-N as reported in (Terada et al. 2007)

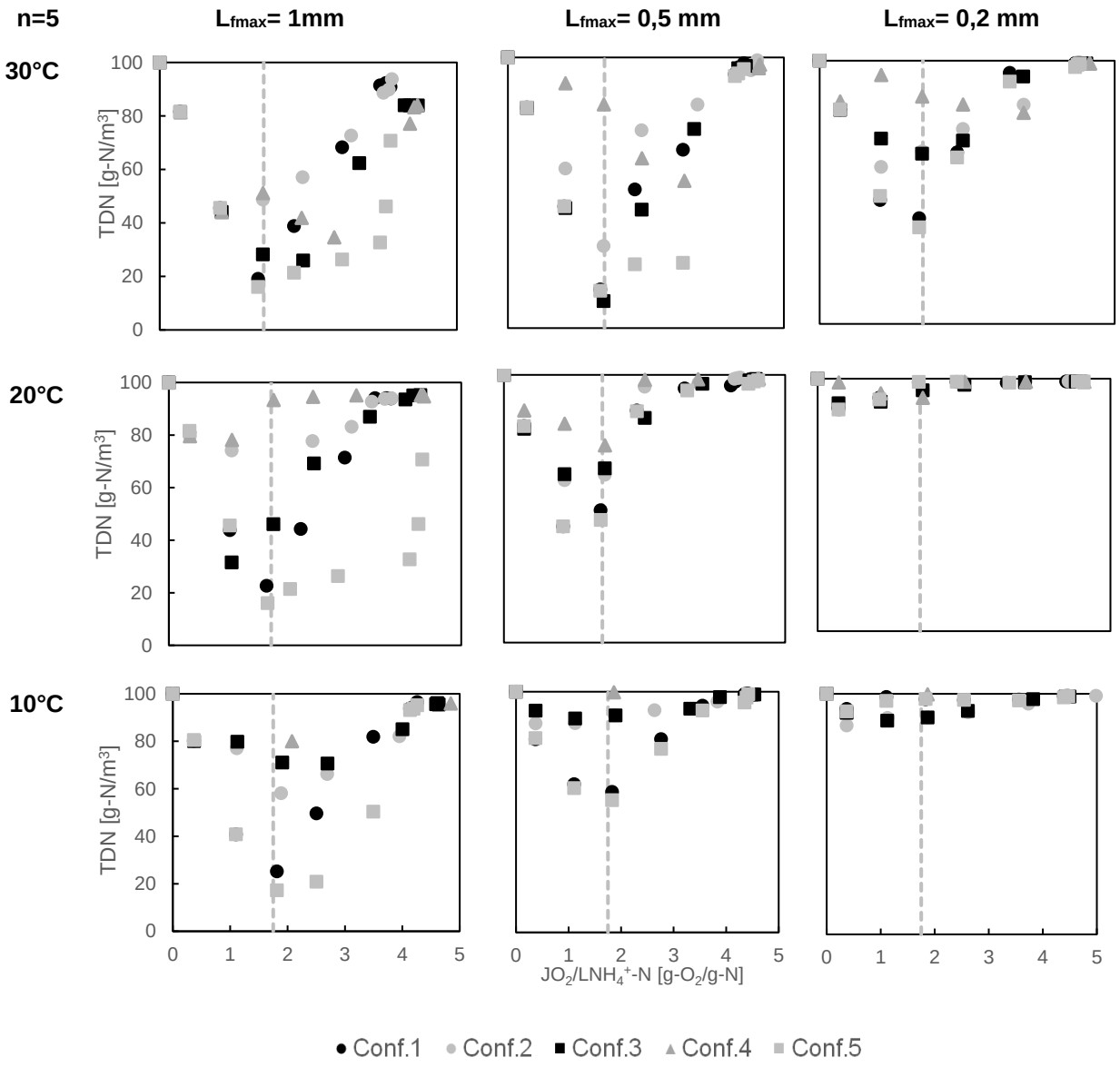

Figure P3. 9. Dependency between TDN and J_{O2}/LNH_4^+-N for all the scenarios with 5 compartments and with airflow ranging from 1 to 50 m3/d. The theoretical point is 1.75 g-O2/g-N as reported in (Terada et al. 2007)

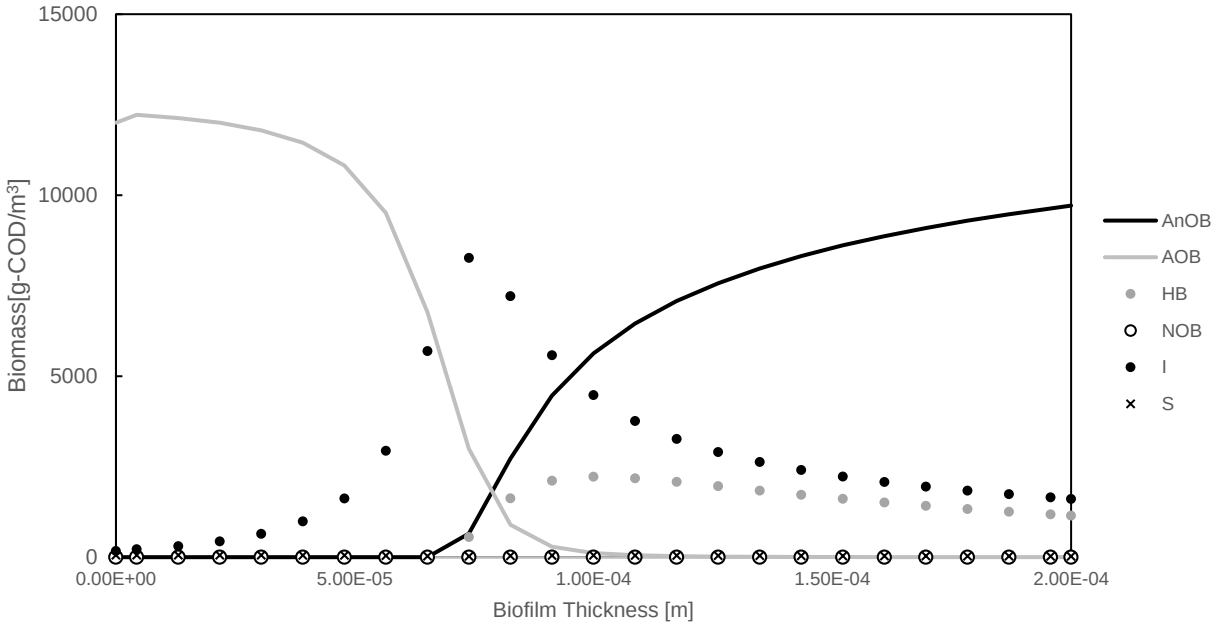

Figure P3. 10. Biomass distribution for the configuration 1 with Gin= 5 m^3/d and Lfmax= 0,2 mm, for all the studied temperatures.

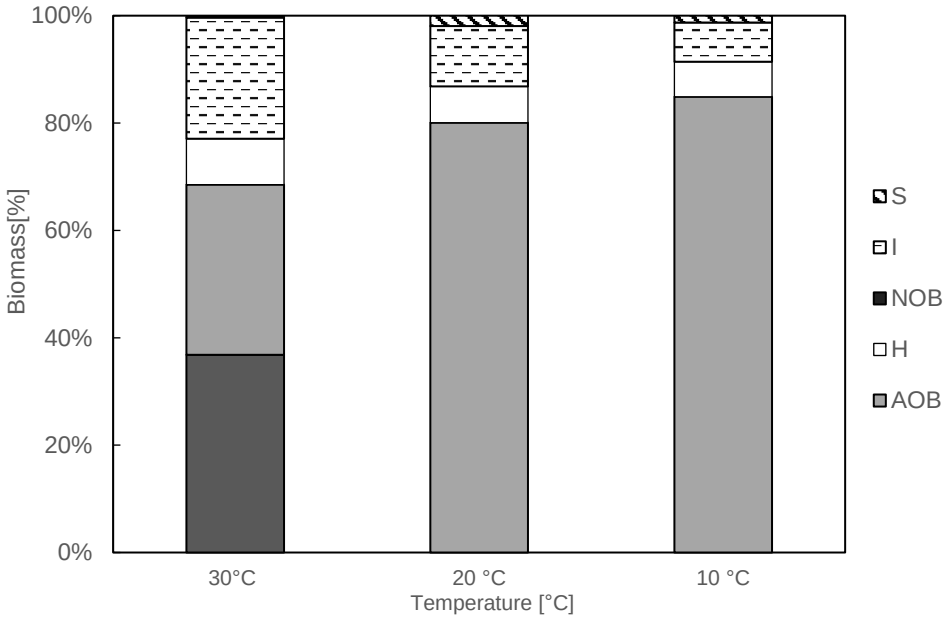

Figure P3. 11.. Biomass stratification in the axial direction for the configuration 1 with T= 30 °C, with Gin= 5 m^3/d and Lfmax= 0,2 mm .

References

Ahmadi Motlagh, A.R., Voller, V.R. and Semmens, M.J. (2006) Advective flow through membrane-aerated biofilms: Modeling results. Journal of Membrane Science 273(1), 143-151.

Alpkvist, E., Picioreanu, C., van Loosdrecht, M.C.M. and Heyden, A. (2006) Three-dimensional biofilm model with individual cells and continuum EPS matrix. Biotechnol Bioeng 94(5), 961-979.

Baeten, J.E., van Loosdrecht, M.C.M. and Volcke, E.I.P. (2017) Improving the accuracy of granular sludge and biofilm reactor simulations in Aquasim through artificial diffusion. Biotechnol Bioeng 114(9), 2131-2136.

Boltz, J.P., Smets, B.F., Rittmann, B.E., van Loosdrecht, M.C.M., Morgenroth, E. and Daigger, G.T. (2017) From biofilm ecology to reactors: a focused review. Water Science and Technology 75(8), 1753-1760.

Casey, E., Glennon, B. and Hamer, G. (1999b) Review of membrane aerated biofilm reactors. Resources, Conservation and Recycling 27(1), 203-215.

Casey, E., Glennon, B. and Hamer, G. (2000a) Biofilm development in a membrane-aerated biofilm reactor: effect of intra-membrane oxygen pressure on performance. Bioprocess Engineering 23(5), 457-465.

Casey, E., Glennon, B. and Hamer, G. (2000b) Oxygen mass transfer characteristics in a membrane-aerated biofilm reactor. Biotechnol Bioeng 62(2), 183-192.

Downing, L.S. and Nerenberg, R. (2008) Effect of oxygen gradients on the activity and microbial community structure of a nitrifying, membrane-aerated biofilm. Biotechnol Bioeng 101(6), 1193-1204.

Gilbert, E.M., Agrawal, S., Schwartz, T., Horn, H. and Lackner, S. (2015) Comparing different reactor configurations for Partial Nitritation/Anammox at low temperatures. Water Research 81, 92-100.

Gilmore, K.R., Terada, A., Smets, B.F., Love, N.G. and Garland, J.L. (2013) Autotrophic Nitrogen Removal in a Membrane-Aerated Biofilm Reactor Under Continuous Aeration: A Demonstration. Environmental Engineering Science 30(1), 38-45.

Han, M., De Clippeleir, H., Al-Omari, A., Wett, B., Vlaeminck, S.E., Bott, C. and Murthy, S. (2016) Impact of carbon to nitrogen ratio and aeration regime on mainstream deammonification. Water Science and Technology 74(2), 375-384.

Hao, Heijnen, J.J. and Van Loosdrecht, M.C.M. (2002a) Model-based evaluation of temperature and inflow variations on a partial nitrification–ANAMMOX biofilm process. Water Research 36(19), 4839-4849.

Hao, X., Heijnen, J.J. and van Loosdrecht, M.C.M. (2002b) Sensitivity analysis of a biofilm model describing a one-stage completely autotrophic nitrogen removal (CANON) process. Biotechnol Bioeng 77(3), 266-277.

Henze, M., Gujer, W., Mino, T. and van Loosedrecht, M. (2000) Activated Sludge Models ASM1, ASM2, ASM2d and ASM3.

Hibiya, K., Terada, A., Tsuneda, S. and Hirata, A. (2003) Simultaneous nitrification and denitrification by controlling vertical and horizontal microenvironment in a membrane-aerated biofilm reactor. Journal of Biotechnology 100(1), 23-32.

Hu, Z., Lotti, T., de Kreuk, M., Kleerebezem, R., van Loosdrecht, M., Kruit, J., Jetten, M.S.M. and Kartal, B. (2013) Nitrogen removal by a nitritation-anammox bioreactor at low temperature. Applied and Environmental Microbiology 79(8), 2807-2812.

IWA (2006) Mathematical Modeling of Biofilms. Scientific and Technical Report Series. , IWA Publishing, London.

Koch, G., Egli, K., Van der Meer, J.R. and Siegrist, H. (2000) Mathematical modeling of autotrophic denitrification in a nitrifying biofilm of a rotating biological contactor. Water Science and Technology 41(4-5), 191-198.

Lackner, S. and Smets, B.F. (2012) Effect of the kinetics of ammonium and nitrite oxidation on nitritation success or failure for different biofilm reactor geometries. Biochemical Engineering Journal 69, 123-129.
Lackner, S., Terada, A. and Smets, B.F. (2008b) Heterotrophic activity compromises autotrophic nitrogen removal in membrane-aerated biofilms: Results of a modeling study. Water Research 42(4), 1102-1112.
Liu, Y., Ngo, H.H., Guo, W., Peng, L., Pan, Y., Guo, J., Chen, X. and Ni, B.-J. (2016a) Autotrophic nitrogen removal in membrane-aerated biofilms: Archaeal ammonia oxidation versus bacterial ammonia oxidation. Chemical Engineering Journal 302, 535-544.
Lotti, T., Kleerebezem, R., Hu, Z., Kartal, B., de Kreuk, M.K., van Erp Taalman Kip, C., Kruit, J., Hendrickx, T.L.G. and van Loosdrecht, M.C.M. (2015a) Pilot-scale evaluation of anammox-based mainstream nitrogen removal from municipal wastewater. Environmental Technology 36(9), 1167-1177.
Lotti, T., Kleerebezem, R. and van Loosdrecht, M.C.M. (2015b) Effect of temperature change on anammox activity. Biotechnol Bioeng 112(1), 98-103.
Martin, K.J. and Nerenberg, R. (2012) The membrane biofilm reactor (MBfR) for water and wastewater treatment: Principles, applications, and recent developments. Bioresource Technology 122, 83-94.
Matsumoto, S., Terada, A. and Tsuneda, S. (2007) Modeling of membrane-aerated biofilm: Effects of C/N ratio, biofilm thickness and surface loading of oxygen on feasibility of simultaneous nitrification and denitrification. Biochemical Engineering Journal 37(1), 98-107.
Ni, B.-J., Smets, B.F., Yuan, Z. and Pellicer-Nàcher, C. (2013) Model-based evaluation of the role of Anammox on nitric oxide and nitrous oxide productions in membrane aerated biofilm reactor. Journal of Membrane Science 446, 332-340.
Pankhania, M., Brindle, K. and Stephenson, T. (1999) Membrane aeration bioreactors for wastewater treatment: completely mixed and plug-flow operation. Chemical Engineering Journal 73(2), 131-136.
Peeters, J., Vicevic, G., Koops, G.H. and Côté, P. (2016) The role of innovative technologies in achieving energy-neutral wastewater treatment. Water Practice and Technology 11(4), 691-701.
Pellicer-Nàcher, C., Franck, S., Gülay, A., Ruscalleda, M., Terada, A., Al-Soud, W.A., Hansen, M.A., Sørensen, S.J. and Smets, B.F. (2014) Sequentially aerated membrane biofilm reactors for autotrophic nitrogen removal: microbial community composition and dynamics. Microbial Biotechnology 7(1), 32-43.
Perez-Calleja, P., Aybar, M., Picioreanu, C., Esteban-Garcia, A.L., Martin, K.J. and Nerenberg, R. (2017) Periodic venting of MABR lumen allows high removal rates and high gas-transfer efficiencies. Water Research 121, 349-360.
Perry, R.H. (1997) Chemical engineering-Hanbooks, manuals>.
Picioreanu, C., van Loosdrecht, M.C.M. and Heijnen, J.J. (1997) Modelling the effect of oxygen concentration on nitrite accumulation in a biofilm airlift suspension reactor. Water Science and Technology 36(1), 147-156.
Reichert, P. (1998) AQUASIM 2.0—Computer program for the identification and simulation of aquatic systems. EAWAG.
Röske, I., Röske, K. and Uhlmann, D. (1998) Gradients in the taxonomic composition of different microbial systems: Comparison between biofilms for advanced waste treatment and lake sediments. Water Science and Technology 37(4), 159-166.
Semmens, M.J. and Essila, N.J. (2001) Modeling Biofilms on Gas-Permeable Supports: Flux Limitations. 127(2), 126-133.
Shanahan, J. and Semmens, M. (2006) Influence of a nitrifying biofilm on local oxygen fluxes across a micro-porous flat sheet membrane. Journal of Membrane Science 277(1-2), 65-74.
Shanahan, J.W. and Semmens, M.J. (2004) Multipopulation Model of Membrane-Aerated Biofilms. Environmental Science & Technology 38(11), 3176-3183.

Strous, M., Heijnen, J.J., Kuenen, J.G. and Jetten, M.S.M. (1998) The sequencing batch reactor as a powerful tool for the study of slowly growing anaerobic ammonium-oxidizing microorganisms. Appl Microbiol Biotechnol 50(5), 589-596.
Strous, M., Van Gerven, E., Kuenen, J.G. and Jetten, M. (1997) Effects of aerobic and microaerobic conditions on anaerobic ammonium-oxidizing (anammox) sludge. Applied and Environmental Microbiology 63(6), 2446-2448.
Terada, A., Lackner, S., Tsuneda, S. and Smets, B.F. (2007) Redox-stratification controlled biofilm (ReSCoBi) for completely autotrophic nitrogen removal: The effect of co- versus counter-diffusion on reactor performance. Biotechnol Bioeng 97(1), 40-51.
Wang, D., Wang, Q., Laloo, A., Xu, Y., Bond, P.L. and Yuan, Z. (2016) Achieving Stable Nitritation for Mainstream Deammonification by Combining Free Nitrous Acid-Based Sludge Treatment and Oxygen Limitation. Scientific Reports 6, 25547.
Wiesmann, U. (1994) Biotechnics/Wastewater, pp. 113-154, Springer Berlin Heidelberg, Berlin, Heidelberg.
Xu, G., Zhou, Y., Yang, Q., Lee, Z.M.-P., Gu, J., Lay, W., Cao, Y., Liu, Y.J.A.M. and Biotechnology (2015) The challenges of mainstream deammonification process for municipal used water treatment. 99(6), 2485-2490.

About the author:

Vanessa Acedo Alonso is a chemical engineer from the Universidad Nacional de Colombia and holds a master degree in water resources and environmental management from the Leibniz Universität Hannover. From 2018 until 2022, she conducted her doctoral research at the Technische Universität Darmstadt as part of the research group water and environmental technology led by Prof. Dr. Susanne Lackner. The focus of her professional endeavors is the development of mechanistic as well as data-driven modelling solutions for optimization of water systems.

From the contents:

This thesis focuses on the modelling of biofilm systems in the wastewater context. It evaluates the impact of two microscale features: microbial community composition and dimensionality on global modelling results i.e. final effluent concentrations. This work explores the implications of implementing these two microscale features trough three biofilm treatment systems relevant to the current wastewater practice:

1. A biologically active granular activated carbon filter for the removal of organic matter as advanced wastewater treatment is modelled trough the combination of a multicomponent adsorption model and a state of the art biofilm model.

2. A moving bed bioreactor for Partial-Nitritation Anammox is used to explore the different growth strategies that heterotrophic bacteria may undergo within a biofilm matrix.

3. A membrane-aerated bioreactor for Partial-Nitritation Anammox is modelled trough two approaches: a one-dimensional and a pseudo two-dimensional model.

For the three systems, the consequences of applying a certain level of complexity in the microscale features are discussed from the practical point of view.

ISBN 978-3-940897-71-8